Studies on thrombopoiesis and spleen tyrosine kinase-mediated signaling in platelets

* * *

Untersuchungen der Thrombopoese und der *spleen tyrosine kinase*-vermittelten Signaltransduktion in Thrombozyten

Doctoral thesis for a doctoral degree
at the Graduate School of Life Sciences,
Julius-Maximilians-Universität Würzburg,
Section Biomedicine

submitted by

Judith Martina Maria van Eeuwijk

from Leerdam, the Netherlands

Würzburg, 2016

Submitted on:

Members of the *Promotionskomitee*:

Chairperson: Prof. Dr. Manfred Gessler

Primary Supervisor: Prof. Dr. Bernhard Nieswandt

Supervisor (Second): Dr. Katrin Heinze

Supervisor (Third): Prof. Dr. Guido Stoll

Date of Public Defense:

Date of Receipt of Certificates:

"One should not pursue goals that are easily achieved. One must develop an instinct for what one can just barely achieve through one's greatest efforts."

- Albert Einstein

Table of contents

Summary

In mammals, anucleate blood platelets are constantly produced by their giant bone marrow (BM) progenitors, the megakaryocytes (MKs), which originate from hematopoietic stem cells. Megakaryopoiesis and thrombopoiesis have been studied intensively, but the exact mechanisms that control platelet generation from MKs remain poorly understood. Using multiphoton intravital microscopy (MP-IVM), thrombopoiesis and proplatelet formation were analyzed in the murine BM in real-time and *in vivo*, identifying an important role for several proteins, including Profilin1, TRPM7 and RhoA in thrombopoiesis. Currently, it is thought that blood cell precursors, such as MKs, migrate from the endosteal niche towards the vascular niche during maturation. In contrast to this paradigm, it was shown that MKs are homogeneously distributed within the dense BM blood vessel network, leaving no space for vessel-distant niches. By combining results from *in vivo* MP-IVM, *in situ* light-sheet fluorescence microscopy (LSFM) of the intact BM as well as computational simulations, surprisingly slow MK migration, limited intervascular space and a vessel-biased MK pool were revealed, contradicting the current concept of directed MK migration during thrombopoiesis.

Platelets play an essential role in hemostasis and thrombosis, but also in the pathogenesis of ischemic stroke. Ischemic stroke, which is mainly caused by thromboembolic occlusion of brain arteries, is among the leading causes of death and disability worldwide with limited treatment options. The platelet collagen receptor glycoprotein (GP) VI is a key player in arterial thrombosis and a critical determinant of stroke outcome, making its signaling pathway an attractive target for pharmacological intervention. The spleen tyrosine kinase (Syk) is an essential signaling mediator downstream of GPVI, but also of other platelet and immune cell receptors. In this thesis, it was demonstrated that mice lacking Syk specifically in platelets are protected from arterial thrombus formation and ischemic stroke, but display unaltered hemostasis. Furthermore, it was shown that mice treated with the novel, selective and orally bioavailable Syk inhibitor BI1002494 were protected in a model of arterial thrombosis and had smaller infarct sizes and a significantly better neurological outcome 24 h after transient middle cerebral artery occlusion (tMCAO), also when BI1002494 was administered therapeutically, i.e. after ischemia. These results provide direct evidence that pharmacological Syk inhibition might become a safe therapeutic strategy. The T cell receptor ζ−chain-associated protein kinase of 70 kDA (Zap-70) is also a spleen tyrosine kinase family member, but has a lower intrinsic activity compared to Syk and is expressed in T cells and natural killer (NK) cells, but not in platelets. Unexpectedly, arterial thrombus formation *in vivo* can occur independently of Syk kinase function as revealed by studies in Syk^{ki} mice, which express Zap-70 under the control of intrinsic Syk promoter elements.

Zusammenfassung

In Säugetieren werden kernlose Thrombozyten durch ihren riesigen Knochenmark- (KM-) Vorläuferzellen, die Megakaryozyten (MK), die von hämatopoetischen Stammzellen stammen, ständig produziert. Megakaryopoese und Thrombopoese wurden schon intensiv untersucht, aber die genauen Mechanismen, die die Thrombozytenproduktion aus MK kontrollieren, bleiben weitgehend unverstanden. Mittels Multiphotonen-Intravitalmikroskopie (MP-IVM) wurden Thrombopoese und Proplättchenbildung im murinen KM in Echtzeit *in vivo* untersucht. Dadurch wurde eine wichtige Rolle für die Proteine Profilin1, TRPM7 und RhoA in der Thrombopoese identifiziert. Derzeit wird angenommen, dass Blutzellvorläufer, wie MK, während der Reifung von der endostalen Nische in Richtung der Gefäßnische migrieren. Im Gegensatz zu diesem Paradigma wurde hier gezeigt, dass MK homogen innerhalb des dichten KM Blutgefäßnetzes verteilt sind, so dass kein Raum für Gefäß-ferne Nischen besteht. Durch Ergebnisse von *in vivo* MP-IVM, *in situ* Licht-Blatt-Fluoreszenzmikroskopie (LSFM) des intakten KM sowie Computersimulationen wurden eine überraschend langsame MK-Migration, ein begrenzter intervaskulärer Raum und eine asymmetrische MK-Verteilung gezeigt, was im Widerspruch zum derzeitig akzeptierten Konzept der gerichteten MK-Migration während der Thrombopoese steht.

Die Thrombozyten spielen eine wesentliche Rolle nicht nur bei der Hämostase und Thrombose, sondern auch in der Pathogenese des ischämischen Schlaganfalls. Der ischämische Schlaganfall, der vor allem durch einen thromboembolischen Verschluss von Gehirnarterien verursacht wird, ist eine der häufigsten Ursachen für Tod und Behinderung weltweit und die Behandlungsmöglichkeiten sind sehr eingeschränkt. Der thrombozytäre Kollagenrezeptor Glykoprotein (GP) VI ist ein wichtiger Faktor in der arteriellen Thrombose und trägt entscheidend zur Pathogenese des ischämischen Schlaganfalls bei, sodass dessen Signalweg ein attraktives Ziel für pharmakologische Interventionen darstellen könnte. Die *spleen tyrosine kinase* (Syk) ist ein wichtiges Molekül im GPVI-Signalweg, aber auch in den Signalkaskaden von anderen Thrombozyten- und Immunzellrezeptoren. Es wurde nachgewiesen, dass Mäuse mit einer thrombozytären Syk-Defizienz, vor arterieller Thrombusbildung und ischämischem Schlaganfall geschützt sind, aber unveränderte Hämostase zeigen. Darüber hinaus wurde gezeigt, dass Mäuse, die mit dem neuartigen, selektiven und oral bioverfügbaren Syk-Inhibitor BI1002494 behandelt wurden, geschützt sind in einem Modell der arteriellen Thrombose. Auch hatten sie kleinere Infarkte und eine deutlich bessere neurologische Funktion 24 Stunden nach der transienten *Arteria cerebri media* Okklusion (tMCAO), auch wenn BI1002494 therapeutisch, d.h. nach der Ischämie, verabreicht wurde. Diese Ergebnisse deuten darauf hin, dass die pharmakologische Hemmung von Syk eine sichere therapeutische Strategie bei Schlaganfall sein könnte. Der

T-Zell Rezeptor *ζ-chain-associated protein kinase of 70 kDa* (Zap-70) ist auch ein *spleen tyrosine kinase*-Familienmitglied, hat aber eine geringere intrinsische Aktivität im Vergleich zu Syk und wird in T-Zellen und *natural killer* (NK) Zellen exprimiert, nicht aber in Thrombozyten. Studien in *Syk^{ki}* Mäusen, die unter der Kontrolle der intrinsischen Syk Promotorelemente Zap-70 exprimieren, ergaben, dass die arterielle Thrombusbildung *in vivo* unabhängig von der Syk-Kinasefunktion stattfinden kann.

Samenvatting

In zoogdieren worden kernloze bloedplaatjes constant door hun grote beenmerg (BM) voorlopercellen, de megakaryocyten (MK), afkomstig van hematopoietische stamcellen, geproduceerd. Megakaryopoïese en trombopoïese zijn tot nu toe intensief bestudeerd, maar de exacte mechanismen die de generatie van bloedplaatjes vanuit MK controleren, blijven slecht begrepen. Met behulp van multiphoton intravitale microscopie (MP-IVM), zijn in real-time en *in vivo*, trombopoïese en proplatelet vorming in het BM van muizen bestudeerd, waarbij een belangrijke rol voor de eitwitten Profilin1, TRPM7 en RhoA in trombopoïese is geïdentificeerd. Momenteel wordt aangenomen dat bloedcelvoorlopers, zoals MK, tijdens de rijping van de endostale niche naar de vasculaire niche migreren. In tegenstelling tot dit paradigma, is hier aangetoond dat MK homogeen verdeeld zijn binnen het dichte bloedvatnetwerk van het BM, waarbij geen ruimte meer is voor bloedvat-verwijderde niches. Door het combineren van de resultaten, verkregen met behulp van *in vivo* MP-IVM, *in situ* licht-blad fluorescentie microscopie (LSFM) van het intacte BM evenals computationele simulaties, zijn, een verrassend langzame MK migratie, een beperkte intervasculaire ruimte en een asymmetrische MK verdeling aangetoond, in tegenspraak tot het huidig geaccepteerde concept van de gerichte MK migratie tijdens de trombopoïese.

Bloedplaatjes spelen een essentiële rol niet alleen in hemostase en trombose, maar ook in de pathogenese van een ischemische beroerte. Een ischemische beroerte, die vooral veroorzaakt wordt door een trombo-embolische occlusie van de hersenslagaders, is een van de belangrijkste oorzaken van overlijden en invaliditeit wereldwijd en de behandelingsmogelijkheden zijn zeer beperkt. De bloedplaatjes collageen receptor glycoproteïne (GP) VI is een belangrijke speler in arteriële trombose en een kritische factor voor de gevolgen van een beroerte, waardoor de signaalweg een aantrekkelijk doelwit voor farmacologische interventie zou kunnen zijn. De *spleen tyrosine kinase* (Syk) is een essentiële signaalmediator in de GPVI-signaalweg, maar ook in signaalwegen van andere bloedplaatjes- en immuuncelreceptoren. In deze thesis is aangetoond, dat muizen die Syk specifiek in bloedplaatjes missen, beschermd zijn tegen de vorming van arteriële trombose en ischemische beroerte, maar ongewijzigde hemostase vertonen. Verder is getoond, dat muizen, die behandeld waren met de nieuwe, selectieve en oraal biologisch beschikbare Syk inhibitor BI1002494, beschermd waren in een model van arteriële trombose. Ook hadden ze kleinere infarcten en een significant beter neurologische functie 24 uur na transiënte middelste cerebrale arterie occlusie (tMCAO), ook toen BI1002494 therapeutisch, dat wil zeggen na ischemie, werd toegediend. Deze resultaten leveren direct bewijs dat farmacologische Syk remming een veilige therapeutische strategie zou kunnen bieden. De T-cel receptor ζ-*chain-associated protein kinase of 70 kDa* (Zap-70) is ook een *spleen tyrosine*

kinase-familielid, maar heeft een lagere intrinsieke activiteit vergeleken met Syk en wordt tot expressie gebracht in T-cellen en *natural killer* (NK) cellen, maar niet in bloedplaatjes. Studies in *Syk^ki* muizen, die Zap-70 onder de controle van intrinsieke Syk promotorelementen tot expressie brengen, laten zien dat arteriële trombusvorming *in vivo* onafhankelijk van Syk kinase functie kan optreden.

1. Introduction

1.1. Hematopoiesis

Hematopoiesis, the process of blood cell formation, begins during embryogenesis in the yolk sac and the aorta-gonad mesonephros region, is taken over by different embryonic organs including the fetal liver and spleen and finally resides in the bone marrow (BM), which functions as the primary lymphoid organ in the adult human body.[1-3] In children, the BM is mainly located in the long bones, like the femur and tibia, whereas in adults it is mostly located in flat bones, like the skull, pelvis, sternum and ribs. The BM contains arteries, carrying oxygen, nutrients and growth factors into the BM and sinusoids, which are specialized venules forming a network of fenestrated vessels allowing cells to enter and leave the circulation. A dense network of arterioles and sinusoids can be found near the endosteum, the interface of bone and BM, which is covered by bone-lining cells such as osteoblasts and osteoclasts. Blood cells and their precursors are located in the extravascular spaces between the sinusoids.[4,5] Hematopoiesis involves hematopoietic stem cells (HSCs), which are capable of self-renewal and are precursors of progenitor cells that become committed to one of the hematopoietic lineages at a later stage.[6] Maintenance and lineage differentiation of the HSC pool in the BM is thought to depend on its specific environment and either occurs via asymmetrical cell division or environmental asymmetry.[7] During asymmetrical cell division, cellular determinants in the cytoplasm like mRNA and/or proteins are localized to only one of the two daughter cells leading to two daughter cells with different cellular fates. Environmental asymmetry depends on the presence of specialized BM niche microenvironments.[7]

1.1.1. Hematopoietic stem cells and bone marrow niches

In 1978, Ray Schofield was the first to propose the concept of the stem cell niche for HSCs in the BM.[8] The BM niche or microenvironment is decisive for the development of HSCs and, depending on the association with adjacent cells and local cytokines in the specific niche or microenvironment, the proliferation or differentiation of HSCs is stimulated (Figure 1). Environmental asymmetry occurs after division of the HSC. According to this model, one daughter cell is exposed to extrinsic signals from the local BM microenvironment promoting lineage differentiation, while the other daughter cell remains in the self-renewing niche, thereby balancing HSC self-renewal and differentiation. Over the past years, significant progress has been made to identify the structure, localization and composition of the HSC niches/microenvironments in the BM and different niche functions have been proposed, such as the quiescent-storage niche and the self-renewal niche.[7] HSCs and distinct subpopulations of HSCs or progenitor cells can also occupy specialized niches.[9]
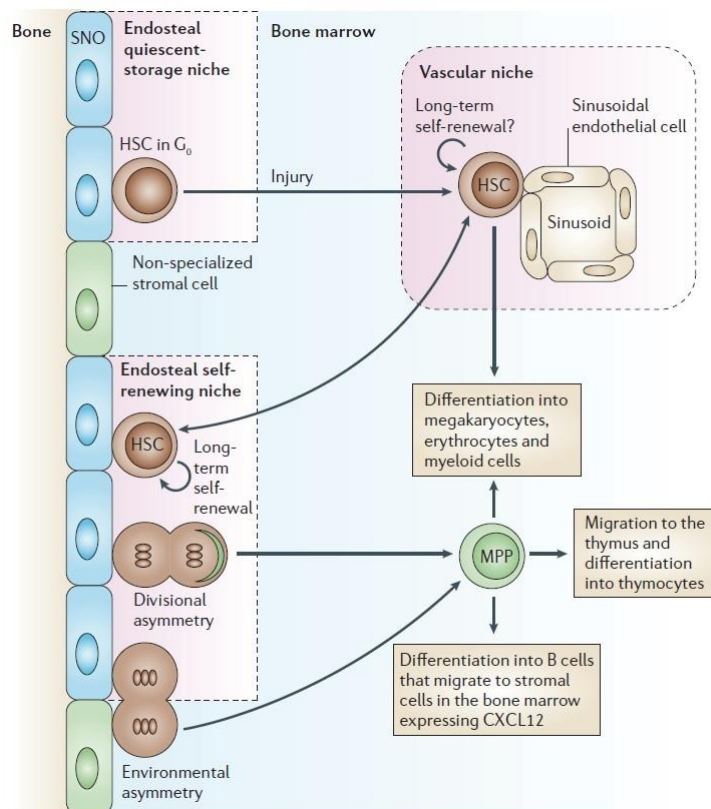
Figure 1. Model of bone marrow hematopoietic stem cell niches. Endosteal bone surfaces are lined with specialized (blue) and non-specialized (green) stromal cells. The osteoblasts (SNOs) function as a regulatory component of the niche and maintain quiescence and prevent differentiation of hematopoietic stem cells (HSCs) in the quiescent-storage niche. In response to injury, these quiescent HSCs might be activated and recruited to the vascular niche. The self-renewal niche contains both quiescent and dividing HSCs. The HSCs are able to differentiate into multipotential progenitors (MPPs), either by asymmetrical cell division or environmental asymmetry. These progenitors can give rise to all hematopoietic lineages, including megakaryocytes (MKs). From: Wilson and Trumpp, 2006[7]

BM niches are likely to be located near the bone surfaces (endosteal niche) and/or associated with sinusoidal endothelium (vascular niche). This concept is, however, heavily debated and it is now thought that in adult BM, multiple niche cell populations from distinct BM zones regulate HSCs for long-term maintenance, proliferation, and differentiation. These zones or niches cooperate to control HSC quiescence and self-renewal and the differentiation of HSCs into progenitor cells to maintain homeostasis. The endosteal niche appears to contain mainly dormant HSCs. Kunisaki *et al.* showed that quiescent HSCs associate specifically with BM arterioles, which are mainly found in the endosteal BM, providing an arteriolar niche.[10] However, a recent report by Acar *et al.* reveals that most HSCs are distant from arterioles and bone surfaces and mainly localize in perisinusoidal niches throughout the BM.[11] In the vascular niche, many proliferating cells, most likely self-renewing HSCs, are located in close contact to the BM sinusoidal endothelial cells (BMECs).[7] A recent report by Itkin *et al.* provided strong evidence to support the concept that BM stem cell maintenance is regulated by distinct blood vessel types with different permeability properties.[12]

Osteoblasts are an essential part of the endosteal niche and are limiting for the niche size and its activity. The osteoblastic cells are a regulatory component of the niche and influence HSC maturation and function.[13] HSCs localize in close proximity to the endosteum and HSC progenitors can be found distributed throughout the central BM.[14,15] On the other hand, it has been shown that HSCs localize adjacent to sinusoid vessels in close contact to perivascular

cells. The HSCs attach to the fenestrated endothelium of the BM sinusoids serving as a niche for adult HSCs.[16] The mesenchymal stromal cells (MSCs) are a component of the perivascular niche and together with the BMECs synthesize cytokines, such as stem cell factor (SCF) and stromal cell-derived factor 1/CXC-chemokine ligand 12 (SDF1/CXCL12), and adhesion molecules like E-selectin and vascular cell-adhesion molecule 1 (VCAM1) that promote HSC maintenance, migration, mobilization and homing.[17-20] HSCs are often found in contact to cells expressing high amounts of SDF1, the so-called CXCL12 abundant reticular (CAR) cells, which are a key component of HSC niches. These cells surround BMECs, but can also be found near the endosteum.[21,22] SDF1 is a chemokine that is required for HSC maintenance, migration and retention in the BM during homeostasis and upon injury. Its expression and secretion is upregulated in situations of increased hematopoietic cell loss, for instance in response to irradiation, chemotherapy or hypoxia.[23,24] SDF1 is the ligand for the CXC-chemokine receptor 4 (CXCR4) and HSC migration only occurs in response to a SDF1 gradient.[25] Mice lacking either SDF1 or CXCR4 show embryonic lethality, indicating an important role for the SDF1-CXCR4 axis in hematopoiesis.[22,26,27]

1.1.2. Megakaryopoiesis

Megakaryocytes (MKs) are the largest cells within the BM with an average diameter of 50-100 μm in humans and up to 50 μm in mice. They are responsible for the production of blood platelets. MKs belong to the myeloid cell lineage and mainly reside in the BM, but can also be found in the spleen and the lungs. MKs are derived from the multipotent HSCs, which differentiate into the common myeloid progenitor (CMP) or colony-forming unit-granulocyte/ erythrocyte/macrophage/megakaryocyte (CFU-GEMM). These cells develop into erythrocyte/ megakaryocyte progenitors (CFU-erythrocyte/megakaryocyte (CFU-EM) and burst-forming unit-EM (BFU-EM)), finally leading to the formation of the direct MK precursor (CFU-Meg) and the differentiation into MKs.[28] Before MKs have the capacity to release platelets, they undergo a complex maturation process, which involves nuclear proliferation. MKs become polyploid by several cycles of DNA replication without terminal cytokinesis, a process called endomitosis, which depends on thrombopoietin (Thpo).[29] Due to endomitosis, the multilobed nucleus of a mature MK can contain between 4 to 128 sets of chromosomes (4N-128N). Concomitantly, maturation of MKs includes cytoplasm expansion by increased protein synthesis, the synthesis of platelet-specific granules and organelles and the formation of a demarcation membrane system (DMS), also known as invaginated membrane system (IMS).[30] The DMS derives from the peripheral plasma membrane and the Golgi apparatus and is an elaborate meshwork of membrane channels containing cisternae and tubules that serve as a membrane reservoir for platelet biogenesis.[31-33] The DMS forms the plasma membrane of newly generated platelets and this is considered to be a Thpo-driven

process.[34-36] Prior to the onset of proplatelet formation from mature MKs and the release of discoid platelets into the circulation, substantial MK cytoplasm remodeling and cytoskeletal rearrangements occur. After proplatelet release, the MK nucleus is extruded and degraded.[29]

The primary regulator for inducing megakaryopoiesis is the cytokine Thpo.[37] Thpo signals through the *myeloproliferative leukemia virus oncogene* (c-Mpl) receptor on MKs and platelets and stimulates the generation of MKs from their HSC progenitors. Hepatocytes are the major source of Thpo and its production is critically regulated by signaling through the hepatic Ashwell-Morell receptor, which recognizes and removes aged platelets.[38] Thpo induces transcription factors such as Fli-1, ETV6, AML1 and GATA1/FOG1, leading to expression of markers like CD42 (GPIb-V-IX complex) or CD41 (GPIIb) that are specific for the platelet lineage.[39,40] During final maturation, under the transcription factor NF-E2, MKs express the late marker and MK/platelet-specific tubulin isoform β1.[28,41] While mice deficient in c-Mpl or Thpo have severely reduced platelet counts, they still successfully produce platelets,[42-44] indicating that MK maturation and platelet biogenesis can occur independently of Thpo. Thpo acts in concert with the cytokines interleukin (IL-) 3, IL-6, IL-11, granulocyte macrophage colony-stimulating factor (GM-CSF), Kit-ligand and the chemokines SDF1, fibroblast growth factor 4 (FGF4) and platelet factor 4 (PF4) to stimulate MK maturation.[28,45] A seminal paper by Avecilla *et al.* shows that chemokine-mediated interactions of MK progenitors with BMECs promote Thpo-independent platelet production. While mice lacking Thpo or its receptor c-Mpl have severely reduced platelet counts, the systemic application of the chemokines SDF1 and FGF4 can restore thrombopoiesis via a vascular endothelial-cadherin (VE-cadherin) dependent mechanism.[18,39]
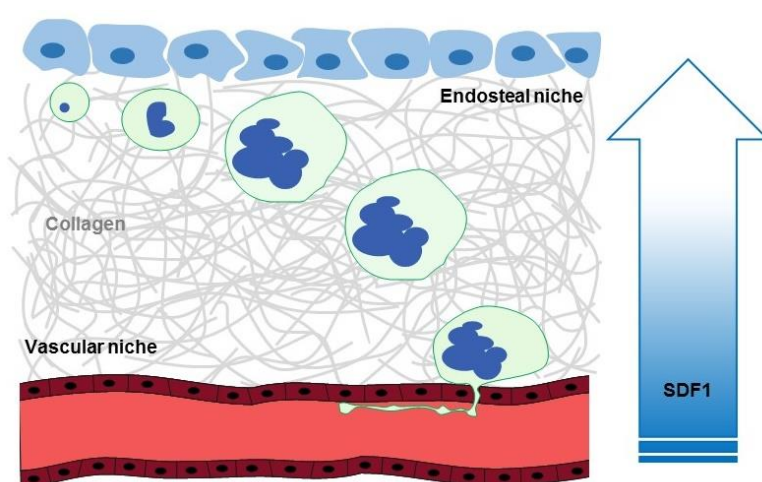
Figure 2. Current concept of MK maturation and migration. During MK maturation, MKs are thought to migrate from the endosteal niche towards the vascular niche. Stromal cell-derived factor 1 (SDF1) enhances thrombopoiesis by promoting the motility and transendothelial migration of MKs. Once the MKs have reached the vascular niche, proplatelets pass the endothelial barrier, releasing platelets into the bloodstream. Modified from Bluteau *et al.*, 2009[45]

During MK maturation, MKs are thought to migrate from the endosteal niche, which is enriched in collagen I, towards the vascular niche, enriched in collagen IV, laminin, von Willebrand factor (vWF), fibronectin and fibrinogen (Figure 2).[18,46,47] Avecilla *et al.* showed

that FGF4 supports the adhesion of MKs to BMECs, enhancing MK survival and maturation. Besides its role in HSC maintenance and migration, SDF1 also modulates thrombopoiesis by promoting the motility and transendothelial migration of MKs.[18,48,49] Recently, Niswander *et al.* further argued in favor of an important role of SDF1 and its downstream signaling through the CXCR4 receptor in MK localization and migration, as intravenous administration of SDF1 enhanced the association of MKs with the BMECs and increased circulating platelet numbers.[50] MKs also interact with the extracellular environment during maturation and migration. To facilitate the penetration of the basement membrane of a sinusoidal vessel or proplatelet extension, MKs form podosomes that degrade and remodel the extracellular matrix (ECM) via matrix metalloproteases (MMPs) in the BM.[51,52] In addition, MKs also have regulatory functions. Recently, Bruns *et al.* and Zhao *et al.* showed that mature MKs regulate HSC quiescence by secretion of PF4 and transforming growth factor β1 (TGF-β1), both negatively regulating HSC cell cycle activity. In response to stress, fibroblast growth factor 1 (FGF1) secretion of MKs overcomes the inhibitory signal of TGF-β1, thereby stimulating HSC expansion.[53,54]

It is known that BMECs support proliferation and differentiation of myeloid and megakaryocytic progenitors, indicating that megakaryopoiesis might be predominantly taking place in the vascular niche.[18,55,56] However, the exact location of MK maturation, the functional significance of MK migration towards the vascular niche for thrombopoiesis and the exact mechanisms of platelet generation from MKs still remain ill-defined.

1.1.3. Thrombopoiesis and proplatelet formation

Platelets are constantly produced by their BM precursors. A mature MK is thought to release up to 5000 platelets *in vivo*, and recent developments in intravital microscopy allowed real-time visualization of proplatelet formation in the BM of living animals.[29,57,58] Although the precise mechanisms still remain elusive, recent *in vivo* studies provide evidence in favor of the following model of thrombopoiesis. Upon MK maturation and migration, polyploid MKs reside in close proximity to the sinusoidal BMECs, where they form distinct transendothelial pseudopods. These pseudopods or proplatelets consist of a thin cytoplasmic shaft containing a central microtubule bundle and bulbous platelet-sized swellings containing actin.[30,34] The proplatelets pass the endothelial barrier and are shed into the circulation, where the final sizing into hundreds of virtually identical platelets from each single MK takes place, most likely due to shear forces in the blood stream.[40,57] The mechanisms that control platelet generation remain poorly understood, but recent work by Zhang *et al.* revealed that endothelial sphingosine-1-phosphate and its receptor S1pR1 on MKs are critical factors guiding the elongation of proplatelet extensions into the BM sinusoids and inducing platelet

release into the blood stream.[58] During normal physiology, the classical process of Thpo-driven thrombopoiesis via proplatelet formation is sufficient to maintain platelet count, but in response to stress, this mechanism might not be efficient enough. Nishimura *et al.* recently identified a novel mechanism of platelet release by IL-1α induced MK rupture, leading to increased platelet counts during acute platelet needs.[59]

Proplatelet formation requires substantial cytoskeletal rearrangements. Microtubules, which consist of αβ-tubulin dimers, are the key components of the machinery that drives proplatelet elongation.[40,60] In addition, microtubules line the proplatelet shaft and the dynein-dependent sliding of the microtubules enables the transport of organelles and granules from the MK body into the proplatelets.[40,60,61] The branching of existing protrusions and the number of proplatelet tips depends on actin polymerization, which is also a critical regulator of platelet sizing.[62,63]

1.1.3.1. Profilin

The dynamic remodeling of the actin cytoskeleton is required for proplatelet formation and among others, proteins such as Profilin1, Wiskott-Aldrich syndrome protein (WASp), Twinfilin1/2a and cofilin are critical in controlling the cytoskeletal rearrangements.[64] In mammals, four different Profilin isoforms have been identified. Profilin1 is ubiquitously expressed and Profilin2 is predominantly expressed in the brain. Profilin3 and 4 are mainly found in the testis.[65-68] Profilin is a small actin-binding protein (15 kDa) and is capable of binding to monomeric actin (G-actin) in a 1:1 molar ratio and was thought to prevent polymerization of actin into filaments (F-actin). However, more recent research revealed that Profilin functions as a nucleotide exchange factor, inducing the exchange of the low energy ADP-G-actin monomers into ATP-G-actin monomers, which are more capable of polymerization.[65,69] Furthermore, Profilin can promote polymerization by regulating the addition of new monomers to growing actin filaments.[70] Besides its actin-binding capacity, Profilin can also bind to phosphatidylinositides, such as phosphatidyl-inositol-4,5-bisphosphate (PIP$_2$), affecting actin and ligand binding and phospholipase C (PLC) γ1 activity.[71] In addition, the poly-L-proline binding domain in Profilin binds proline-rich regions in different proteins, regulating several processes, such as membrane trafficking, focal contact formation and actin dynamics. Furthermore, Profilin is involved in the regulation of signaling pathways of small Rho-GTPases.[72,73]

1.1.3.2. Transient receptor potential melastatin 7 channel

Besides remodeling of the actin cytoskeleton, its contractility is also required for the structural integrity of the cell and processes like cell adhesion and migration. Non-muscle myosin II A (NMMIIA) is a member of the motor protein superfamily and serves as an actin-binding protein with actin cross-linking and contractile properties, thereby regulating cytoskeletal reorganization and processes requiring cellular reshaping and movement.[74,75] Myosin filaments produce tension on and drive the sliding of the actin filaments. Myosin is regulated by phosphorylation of its light and heavy chains. The heavy chain of myosin II A can be phosphorylated by the transient receptor potential melastatin 7 (TRPM7) channel.[76] The ubiquitously expressed plasma membrane protein TRPM7 consists of a transmembrane ion channel and a cytosolic α-type serine/threonine protein kinase domain. TRPM7 is a constitutively active ion channel, which is highly selective for divalent cations, such as magnesium (Mg^{2+}), calcium (Ca^{2+}) and zinc (Zn^{2+}). TRPM7 plays a central role in Mg^{2+} homeostasis, cell motility, proliferation and differentiation and is critical for early embryonic development.[77] In addition to the regulation of myosin II A via phosphorylation by TRPM7, the intracellular magnesium concentration ($[Mg^{2+}]_i$) also contributes to the actomyosin contractility by modulating the actin-binding affinity of myosin II A.[78] Myosin II A activity is also linked to platelet biogenesis, since its suppression through phosphorylation enables the increase of MK ploidy and proplatelet formation, whereas its re-activation by shear stress leads to the proper sizing of platelets.[79]

1.2. Platelets

Platelets are small anucleate discoid-shaped blood cells with a diameter of 3-4 μm in humans and 1-2 μm in mice and are the smallest and second most abundant cell type in the blood. Platelets are constantly produced by MKs to maintain a normal range of circulating platelets (150 x 10^3 – 400 x 10^3 platelets/μl in humans and ~1,000 x 10^3 platelets/μl in mice). The life span of platelets is restricted to 10 days in humans and 5 days in mice and due to their short life span, platelets are continuously replenished and thus provide a paradigmatic system to study hematopoiesis. Aged, dysfunctional or pre-activated platelets are cleared from the circulation by resident macrophages in the reticuloendothelial system of the spleen and liver.[80]

Platelets play an essential role in hemostasis and thrombosis, but they are also critically involved in several other (patho)physiological processes, including embryonic development, cancer metastasis, wound healing, angiogenesis and maintenance of the vascular integrity during inflammation.[81-83]

Platelets contain different types of organelles and granules, such as mitochondria, glycogen stores, peroxisomes, α- and dense-granules and lysosomes.[28,84] α-granules are the most abundant platelet granules and store platelet adhesion proteins (e.g. fibrinogen, fibronectin, vWF, P-selectin), coagulation factors, chemokines (e.g. PF4), growth factors and glycoproteins (e.g. αIIbβ3). Dense granules are smaller, less abundant and contain many inorganic molecules, such as adenosine diphosphate (ADP), adenosine triphosphate (ATP), Ca^{2+}, thromboxane A2 (TxA_2), polyphosphates, catecholamines and 5-hydroxytryptamine (5-HT). Lysosomes store enzymes that are required for the degradation of carbohydrates, proteins and lipids. In addition, platelets contain the open canalicular system (OCS), the dense tubular system (DTS), an actin-based cytoskeletal network and a peripheral microtubule coil. The OCS consists of plasma membrane invaginations and serves as a membrane reservoir, allowing surface area increase following platelet activation and shape change. The DTS derives from residual endoplasmatic reticulum and is thought to be a Ca^{2+} reservoir.[85-87]

1.3. Platelet activation and thrombus formation

Under normal physiological conditions, most of the circulating platelets never come into contact with components of the ECM. However, at sites of vascular wall damage, for example upon injury or atherosclerotic plaque rupture, thrombogenic components of the ECM become exposed. Subendothelial matrix components, including vWF, fibrillar collagens and laminins, come into contact with the flowing blood, initiating the activation, adhesion and aggregation of platelets and subsequent thrombus formation. This process is essential to seal vessel lesion, minimize blood loss and prevent infection. Under pathological conditions, however, platelet aggregation can lead to uncontrolled thrombus formation, possibly causing arterial occlusion or embolism, leading to acute ischemic disease states, such as myocardial infarction or stroke. These pathologies are currently the primary causes of death and disability in the industrialized world.[88] Platelet activation is a tightly regulated multistep process and can be divided into three major steps: (1) tethering and platelet adhesion to the exposed ECM; (2) platelet activation and granule release and (3) firm adhesion, platelet aggregation and thrombus growth (Figure 3).[89] Tethering of the platelets occurs under intermediate or high shear conditions (1,000-10,000 s^{-1}), which are found in arterioles or stenosed arteries. The initial contact of circulating platelets to exposed components of the ECM is facilitated by the interaction of the glycoprotein (GP) Ib-V-IX receptor complex with vWF immobilized on collagen.[90-93] This transient and weak interaction leads to rapid deceleration and 'rolling' of the circulating platelets and enables the interaction of the ECM component collagen with the central activating platelet collagen receptor, GPVI.[94-96]
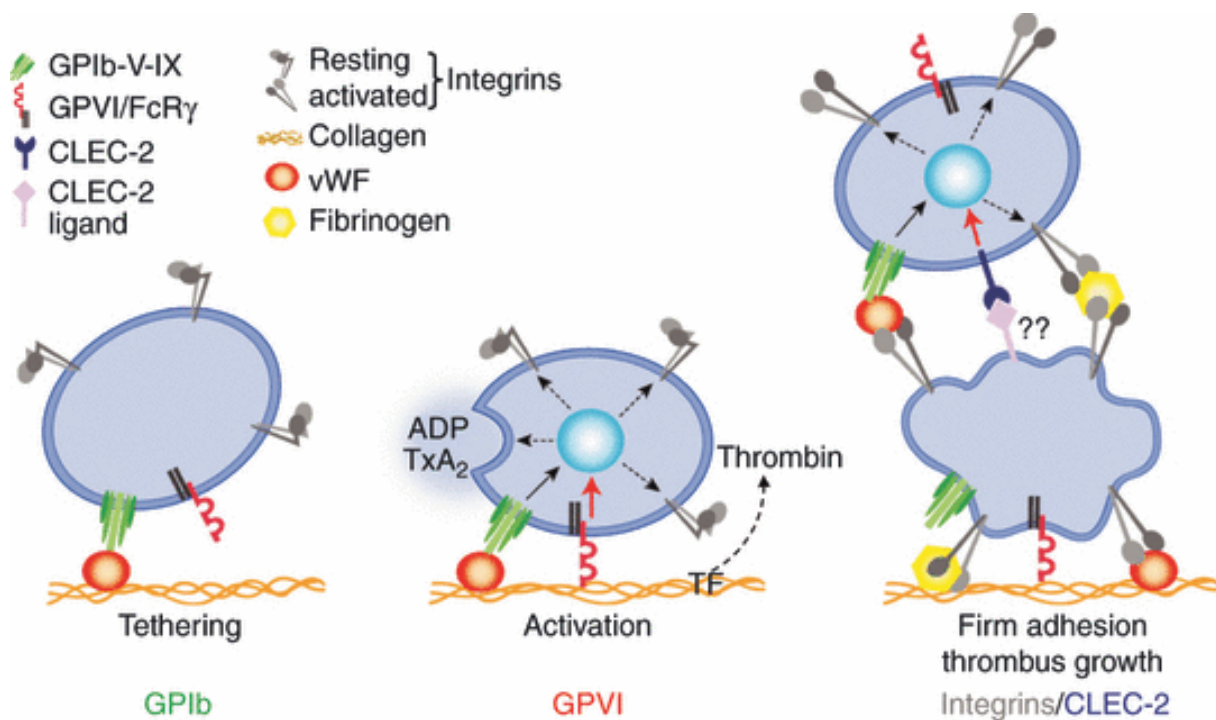
Figure 3. Multistep process of platelet adhesion, activation and thrombus formation. Upon vascular wall injury, tethering of circulating platelets to exposed components of the ECM is facilitated by the GPIb-vWF interaction. This enables the binding of GPVI to collagen, leading to intracellular signaling and the release of second wave mediators, like ADP and TxA$_2$. Exposed TF triggers thrombin generation, which contributes to platelet activation. The cellular signaling events induce the conversion of integrins to a high-affinity state, resulting in firm platelet adhesion and thrombus growth. From: Nieswandt *et al.*, 2011[97]

Cross-linking of GPVI by collagen induces an intracellular signaling cascade, culminating in an increase in intracellular calcium levels ([Ca^{2+}]$_i$), surface exposure of negatively charged procoagulant phosphatidylserine (PS), cytoskeletal rearrangements and the mobilization of α- and dense granules, leading to the release of second wave mediators, including ADP and TxA$_2$.[97,98] In addition, exposed tissue factor (TF) triggers thrombin generation (extrinsic coagulation pathway). This is also induced by the release of polyphosphates from the dense granules, leading to the activation of factor XII and the intrinsic pathway of coagulation, culminating in the cleavage of the proenzyme prothrombin (factor II) to thrombin.[99] Thrombin is a potent platelet activator and converts fibrinogen to fibrin. The soluble agonists ADP, TxA$_2$ and thrombin bind to and activate G protein-coupled receptors (GPCRs) (G$_q$, G$_{12/13}$ and G$_i$), inducing platelet activation and additional recruitment of platelets to the growing thrombus.[100] Finally, firm adhesion, platelet aggregation and thrombus growth is mediated by the conformational change of integrin adhesion receptors. The extra- and intracellular signaling events induce the conversion of the integrins from a low (inactive) to a high (active) affinity state (inside-out signaling), allowing the interaction of the activated integrins with their ligands (outside-in signaling).[89,101] The major platelet integrin, αIIbβ3 (GPIIb/IIIa; CD41), is able to bind to fibrinogen or exposed ECM components, such as collagen-bound vWF,

fibronectin and vitronectin. Platelet binding to fibrinogen enables bridging of adjacent platelets, inducing the growth and formation of a stable thrombus. Integrin $\alpha IIb\beta3$ binding to ECM components leads to firm platelet adhesion. This is further mediated by binding of high-affinity $\beta1$- and $\beta3$-integrins to collagen ($\alpha2\beta1$), fibronectin ($\alpha5\beta1$), laminin ($\alpha6\beta1$) and vitronectin ($\alpha v\beta3$).[89,102,103] The activation of platelets also results in the rearrangement of the actin and tubulin cytoskeleton, leading to the formation of membrane protrusions, such as filopodia and lamellipodia.[104]

Platelet activation is mediated by two major signaling pathways (Figure 4): signaling via the GPCRs or the (hem)immunoreceptor tyrosine-based activation motif (ITAM)-bearing receptors, which are described in more detail in section 1.3.1 and 1.3.2. Both signaling pathways culminate in the activation of PLC isoforms, leading to hydrolysis of PIP_2 to inositol-1,4,5-trisphosphate (IP_3) and diacyl-glycerol (DAG).[105] IP_3 binds to the IP_3 receptor on the endoplasmatic reticulum membrane, inducing Ca^{2+} release from the intracellular stores. Subsequently, the Ca^{2+} store content decreases, stimulating the Ca^{2+} channels in the plasma membrane to open, a process called store-operated Ca^{2+} entry (SOCE), which is mediated by stromal interaction molecule 1 (STIM1) and Ca^{2+} release-activated calcium channel protein 1 (Orai1).[106] This results in increased $[Ca^{2+}]_i$, leading to integrin activation, platelet shape change, granule secretion and platelet aggregation.[105]

1.3.1. G protein-coupled receptor signaling in platelets

Soluble mediators, like ADP, TxA_2 and thrombin, signal through GPCRs (Figure 4).[100] ADP binds to the $P2Y_1$ and $P2Y_{12}$ receptors that activate the heterotrimeric G proteins G_q and G_i, respectively. TxA_2 stimulates the TxA_2 receptor (TP) activating G_q and thrombin activates the protease-activated receptor (PAR) 1/4 and PAR 3/4 on human and mouse platelets, respectively, which mainly activate G_q and $G_{12/13}$.[100,107] Stimulation of G_q leads to the activation of the PLCβ isoforms, inducing hydrolysis of PIP_2 to IP_3 and DAG, ultimately leading to integrin activation and granule secretion. Activation of the $P2Y_{12}$ receptor stimulates G_i, which inhibits adenylyl cyclase (AC) activity and activates phosphatidylinositide 3-kinase (PI3K). PI3K hydrolyses PIP_2 to PIP_3, thereby activating Akt, which ultimately leads to integrin activation. G_z is a member of the G_i protein subfamily and can be found coupled to the epinephrine receptor, the alpha-2A adrenergic receptor (α_{2A}). Similar to G_i, G_z inhibits AC activity. The activation of $G_{12/13}$ stimulates the Rho-guanine nucleotide-exchange factors (GEFs). Rho GTPases cycle between a guanosine-5'-triphosphate (GTP)-bound active and a guanosine diphosphate (GDP)-bound inactive state. Rho-GEFs stimulate the exchange of GDP to GTP and thereby activate GTPases of the Rho family.[100,105]
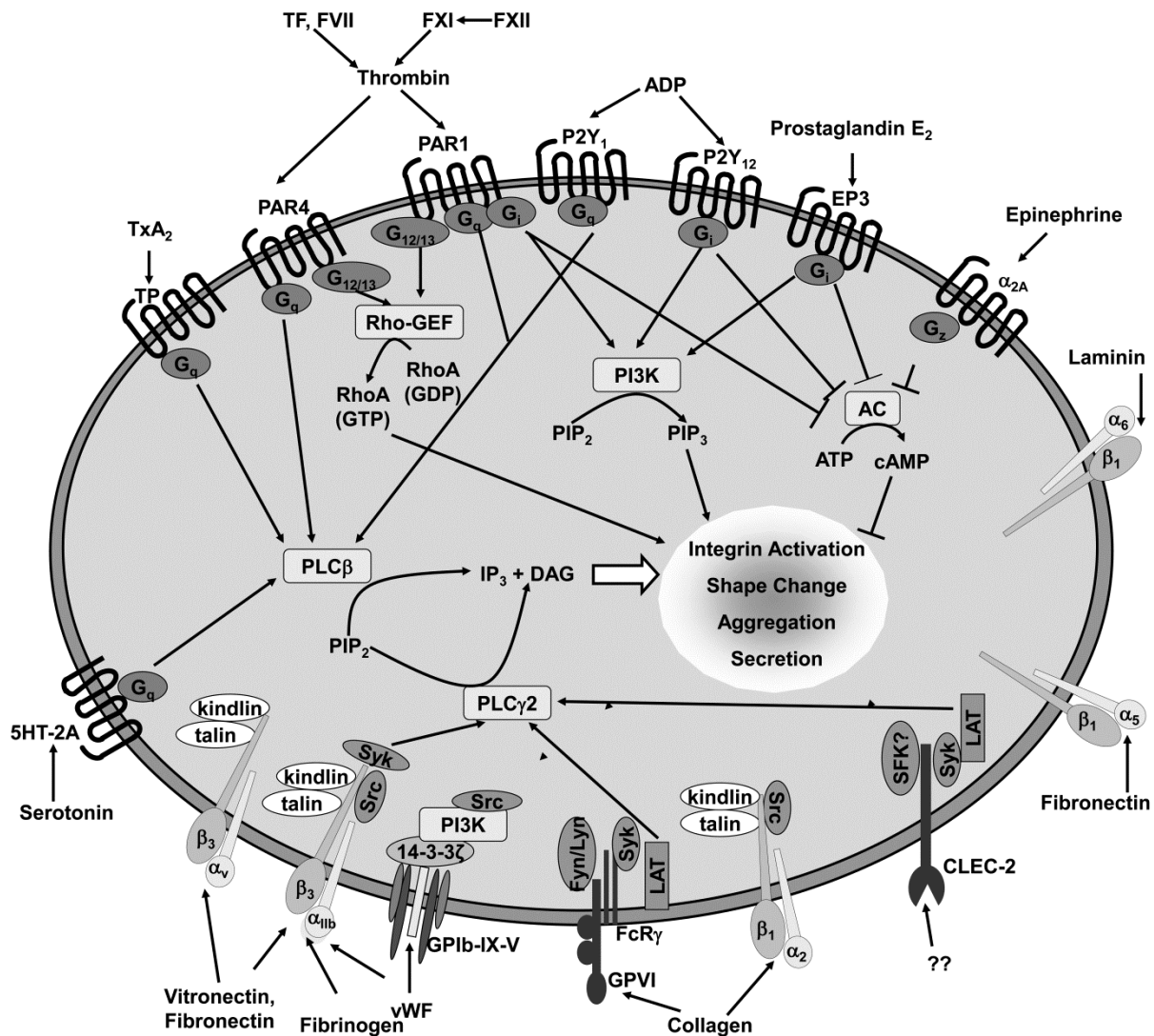
Figure 4. Major signaling pathways in platelets. Soluble agonists, including ADP, TxA$_2$ and thrombin, signal through GPCRs and activate downstream effectors, culminating in the activation of PLCβ. Platelet activating receptors, including GPVI, CLEC-2 and active integrins induce PLCγ2 activation upon ligand binding. The activation of the PLC isoforms finally leads to enhanced integrin activation, platelet shape change, aggregation and secretion. From: Stegner and Nieswandt, 2011[105]

1.3.1.1. Ras homolog gene family, member A

Small GTPases of the Rho family are known to be critical regulators of cytoskeletal rearrangements in platelets.[108,109] Ras homolog gene family, member A (RhoA) regulates the actin cytoskeleton in the formation of stress fibers and mediates platelet shape change from discoid to spherical following activation.[110,111] The Rho-GEFs activate RhoA, which binds to and activates Rho-associated protein kinase (ROCK), leading to ROCK phosphorylation and inhibition of the MLC phosphatase, resulting in increased phosphorylation of the myosin light chain (MLC), inducing actin remodeling.[110,112] Studies in MK- and platelet-specific RhoA-deficient mice showed that RhoA signaling is essential for platelet shape change and

contributes to integrin αIIbβ3 activation, granule release, clot retraction *in vitro* and arterial thrombus formation and stability *in vivo*.[111] Although Rho GTPases, such as RhoA are known to be critical regulators of cytoskeletal rearrangements in platelets, little is known about their specific roles during platelet biogenesis. The moderate thrombocytopenia observed in RhoA-deficient mice suggests that RhoA is necessary for platelet production. Recent studies revealed a minor shift to higher mean ploidy levels and slightly increased numbers of BM MKs in MK-specific RhoA-deficient mice, but the role of RhoA in platelet biogenesis remains poorly understood.[111,113]

1.3.2. (Hem)immunoreceptor tyrosine-based activation motif signaling in platelets

The second major signaling pathway in platelets involves signaling via the (hem)ITAM-bearing receptors (Figure 5). An ITAM is a highly conserved sequence of four amino acids, which is repeated twice in the cytoplasmic tail of several hematopoietic immunoglobulin (Ig) receptors, including Fc receptors (FcR), T and B cell receptors (TCR, BCR) and C-type lectin-like receptors. The motif is defined by the presence of two YxxL/I motifs separated by 6-12 amino acids ($YxxL/Ix_{(6-12)}YxxL/I$).[114] Human platelets express three ITAM-bearing receptors: the Fc receptor FcγRIIA, GPVI and the hemITAM C-type lectin-like receptor 2 (CLEC-2), whereas mouse platelets only express GPVI and CLEC-2. FcγRIIA signals through an ITAM in its cytoplasmic tail and is critically involved in immune-mediated thrombocytopenia and thrombosis, but also enhances integrin outside-in signaling via spleen tyrosine kinase (Syk).[81,115] GPVI signals via the non-covalently associated ITAM-bearing FcR γ-chain. Upon ligand-induced receptor activation of GPVI, the tyrosine residues in the ITAM become phosphorylated by Src family kinases (SFKs), such as Fyn and Lyn, inducing the recruitment and activation of tandem Src homology (SH)2 domain-containing Syk.[81,98] In contrast to classical ITAM signaling, recent studies suggest that Syk itself phosphorylates the hemITAM within CLEC-2, whereas the SFKs together with Syk are involved in the regulation of downstream signaling.[116] The downstream signaling cascade involves a large number of adaptor and effector proteins, such as the linker for activated T cells (LAT), the SH2 domain-containing leukocyte protein of 76 kDa (SLP-76) and growth factor receptor-bound protein 2 (Grb2), ultimately leading to the activation of effector enzymes, such as PI3K and PLCγ2.[81,117] Subsequently, Ca^{2+} mobilization, integrin activation and granule secretion are induced.
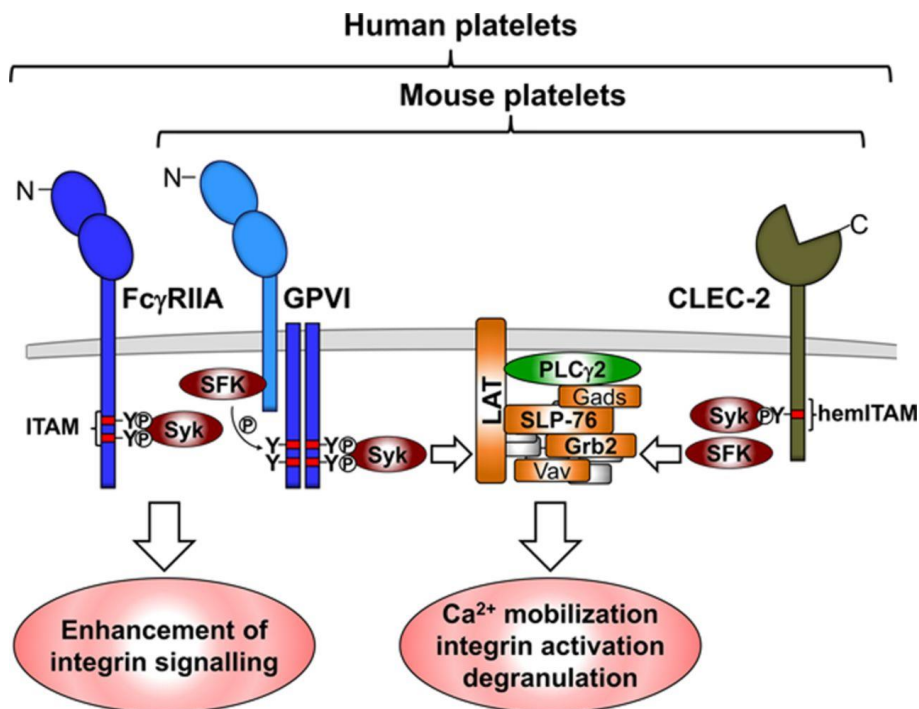
Figure 5. (hem)ITAM signaling in platelets. The Fc receptor FcγRIIA is expressed on human, but not on mouse platelets and signals through an ITAM, thereby enhancing integrin outside-in signaling via Syk. GPVI is non-covalently associated with the ITAM-bearing FcR γ-chain. Ligand-induced receptor activation initiates phosphorylation of the tyrosine residues in the ITAM by SFKs, leading to the recruitment and activation of Syk. Syk initiates a downstream signaling cascade that involves a large number of adaptor and effector proteins, such as LAT, SLP-76 and Grb2, culminating in the activation of PLCγ2. CLEC-2 contains one copy of the YxxL motif (hemITAM), which becomes phosphorylated by Syk. Syk together with the SFKs regulate a downstream signaling cascade similar to that found downstream of GPVI, leading to Ca²⁺ mobilization, integrin activation and granule secretion. From: Stegner *et al.*, 2014[81]

1.3.2.1. Glycoprotein VI

Platelets express several receptors that are able to interact with collagens, such as $\alpha2\beta1$ and GPVI. Integrin $\alpha2\beta1$ mainly mediates adhesion, whereas GPVI is the central and indispensable activating collagen receptor on the platelet surface.[94,117] GPVI is a 62 kDa type I transmembrane protein that belongs to the Ig superfamily of surface receptors and is exclusively expressed on MKs and platelets.[118] The extracellular part of GPVI consists of two IgG domains bearing the collagen binding site, followed by a mucin-like region containing O-glycosylation sites, a transmembrane region and a cytoplasmic tail.[94,98] The cytoplasmic tail is short, comprising only 51 amino acids in human and 27 amino acids in mice and contains a calmodulin binding motif and a proline-rich region, which is recognized by the SH3 domain of the SFKs Fyn and Lyn.[119,120]

The transmembrane region of GPVI contains a positively charged arginine that is essential for the non-covalent association with the FcR γ-chain. The FcR γ-chain is required for initiation of downstream signaling and serves as the signal transducing subunit of the

GPVI/FcR γ-chain complex.[94] Each FcR γ-chain contains one ITAM and is expressed as a covalently linked homodimer. One GPVI molecule associates with one FcR γ-chain dimer and only the dimeric form of GPVI binds collagen with a high affinity.[117,121] GPVI specifically recognizes the glycine-proline-hydroxyproline (GPO) repeats within collagen.[94] Platelet activation via GPVI can also be induced by the specific agonists collagen-related peptide (CRP), which is composed of repeated GPO motifs, and the snake venom toxin convulxin (CVX), which is capable of clustering four GPVI proteins and therefore a strong agonist.[94] Ligand-induced crosslinking of GPVI leads to phosphorylation of the FcRγ-chain ITAM, inducing downstream signaling and finally activation of PI3K and PLCγ2.[122] Signaling through the GPVI/FcR γ-chain is, among others, negatively regulated by immunoreceptor tyrosine-based inhibition motif (ITIM) containing receptors, including platelet endothelial cell adhesion molecule 1 (PECAM-1), Carcinoembryonic antigen-related cell adhesion molecule 1 (CEACAM1) and G6b-B.[117]

Since GPVI is a MK- and platelet specific receptor, it may represent an attractive potential target for antithrombotic therapy. Patients with a congenital deficiency of GPVI or autoantibody-mediated GPVI deficiency only suffered from a mild bleeding disorder, but platelet aggregation and thrombus formation *ex vivo* on collagen were impaired.[98,123] In experimental models, the deficiency, blockade or immunodepletion of GPVI provide a strong protection from arterial thrombosis without or only moderately affecting hemostasis.[98,124] Besides its crucial role in occlusive arterial thrombosis, GPVI has been identified as a critical modulator of several thrombo-inflammatory disease states, including ischemic stroke, loss of vascular integrity at sites of inflammation, rheumatoid arthritis, atheroprogression and tumor metastasis.[125-130]

Different possibilities exist to target GPVI, including the direct blockade of the ligand binding site on GPVI, immunodepletion or downregulation of the GPVI receptor using monoclonal antibodies and targeting of the GPVI signaling pathway.[98] Receptor blockade can be achieved by using a F(ab) fragment of an anti-GPVI antibody.[131] *In vivo* administration of monoclonal anti-GPVI antibodies (JAQ1-3) induces specific and irreversible removal of the receptor from the surface of circulating platelets, leading to a knockout-like phenotype.[132-134] To induce GPVI downregulation, two principal pathways exist in platelets, namely ectodomain shedding by the metalloproteinases *A disintegrin and metalloprotease* (ADAM)10 and ADAM17, generating a soluble GPVI fragment and a transmembrane remnant, and internalization/degradation of the GPVI receptor.[134-137] Both processes require signaling through the FcR γ-chain ITAM.[136] Ectodomain shedding appears to be the predominant mechanism of antibody-induced GPVI loss, however, downregulation *in vivo* seems to involve another sheddase, since antibody-induced shedding of GPVI still occurs in

mice lacking ADAM10 and ADAM17.[135,137] To reduce GPVI activity, molecules in the downstream signaling pathway, for example the kinase Syk, could be targeted. Several Syk inhibitors have been developed and clinically used[138-145] and Syk might be a potential antithrombotic target.

1.3.2.2. C-type lectin-like receptor 2

CLEC-2 plays a crucial role in different (patho)physiological processes, such as thrombosis and hemostasis, tumor metastasis, maintenance of the integrity of high endothelial venules, maintenance of the vascular integrity during inflammation, lymph node development and blood/lymph vessel separation.[146-149]

CLEC-2 is a 32 kDa type II transmembrane protein, that is highly expressed on MKs and platelets and, in addition, at lower levels on different immune cells and liver sinusoidal cells.[117,150] CLEC-2 was identified as the receptor for the snake venom toxin rhodocytin (Rhod) and the glycoprotein podoplanin, the only known physiological ligand of CLEC-2.[151,152] Podoplanin is expressed in different tissues, including lymphatic endothelial cells, type 1 lung alveolar cells, kidney podocytes, lymph node stromal cells and is also expressed on tumor cells.[151,153] However, podoplanin is not expressed on platelets and vascular endothelial cells. Mice lacking either CLEC-2 or podoplanin, fail to separate blood and lymphatic vessels during development, leading to embryonic or neonatal lethality associated with blood-filled lymphatics and severe edema formation.[154-157] The interaction of podoplanin with CLEC-2 induces platelet activation and aggregation leading to closing of the blood-lymphatic shunts. Blood-filled lymphatics can also be found in mice lacking key (hem)ITAM-signaling molecules, such as Syk, SLP-76 and PLCγ2, but the exact mechanism in separation of blood and lymphatic vessels remains poorly understood.[147,154,158]

CLEC-2 contains a conserved YxxL motif in its cytoplasmic tail, which mediates downstream signaling. This motif is similar to the ITAM, however, only one copy of the sequence is present within the protein, therefore it is called a hemITAM.[151] CLEC-2 is expressed as a homodimer on the platelet surface and upon ligand binding, clustering of the receptor brings together two hemITAM domains, which, upon phosphorylation, serve as a binding site for the two SH2 domains of Syk.[151,159] The signaling pathway downstream of CLEC-2 resembles the GPVI signaling pathway and involves similar molecules, such as Syk, SFKs, LAT, SLP-76 and PLCγ2.[117,151] However, recent studies suggest a difference in the phosphorylation events and recruitment of SFKs and Syk. Following GPVI receptor activation, phosphorylation of the ITAM on the FcR γ-chain is mediated by the SFKs Fyn and Lyn, leading to the recruitment and activation of Syk, whereas Syk itself phosphorylates the hemITAM within CLEC-2, while the SFKs are involved in the regulation of downstream signaling.[116]

CLEC-2 also plays an important role in the stabilization of platelet thrombi and studies on the role of CLEC-2 in thrombosis and hemostasis revealed the receptor as a potential target for antithrombotic therapy.[155,160] Immunodepletion of CLEC-2 from the surface of circulating platelets or CLEC-2 deficiency in mice led to impaired aggregate formation *in vitro* and abolished thrombus formation *in vivo,* while bleeding times are only moderately prolonged.[155,160] However, the combined deficiency of CLEC-2 and GPVI resulted in a dramatic hemostatic defect and inflammation-induced hemorrhage, demonstrating a functional redundancy of these two receptors.[128,133] Therefore, the suitability of CLEC-2 as a safe antithrombotic therapy target needs to be reconsidered. Since podoplanin is not expressed in platelets and vascular endothelial cells, the mechanism that contributes to CLEC-2 dependent thrombus stabilization, may involve a yet unidentified CLEC-2 ligand.[160]

Similar to GPVI, CLEC-2 can be immunodepleted from the surface of platelets by a monoclonal anti-CLEC-2 antibody (INU1), resulting in a knockout-like phentotype.[133,160,161] INU1 induces receptor downregulation and a severe, but transient thrombocytopenia.[133,160,161] The INU1-induced receptor downregulation occurs through SFK-dependent receptor internalization *in vitro* and *in vivo*, whereas the thrombocytopenia is Syk-dependent. This indicates that CLEC-2 downregulation occurs through receptor internalization and this mechanism can be uncoupled from the associated antibody-induced thrombocytopenia.[161]

1.3.2.3. Spleen tyrosine kinase

The adaptive recognition of self and foreign antigens is mediated by the classical immunoreceptors, such as the BCR, TCR and FcR. These receptors or their associated transmembrane adaptors contain and signal through ITAMs, which become phosphorylated during receptor activation, primarily by SFKs. The phosphorylation of the tyrosine residues induces the recruitment of the tandem SH2 domain-containing Syk (BCR and FcR) or the related protein ζ-chain-associated protein kinase of 70 kDa (Zap-70) (TCR), initiating a downstream signaling cascade. In addition to the immunoreceptors, Syk is also activated by GPVI, C-type lectins and integrin receptors.[162-165] The downstream signaling of Syk or Zap-70 involves molecules, such as Vav proteins, PLCγ isoforms, PI3Ks and SLP family members. These molecules induce activation of other downstream processes, including PKC signaling, Rho-mediated cytoskeletal rearrangements, reactive oxygen species (ROS) production and transcriptional regulation.[162]

Syk plays a crucial role in adaptive immune receptor signaling, but is also involved in other (patho)physiological processes, including cellular adhesion, innate pathogen recognition, damage recognition, bone metabolism, platelet activation, vascular development, allergy, autoimmune diseases and hematological malignancies.[162]

Syk is highly expressed in hematopoietic cells, but it is also expressed in other tissues, such as fibroblasts, epithelial cells, breast tissue, neuronal cells and vascular endothelial cells.[166] Syk is a 72 kDa multiple-domain cytoplasmic tyrosine kinase that contains two tandem SH2 domains and a carboxy-terminal tyrosine kinase domain. The two SH2 domains are linked by interdomain A and the C-terminal SH2 domain and the kinase domain are linked by interdomain B. Syk-B, an alternatively spliced form of Syk lacks 23 amino acids of interdomain B, but the generation of this isoform is poorly understood.[162,167] In the resting state, the kinase domain of Syk is inactive or autoinhibited, but upon binding of the SH2 domains to the phosphorylated ITAMs, the domain can be activated. In addition, the tyrosine residues in interdomain A and B can become phosphorylated, inducing kinase activation. The dual activation of Syk provides rapid activation by ITAM binding and sustained activation by autophosphorylation, which could even occur in the absence of binding to phosphorylated ITAMs. The phosphorylation of the tyrosine residues in Syk allows binding of different molecules, resulting in downstream signaling or the degradation of Syk.[162] Its function can be negatively regulated by SH2 domain-containing protein tyrosine phosphatase 1 (SHP1) and the E3 ubiquitin ligase Casitas B-lineage lymphoma (CBL).[168,169] Syk deficiency in mice leads to perinatal lethality and blocked B-cell development, leading to the lack of mature B cells.[170,171] Syk plays an important role in the conversion of pro-B cells into pre-B cells and is required for the maturation of transitional B cells.[170,172] Syk also has a critical role in pre-TCR signaling, FcεRI signaling in mast cells and FcγR signaling in neutrophils and macrophages.[173-176]

Due to its central role in immunological processes, several Syk inhibitors have been developed and clinically used, including R112[143], PRT-060318[145], the prodrug fostamatinib (R788)[138,139] and its active metabolite R406.[140] However, these inhibitors have a rather limited specificity and adverse effects.[177] Recently, entospletinib (GS-9973), a more selective and orally efficacious Syk inhibitor was developed[141] and phase II trials are underway to assess its effectiveness in treating leukemia.[178] Syk inhibitors have been used in the treatment of allergy,[143] B cell malignancies,[138] heparin-induced thrombocytopenia[145] and autoimmune diseases like rheumatoid arthritis[139] and immune thrombocytopenic purpura.[144]

Several platelet functions rely on Syk signaling, including GPVI and CLEC-2 receptor signaling. In addition, Syk has been proposed to contribute to outside-in signaling of platelet integrin αIIbβ3.[179-181] Studies using Syk inhibitors or Syk-deficient mice (radiation chimeras) provide minimal evidence for a role for Syk in thrombosis and hemostasis.[145,182,183] Thrombus formation *ex vivo* and *in vivo* was strongly inhibited, without affecting hemostasis, therefore Syk could be a potential antithrombotic target.

1.3.2.4. Z-chain-associated protein 70

As mentioned in section 1.3.2.3, Zap-70 is a downstream mediator of the immunoreceptor TCR and is mainly expressed in T cells and natural killer (NK) cells.[184] Like Syk, Zap-70 contains two tandem SH2 domains and a carboxy-terminal tyrosine kinase domain. The domains are connected by two linker regions, interdomain A and B. In comparison to Syk, Zap-70 lacks 11 amino acids in the interdomain B and has a much lower intrinsic kinase activity.[162] It is thought that due to the shorter linker region, the structure of Zap-70 is less flexible and therefore, it would be more difficult to bridge two hemITAMS or to bind phosphorylated tyrosine residues with a bigger distance between them.[185,186] Following TCR engagement, the ITAMs present in the cytoplasmic tails of the TCR ζ homodimer and CD3 become phosphorylated by SFKs Lck or Fyn. This leads to the recruitment of the SH2 domain-containing Zap-70 and disassembly of the autoinhibited, inactive conformation, allowing the kinase domain to adopt an active confirmation.[187,188] Subsequently, Lck or autophosphorylation of the tyrosine residues activate the kinase domain and Zap-70 activates the downstream targets LAT and SLP-76, leading to T cell activation. In addition, Zap-70 can recruit additional signaling proteins, such as CBL, Vav, Lck and PLCγ to the stimulated TCR complex by interaction with the phosphorylated tyrosine residues.[184] In contrast to Syk, Zap-70 is not able to phosphorylate the ITAM residues itself and is therefore more dependent on SFKs for its activation and the unique ability to enhance the activation of mitogen-activated protein kinase (MAPK) p38.[167,189] Zap-70 deficient humans and mice fail to produce functional T cells and suffer from severe combined immunodeficiency (SCID).[190-192] Zap-70 plays an important role in thymocyte development and pre-TCR signaling, specifically during thymic selection at the double negative and double positive stage.[171,192,193] In addition, Zap-70 is expressed throughout B cell development and participates in pre-BCR signaling, and its expression is associated with increased BCR signaling in B-cell chronic lymphocyte leukemia.[184,194] Furthermore, decreased function of Zap-70 is associated with autoimmune disease.[195]

1.4. Imaging modalities

Over the last few decades, the processes of megakaryopoiesis and thrombopoiesis have been studied intensively, but mainly *in vitro* using cultured MKs or *ex vivo* using BM explants and histological sections of the BM, since *in vivo* investigations are complicated by the anatomic inaccessibility of the BM. However, to further understand these processes, visualization of the localization and morphology of MKs as well as the generation of platelets within the intact BM *ex vivo* and real-time *in vivo* would be of great benefit. Recent developments in imaging methods enable us to observe dynamic cellular events *in vivo* using

multiphoton intravital microscopy (MP-IVM) and to observe the intact three-dimensional (3D) structure of different tissues *ex vivo* using light-sheet fluorescence microscopy (LSFM).

1.4.1. Multiphoton intravital microscopy

IVM enables the microscopic imaging of a living animal and combining this method with MP imaging allows us to visualize and analyze the murine BM real-time and *in vivo*. Mazo *et al.* described an IVM technique to study physiologically perfused murine BM microvessels using fluorescence microscopy and characterized the anatomy of the skull BM microvasculature.[196] The flat bones forming the calvaria of the murine skull contain BM. Imaging of the BM in the frontoparietal skull without surgical manipulation of the bone is achievable, since the thin layer of bone covering the BM cavities is sufficiently transparent.[196] However, light scattering, due to refractive index mismatches in heterogeneous tissues, has hampered imaging within living tissues or thick samples using fluorescence microscopy. Light scattering leads to the degradation of resolution and contrast with increasing tissue depth and high resolution imaging eventually becomes impossible. Confocal microscopy improves the image quality, but also has its limitations, since excitation of the sample often leads to photodestruction of the fluorophore (photobleaching) or photodynamic damage to the specimen (photodamage). These drawbacks can be evaded by the use of MP microscopy. In 1931, Maria Göppert-Mayer first predicted the possibility of MP excitation, but it was only after the invention of the laser, that it was experimentally confirmed.[197] A seminal paper by Denk *et al.* showed the application of two-photon excitation to laser scanning microscopy and the capability of MP microscopy for biology.[198,199] The key difference between confocal microscopy and MP microscopy is the excitation of the fluorescent molecules. In one photon excitation, used in confocal microscopy, a laser with a short wavelength (high energy) can excite or energize electrons (Figure 6). An electron of, for example, a fluorescent molecule then absorbs a single photon of the excitation light. This raises the energy level of the electron to an excited state (S1). During the excitation period, some of the energy is lost and the remaining energy is emitted as a photon. The energy level of the electron falls back to the lowest-energy state, the ground state (S0). The emitted photon carries less energy and has a longer wavelength. In MP excitation, a femtosecond pulsed mode-locked laser with a longer wavelength is used. The short pulses of the laser induce the packing of available excitation photons into short temporal intervals. This increases the probability for a fluorescent molecule to simultaneously absorb two or more long wavelength photons (low energy), thus combining the energy of two photons to reach the excited state (S1) (Figure 6).[198,199] Subsequently, fluorescence is only generated in the focal plane, where the light intensity is high, allowing intrinsic optical sectioning of the specimen. A detector pinhole is not required, since all fluorescence photons contribute to the signal and fluorescence from off-focus locations does not need to be

rejected.[199] The advantages of MP microscopy compared to confocal microscopy are reduced photobleaching and photodamage and, due to the use of longer excitation wavelengths, an increased penetration depth. This allows imaging of thick samples and long term observations *in vivo*.[199]
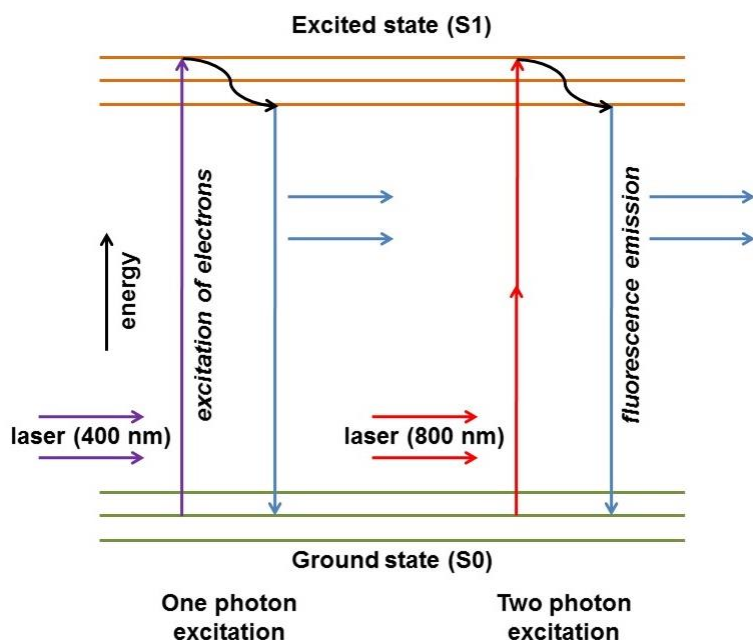
Figure 6. Jablonski diagram illustrating one photon and two photon excitation. One photon excitation occurs upon excitation of electrons by a laser with a short wavelength (high energy), leading to the absorption of a single photon. Two photon excitation occurs through the absorption of two lower energy photons. Using a femtosecond pulsed mode-locked laser, available excitation photons are packed into short temporal intervals, increasing the probability for a fluorescent molecule to simultaneously absorb two long wavelength photons (low energy). The subsequent fluorescence emission is the same for both processes.

It is of our interest to study thrombopoiesis and visualize and analyze the murine BM real-time and *in vivo*. Junt *et al.* previously demonstrated the dynamic visualization of thrombopoiesis within the BM using MP-IVM.[57] *In vivo*, they were able to identify MKs extending proplatelet-like protrusions into the microvessels of the BM, which were released in the blood stream, most likely due to shear forces, and serve as an intravascular platelet source.[57] Other, more recent publications confirm that MP-IVM is an insightful tool for studying thrombopoiesis.[58,59]

1.4.2. Light-sheet fluorescence microscopy

Although MP-IVM allows imaging of thick specimens and *in vivo* imaging, it does have two main limitations, namely a relatively small imaging window and a limited penetration depth of approximately 300 µm to 500 µm. LSFM, also known as selective plane illumination microscopy (SPIM), enables the visualization of large tissue specimens in 3D with a subcellular resolution, a faster acquisition time, lower signal-to-noise ratio and lower photobleaching and photodamage effects in comparison to MP microscopy.[200,201] In 1903, Siedentopf and Zsigmondy, described the first, simple version of a LSFM using sunlight to observe gold particles.[201] However, it took until 1993 for Voie *et al.* to develop the orthogonal-

plane fluorescence optical sectioning (OPFOS) and to image whole fluorophore-stained and cleared cochleas.[202] A seminal paper by Huisken *et al.* accelerated the development and use of LSFM. They were able to visualize embryogenesis in *Drosophila melanogaster in vivo*, thereby showing that LSFM is a useful method for imaging large, living biological specimens.[203] Dodt *et al.* further improved image quality by adding dual-sided illumination to LSFM, making the illumination of large specimens such as the brain more uniform throughout the specimen.[204] LSFM uses a thin sheet of light to illuminate and optically section the transparent specimen, thereby generating sections that are suitable for 3D reconstruction of the whole tissue (Figure 7). The focal point of the light sheet is positioned within the specimen chamber, which contains either a physiological solution or a clearing solution. The specimen is attached to a glass rod and is placed at the intersection of the focal point of the light sheet and the focal plane of the detecting objective, where the fluorescence emission is detected orthogonally to the illumination pathway. The light sheet excites fluorescence in the specimen, which is collected by the detection optics and projected onto a camera. To obtain the 3D structure, the sample is moved through the light sheet in small increments, acquiring a stack of optical sections.[200,201]
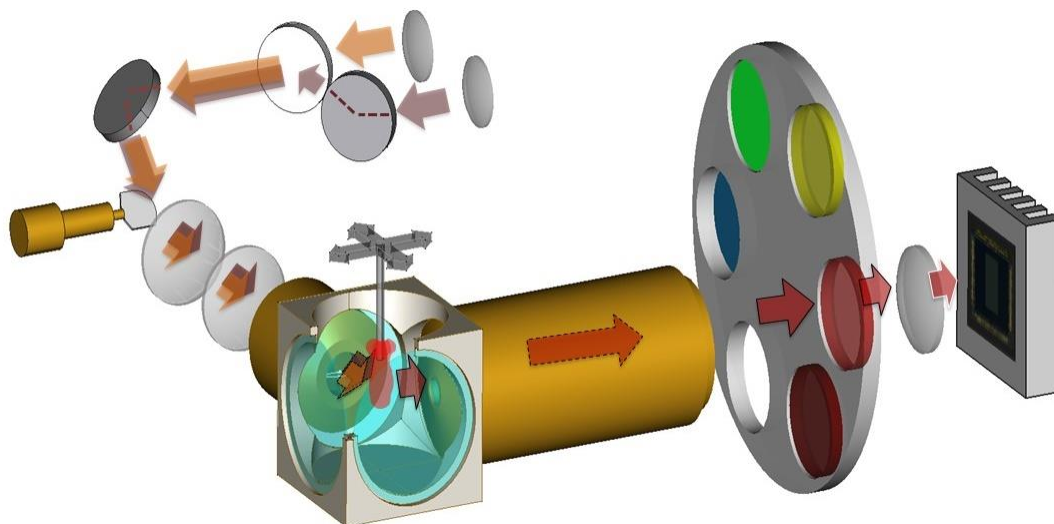
Figure 7. Schematic overview of a custom-built light-sheet fluorescence microscope. A thin sheet of light is generated (arrows), illuminating the sample (red) from one side. The focal plane of the light sheet is positioned within the clearing solution-containing specimen chamber. The specimen is attached to a glass rod and placed at the intersection of the excitation and detection pathway. The fluorescence emission is detected orthogonally to the illumination pathway and projected onto a camera. Image courtesy of Katrin G. Heinze.

The imaging process is mainly conducted *ex vivo*, since most samples need to undergo a clearing process to become transparent to allow penetration of the laser light sheet. Clearing is achieved by immersing the specimen in a solution with the same refractive index as protein. By matching the refractive indices, light is not scattered and, when no absorption

occurs, the specimen turns transparent. Tissue clearing methods were already used a century ago to study the anatomy of the heart and have been developed since, mainly for soft tissues, such as embryonic tissue and brain.[204] In general, tissue is dehydrated and subsequently immersed in an optical clearing solution, such as glucose, glycerol, benzyl alcohol benzyl benzoate (BABB or Murray's clear) or dibenzyl ether (DBE).[205,206] However, dehydration and clearing of tissues expressing fluorescent proteins, such as green fluorescent protein (GFP), degraded the fluorescent signal, thereby preventing its detection. Therefore, to preserve fluorescent signals, new clearing agents have recently been developed, such as 3DISCO, CLARITY and Sca*l*eS.[205-207]

2. Aim of the study

In order to understand the regulatory mechanisms of hematopoiesis, it is important to determine the spatiotemporal organization of blood cell precursors within the BM and their interaction with the BM microenvironment. Therefore, the major aim of this thesis was the establishment of imaging modalities to visualize these cellular processes *in vitro* and *in vivo*.

Megakaryopoiesis and thrombopoiesis have been studied intensively, but the exact mechanisms that control platelet generation from MKs remain poorly understood. Recent developments in IVM enable us to study thrombopoiesis and proplatelet formation in the murine BM real-time and *in vivo*. The first aim of this thesis was to establish MP-IVM to study thrombopoiesis and proplatelet formation and to identify the role of Profilin1, TRPM7 and RhoA in thrombopoiesis *in vivo* using MP-IVM.

Currently, it is thought that blood cell precursors, such as MKs, migrate from the endosteal niche towards the vascular niche during maturation. However, the exact location of MK maturation and the functional significance of MK migration towards the vascular niche for thrombopoiesis still remain ill-defined. Therefore, the second aim of this thesis was to visualize the distribution and morphology of MKs in the intact BM using LSFM.

Platelets are constantly produced by their BM precursors. In platelets, Syk is an essential signaling mediator downstream of immune cell receptors, but also of GPVI and CLEC-2. However, only limited evidence exists on the role of Syk in hemostasis, arterial thrombosis and ischemic stroke. Thus, the third aim of this thesis was to identify the pathophysiological significance of Syk deficiency and to determine if Syk could be a potential anti-thrombotic target.

Zap-70 has a lower intrinsic activity compared to Syk and is expressed in T cells and NK cells, but not in platelets. To assess if Syk and Zap70 exhibit interchangeable functions *in vivo*, a knock-in mouse was generated, which expresses Zap-70 under the control of intrinsic Syk promoter elements. The fourth aim of this thesis was to investigate the consequence of the kinase replacement for platelet function *in vitro* and *in vivo*.

3. Materials and Methods

3.1. Materials

3.1.1. Reagents and chemicals

Acetic acid	Roth (Karlsruhe, Germany)
Adenosine diphosphate (ADP)	Sigma-Aldrich (Schnelldorf, Germany)
Agarose	Roth (Karlsruhe, Germany)
Amersham® Hyperfilm®, ECL	GE Healthcare (Little Chalfont, UK)
Ammonium persulphate (APS)	Roth (Karlsruhe, Germany)
Apyrase (grade III)	Sigma-Aldrich (Schnelldorf, Germany)
Atipamezole	Pfizer (Karlsruhe, Germany)
β-mercaptoethanol	Roth (Karlsruhe, Germany)
Benzyl alcohol	Sigma-Aldrich (Schnelldorf, Germany)
Benzyl benzoate	Sigma-Aldrich (Schnelldorf, Germany)
Bovine serum albumin (BSA)	AppliChem (Darmstadt, Germany)
Bromophenol blue	Sigma-Aldrich (Schnelldorf, Germany)
Collagen Horm® suspension + SKF sol.	Takeda (Linz, Austria)
Complete protease inhibitor cocktail	Roche Diagnostics (Mannheim, Germany)
Convulxin	Enzo Life Sciences (Lörrach, Germany)
Cryo-Gel	Leica Biosystems (Wetzlar, Germany)
Cyanoacrylate	Weicon (Münster, Germany)
Deoxynucleotide triphosphates (dNTP) mix	Thermo Fisher (Schwerte, Germany)
4',6-diamidino-2-phenylindole (DAPI) Fluoromount-G	Southern Biotech (Birmingham, AL, USA)
Dimethyl sulfoxide (DMSO)	Sigma-Aldrich (Schnelldorf, Germany)
Disodium hydrogen phosphate (Na_2HPO_4)	Roth (Karlsruhe, Germany)
Dulbecco's Modified Eagle Media (DMEM)	Gibco (Karlsruhe, Germany)
Enhanced chemiluminescence (ECL) detection substrate	MoBiTec (Göttingen, Germany)
Ethanol	Sigma-Aldrich (Schnelldorf, Germany)
Ethylenediaminetetraacetic acid (EDTA)	AppliChem (Darmstadt, Germany)
Ethylene glycol tetraacetic acid (EGTA)	Sigma-Aldrich (Schnelldorf, Germany)
Fat-free dry milk	AppliChem (Darmstadt, Germany)
Fentanyl	Janssen-Cilag (Neuss, Germany)
Fetal calf serum (FCS)	Perbio (Bonn, Germany)
Fibrinogen from human plasma (F3879)	Sigma-Aldrich (Schnelldorf, Germany)

Fibrinogen from human plasma (F4883)	Sigma-Aldrich (Schnelldorf, Germany)
Flumazenil	AlleMan Pharma (Pfullingen, Germany)
GeneRuler DNA Ladder Mix	Thermo Fisher (Schwerte, Germany)
Glucose	Roth (Karlsruhe, Germany)
Glycerin	Roth (Karlsruhe, Germany)
Glycerol	Roth (Karlsruhe, Germany)
Glycine	Sigma-Aldrich (Schnelldorf, Germany)
Heparin	Ratiopharm (Ulm, Germany)
Hoechst 33258	Biomol (Hamburg, Germany)
4-(2-hydroxyethyl)-1-piperazine-ethanesulfonic acid (HEPES)	Roth (Karlsruhe, Germany)
IGEPAL® CA-630	Sigma-Aldrich (Schnelldorf, Germany)
Immobilon-P transfer membrane, PVDF	Merck Millipore (Darmstadt, Germany)
Indomethacin	Sigma-Aldrich (Schnelldorf, Germany)
Iron-III-chloride hexahydrate ($FeCl_3 \cdot 6\ H_2O$)	Roth (Karlsruhe, Germany)
Isofluran CP®	cp-pharma (Burgdorf, Germany)
Isopropanol	Roth (Karlsruhe, Germany)
Magnesium chloride ($MgCl_2$)	Roth (Karlsruhe, Germany)
Medetomidine	Pfizer (Karlsruhe, Germany)
Methanol	Sigma-Aldrich (Schnelldorf, Germany)
Midazolam	Roche Diagnostics (Mannheim, Germany)
Midori Green Advanced DNA stain	Nippon Genetics Europe (Düren, Germany)
Monopotassium phosphate (KH_2PO_4)	Sigma-Aldrich (Schnelldorf, Germany)
3-(N-morpholino)propanesulfonic acid (MOPS)	AppliChem (Darmstadt, Germany)
Naloxone	AlleMan Pharma (Pfullingen, Germany)
Neomycin Sulfate	Bela-Pharm (Vechta, Germany)
NuPAGE® LDS Sample Buffer (4x)	Life Technologies (Darmstadt, Germany)
PageRuler Prestained Protein Ladder	Thermo Fisher (Schwerte, Germany)
Paraformaldehyde (PFA)	Sigma-Aldrich (Schnelldorf, Germany)
Phenol/chloroform/isoamyl alcohol	Roth (Karlsruhe, Germany)
Phosphate-buffered saline (PBS)	Life Technologies (Darmstadt, Germany)
Plerixafor (AMD3100)	Selleckchem, Munich, Germany
Potassium chloride (KCl)	Roth (Karlsruhe, Germany)
Propidium iodide (PI)	Life Technologies (Darmstadt, Germany)
Prostacyclin (PGI_2)	Calbiochem (Bad Soden, Germany)
Protease inhibitor cocktail	Sigma-Aldrich (Schnelldorf, Germany)

Proteinase K, recombinant, PCR grade	Thermo Fisher (Schwerte, Germany)
Rotiphorese® Gel 30 (37,5:1) acrylamide	Roth (Karlsruhe, Germany)
SeeBlue® Plus2 pre-stained standard	Life Technologies (Darmstadt, Germany)
Sodium azide (NaN_3)	Sigma-Aldrich (Schnelldorf, Germany)
Sodium bicarbonate ($NaHCO_3$)	Sigma-Aldrich (Schnelldorf, Germany)
Sodium chloride (NaCl)	AppliChem (Darmstadt, Germany)
Sodium citrate	AppliChem (Darmstadt, Germany)
Sodium dodecyl sulfate (SDS)	Sigma-Aldrich (Schnelldorf, Germany)
Sodium fluoride (NaF)	Sigma-Aldrich (Schnelldorf, Germany)
Sodium orthovanadate (Na_3VO_4)	Sigma-Aldrich (Schnelldorf, Germany)
SRP4388 (SDF1 alpha)	Sigma-Aldrich (Schnelldorf, Germany)
Sucrose	Sigma-Aldrich (Schnelldorf, Germany)
10x Taq Buffer (+KCl, -MgCl2)	Thermo Fisher (Schwerte, Germany)
Taq DNA polymerase	Thermo Fisher (Schwerte, Germany)
N,N,N',N'-Tetramethylethylenediamine (TEMED)	Roth (Karlsruhe, Germany)
Thrombin from human plasma	Roche Diagnostics (Mannheim, Germany)
Thrombin from human plasma	Sigma-Aldrich (Schnelldorf, Germany)
Tissue-Tek® O.C.T.™ Compound	Sakura Finetek (Staufen, Germany)
2,3,5-triphenyltetrazolium chloride (TTC)	Sigma-Aldrich (Schnelldorf, Germany)
Tris(hydroxymethyl)aminomethane (Tris)	Roth (Karlsruhe, Germany)
Tween® 20	Roth (Karlsruhe, Germany)
U46619	Enzo Life Sciences (Lörrach, Germany)
Western Lightning® Plus-ECL	PerkinElmer (Baesweiler, Germany)

Collagen-related peptide (CRP) was kindly provided by Dr. Steve Watson (University of Birmingham, UK). Rhodocytin was a generous gift from Dr. Johannes Eble (University Hospital, Frankfurt, Germany). Primers were obtained from Metabion (Planegg-Martinsried, Germany). All other non-listed chemicals were obtained from AppliChem (Darmstadt, Germany), Roth (Karlsruhe, Germany) or Sigma-Aldrich (Schnelldorf, Germany).

3.1.2. Materials

18G x 1 ½", 20G x 1 ½", 26G x 1 ½" needles	BD Biosciences (Heidelberg, Germany)
Glass coverslips (24 x 60 mm)	Roth (Karlsruhe, Germany)
Glass vials	Hartenstein (Würzburg, Germany)
Heparinized capillaries	Hartenstein (Würzburg, Germany)
Metal plate skull holder	Boer Metaal en Draad (Deil, Netherlands)
Microcapillaries (50 μl and 100 μl)	Hartenstein (Würzburg, Germany)
Perma-Hand silk suture (3-0, 4-0, 7-0)	Ethicon (Somerville, NJ, USA)
Syringes (1 ml)	Dispomed (Gelnhausen, Germany)
Syringe filters (0.22 μm and 0.45 μm)	Roth (Karlsruhe, Germany)
Well plates (6-well, 12-well and 24-well)	Greiner (Frickenhausen, Germany)

3.1.3. Labeling kits and fluorophores

Alexa Fluor 488 protein labeling kit	Life Technologies (Darmstadt, Germany)
Alexa Fluor 546 protein labeling kit	Life Technologies (Darmstadt, Germany)
Alexa Fluor 594 protein labeling kit	Life Technologies (Darmstadt, Germany)
Alexa Fluor 647 protein labeling kit	Life Technologies (Darmstadt, Germany)
Alexa Fluor 750 SAIVI™ Rapid Antibody Labeling Kit	Life Technologies (Darmstadt, Germany)
DyLight™ 488 antibody labeling kit	Life Technologies (Darmstadt, Germany)
Fluorescein (FITC)	Life Technologies (Darmstadt, Germany)
R-Phycoerythrin (PE)	EUROPA (Cambridge, UK)
Tetramethylrhodamine dextran (2 MDa)	Life Technologies (Darmstadt, Germany)

3.1.4. Antibodies

3.1.4.1. Commercial primary and secondary antibodies

Goat anti-rabbit IgG	Life Technologies (Darmstadt, Germany)
Goat anti-rabbit IgG-HRP	Cell Signaling (Danvers, MA, USA)
Goat anti-rat IgG	Life Technologies (Darmstadt, Germany)
Hamster anti-CD29 (β1-int.)-FITC (HMβ1-1)	BioLegend (San Diego, CA, USA)
Mouse anti-α-tubulin (B-5-1-2)	Sigma-Aldrich (Schnelldorf, Germany)
Platelet depletion antibody (# R300)	Emfret Analytics (Eibelstadt, Germany)
Rabbit anti-β1-tubulin	Sigma-Aldrich (Schnelldorf, Germany)
Rabbit anti-PLCγ2	Santa Cruz (Dallas, TX, USA)
Rabbit anti-Syk (N-19)	Santa Cruz (Dallas, TX, USA)
Rabbit anti-total-Syk (D1I5Q)	Cell Signaling (Danvers, MA, USA)
Rabbit anti-Zap-70 (99F2)	Cell Signaling (Danvers, MA, USA)

Rat anti-CD105 (endoglin) (MJ7/18) BioLegend (San Diego, CA, USA)

Rat anti-CD41-FITC (MWReg30) BD Biosciences (Heidelberg, Germany)

3.1.4.2. Monoclonal rat antibodies

Monoclonal antibodies generated and/or modified in our laboratory. Antibodies were fluorescently labeled using antibody labeling kits.

Antibody	Clone	Isotype	Antigen	Reference
p0p3	7A9	IgG2a	GPIbα	[208]
p0p4	15E2	IgG2b	GPIbα	[208]
p0p5	13G12	IgG1	GPIbα	[209]
p0p/B	57E12	IgG2b	GPIbα	[209]
DOM2	89H11	IgG2a	GPV	[210]
p0p6	56F8	IgG2b	GPIX	[210]
JAQ1	98A3	IgG2a	GPVI	[211]
INU1	11E9	IgG1	CLEC-2	[160]
ULF1	97H1	IgG2a	CD9	unpublished
JER1	10B6	IgG1	CD84	[212]
LEN1	12C6	IgG2b	α2	[211]
LEN/B	23C11	-	α2β1	[213]
BAR-1	25B11	IgG1	α5	[214]
EDL1	57B10	IgG2a	β3	[208]
MWReg30	5D7	IgG1	αIIbβ3	[215]
JON2	14A3	IgG2b	αIIbβ3	[210]
JON/A	4H5	IgG2b	αIIbβ3	[209]
WUG 1.9	5C8	IgG1	P-selectin	[132]

3.1.5. Buffers

If not stated otherwise, all buffers were prepared and diluted using deionized water obtained from a MilliQ Water Purification System (Millipore, Schwalbach, Germany). pH was adjusted with HCl or NaOH.

Blocking buffer

BSA or fat-free dry milk	5%
in washing buffer	

Clearing solution (BABB)

Benzyl alcohol	1 part
Benzyl benzoate	2 parts

Decalcification buffer, pH 7.4

EDTA	10%
in PBS	

Laemmli SDS sample buffer (4x)

Tris-HCl, pH 6.8	200 mM
Glycerol	40%
Bromophenol blue	0.04%
SDS	8%
β-mercaptoethanol (reducing conditions)	20%

Laemmli running buffer for SDS-PAGE

Tris	0.25 M
Glycine	1.92 M
SDS	35 mM

Loading dye solution (6x) for analysis of PCR products

Tris buffer (150 mM)	33%
Glycerin	60%
Bromophenol blue	0.04%

Lysis buffer for DNA isolation

Tris base	100 mM
EDTA	5 mM
NaCl	200 mM
SDS	0.2%
Proteinase K (20 mg/ml)	100 μg/ml

Lysis buffer for platelet lysates, pH 8.0

Tris, pH 7.4	15 mM
NaCl	155 mM
EDTA	1 mM
NaN_3	0.005%
IGEPAL CA-630	1%
Protease inhibitor cocktail	1%

MOPS buffer (20x)

MOPS	1 M
Tris base	1 M
SDS	69.3 mM
EDTA	20.5 mM

PBS/EDTA

EDTA	5 mM
in PBS	

Paraformaldehyde (PFA), pH 7.2

PFA	4%
in PBS	

Phosphate-buffered saline (PBS), pH 7.14

NaCl	137 mM
KCl	2.7 mM
KH_2PO_4	1.5 mM
Na_2HPO_4	8 mM

Separating gel buffer (SDS-PAGE), pH 8.8

Tris-HCl	1.5 M

Sodium citrate buffer, pH 7.0

Sodium citrate	0.129 M

Stacking gel buffer (SDS-PAGE), pH 6.8

Tris-HCl	0.5 M

Stripping buffer

Tris-HCl, pH 6.8	62.5 mM
SDS	2%
β-mercaptoethanol	100 mM

TAE buffer (50x)

Tris base	0.2 M
Acetic acid	5.7%
EDTA (0.5 M, pH 8.0)	10%

TE buffer, pH 8.0

Tris base	10 mM
EDTA	1 mM

Transfer buffer

Tris-Ultra	50 mM
Glycine	40 mM
Methanol	20%

Tris-buffered saline (TBS), pH 7.3

Tris-HCl	20 mM
NaCl	137 mM

Tyrode-HEPES (Tyrode's) buffer, pH 7.4

NaCl	137 mM
KCl	2.7 mM
$NaHCO_3$	12 mM
NaH_2PO_4	0.43 mM
$CaCl_2$	1 mM
$MgCl_2$	1 mM
HEPES	5 mM
BSA	0.35%
Glucose	0.1%

Washing buffer (TBS-T)

Tween® 20	0.1%
in TBS (1x)	

3.1.6. Mice

Syk^{fl/fl},[161] *RhoA*^{fl/fl},[216] *Pfn1*^{fl/fl} [217] and *Trpm7*^{fl/fl} [218] mice were intercrossed with mice carrying the Cre-recombinase under the *Pf4* promoter to generate megakaryocyte and platelet-specific knockout mice.[219] *Syk*[Zap70/Zap70] mice were generated as previously described.[220] *Flk1-mCherry*[221] were kindly provided by Mary E. Dickinson (Houston, Texas). *Tie2-Cre/R26-tdRFP*[222] were kindly provided by Friedemann Kiefer (Münster, Germany). *CD41-YFP*[223] and *Lys-eGFP*[224] mice were kindly provided by Thomas Graf (Barcelona, Spain). *Thy1-eGFP*[225] mice were kindly provided by Anna-Lena Sirén (Würzburg, Germany). C57BL/6JRj mice were obtained from Janvier Labs (Saint-Berthevin, France). All mice used in experiments were 8 to 12 weeks old and sex-matched, if not stated otherwise. Animal studies were approved by the district government of Lower Franconia (Bezirksregierung Unterfranken).

3.1.6.1. Generation of fetal liver chimeric and bone marrow chimeric mice

The insertion of Zap-70 cDNA into the first coding exon of Syk resulted in perinatal lethality of the *Syk*[Zap70/Zap70] mice and therefore fetal liver chimeric mice and bone marrow chimeric mice were generated. Recipient C57BL/6JRj mice at 6 weeks of age were lethally irradiated with 10 Gray. For fetal liver chimeric mice, female mice were time-mated and the livers of 13.5 to 14.5 day old mouse embryos were isolated. For bone marrow chimeric mice, the femur and tibia of donor mice were prepared and bone marrow was flushed out with a 22G needle into cold DMEM. A single cell suspension was prepared and cells were counted in a Neubauer chamber. 4 million cells diluted in 150 µl DMEM were intravenously injected into one recipient mouse. Mice were treated with 2 g/l neomycin in water for the following 6 weeks.

3.2. Methods

3.2.1. Mouse genotyping

3.2.1.1. Mouse genotyping by flow cytometry

CD41-YFP mice were genotyped by flow cytometry. 50 µl blood were drawn from the retro-orbital plexus of anesthetized mice using heparinized capillaries and collected in a tube containing 300 µl heparin in TBS (20 U/ml, pH 7.3). Blood was diluted 1:20 with Ca^{2+}-free Tyrode's buffer or 1x PBS and either stained with saturating amounts of anti-αIIb-PE antibodies for 15 minutes (min) at room temperature (RT) to determine surface protein expression or left unstained to determine the percentage of YFP-positive platelets. The reaction was stopped by the addition of 500 µl 1x PBS and samples were analyzed on a FACSCalibur (BD Biosciences, Heidelberg, Germany).

3.2.1.2. Isolation of genomic DNA from mouse tissue

Mouse ear punch samples were lysed in 500 μl DNA lysis buffer containing 100 μg/ml proteinase K. The samples were incubated overnight (o/n) at 56 ºC under shaking conditions (900 rpm, Eppendorf Thermomixer). Phenol/chloroform/isoamyl alcohol mixture (500 μl) was added to each sample and upon vigorous shaking, the samples were centrifuged at 10,000 rpm for 10 min at RT. The upper phase (approximately 440 μl) was transferred to reaction tubes containing 500 μl isopropanol and upon vigorous shaking, the samples were centrifuged at 14,000 rpm for 10 min at 4ºC. The supernatant was discarded and the DNA pellet was washed with 500 μl 70% ethanol and centrifuged again at 14,000 rpm for 10 min at 4ºC. The DNA pellet was allowed to dry at 37 ºC for 30 min and solubilized in 70 μl TE buffer for 30 min at 37 ºC under stirring conditions. 1-2 μl of DNA was used for a polymerase chain reaction (PCR).

3.2.1.3. Mouse genotyping by PCR

Genotyping was accomplished by PCR using different mixtures of primers and PCR programs as indicated below.

Detection of the *Syk* floxed allele by PCR

Primers:

Syk_flox_F	5' GGT GCC TAC AGG TCT ACA GC 3'
Syk_flox_R	5' AAC CTG GTA ATT TCA TAA CGC C 3'

Pipetting scheme:

DNA	1 μl
Syk_flox_F (1:10 in H_2O, stock: 100 pmol/μl)	1 μl
Syk_flox_R (1:10 in H_2O, stock: 100 pmol/μl)	1 μl
dNTPs (10 mM)	1 μl
10x Taq buffer (+KCl, -$MgCl_2$)	2.5 μl
$MgCl_2$ (25 mM)	2.5 μl
Taq polymerase (5 U/μl)	0.25 μl
H_2O	15.75 μl

PCR program:

96ºC	3:00 min	
94ºC	0:30 min	
56ºC	0:30 min	35 cycles
72ºC	1:00 min	
72ºC	10:00 min	
4ºC	∞	

Resulting band size:

wt: 198 bp

floxed allele: 285 bp

Detection of the *Pf4-Cre* transgene by PCR

Primers:

Pf4-Cre_F   5' CCC ATA CAG CAC ACC TTT 3'

Pf4-Cre_R   5' TGC ACA GTC AGC AGG TT 3'

Pipetting scheme:

DNA	1 μl
Pf4-Cre_F (1:10 in H_2O, stock: 100 pmol/μl)	1 μl
Pf4-Cre_R (1:10 in H_2O, stock: 100 pmol/μl)	1 μl
dNTPs (10 mM)	1 μl
10x Taq buffer (+KCl, -$MgCl_2$)	2.5 μl
$MgCl_2$ (25 mM)	2.5 μl
Taq polymerase (5 U/μl)	0.25 μl
H_2O	15.75 μl

PCR program:

95ºC	5:00 min	
95ºC	0:30 min	
58ºC	0:30 min	35 cycles
72ºC	0:45 min	
72ºC	5:00 min	
4ºC	∞	

Resulting band size:

wt: no PCR product

Pf4-Cre positive: 450 bp

Detection of the wildtype *Syk* allele *(Syk$^{Zap70/Zap70}$)* by PCR

Primers:

Syk_WT_F   5' GCA CTC TAA GCT TGT ATC CCT GTG G 3'

Syk_WT_R   5' GCA GCA CAC AGG CAT CTG CTA TCC 3'

Pipetting scheme:

DNA	1 μl
Syk_WT_F (1:10 in H_2O, stock: 100 pmol/μl)	1 μl
Syk_WT_R (1:10 in H_2O, stock: 100 pmol/μl)	1 μl
dNTPs (10 mM)	1 μl
10x Taq buffer (+KCl, -$MgCl_2$)	2.5 μl
$MgCl_2$ (25 mM)	2.5 μl

Taq polymerase (5 U/μl)	0.25 μl
H$_2$O	15.75 μl

PCR program:

95ºC	5:00 min	
95ºC	0:30 min	
60ºC	0:45 min	30 cycles
72ºC	1:00 min	
72ºC	5:00 min	
4 ºC	∞	

Resulting band size:

wt:	661 bp

Detection of the *Zap70* allele *(Syk$^{Zap70/Zap70}$*) by PCR

Primers:

Syk_KI_F	5' AAA TCG GCA AAA TCC CTT ATA AAT C 3'
Syk_KI_R1	5' GAA GAA CGA GAT CAG CAG C 3'
Syk_KI_R2	5' CCT GAT GAG GTT CTC CTT C 3'

Pipetting scheme:

DNA	1 μl
Syk_KI_F (1:10 in H$_2$O, stock: 100 pmol/μl)	1 μl
Syk_KI_R1 (1:10 in H$_2$O, stock: 100 pmol/μl)	1 μl
Syk_KI_R2 (1:10 in H$_2$O, stock: 100 pmol/μl)	1 μl
dNTPs (10 mM)	1 μl
10x Taq buffer (+KCl, -MgCl$_2$)	2.5 μl
MgCl$_2$ (25 mM)	2.5 μl
Taq polymerase (5 U/μl)	0.25 μl
H$_2$O	14.75 μl

PCR program:

95ºC	5:00 min	
95ºC	0:30 min	
60ºC	0:45 min	30 cycles
72ºC	1:00 min	
72ºC	5:00 min	
4 ºC	∞	

Resulting band size:

Zap70:	142 bp

3.2.1.4. Agarose gel electrophoresis

Agarose (final concentration (f.c.) 1.5%) was dissolved in 1x TAE buffer and boiled in a microwave. When the temperature of the solution had decreased to approximately 60°C, 5 μl Midori green per 100 μl solution were added and the fluid was poured into a tray with a comb. After solidification of the gel, the tray was positioned in an electrophoresis chamber containing 1x TAE buffer. 4 μl 6x loading dye solution were added to 20 μl DNA and the samples were loaded into the gel slots. For size separation, DNA samples were run for 30 min at 120-160 V and a DNA ladder was used to determine the size of the PCR products.

3.2.2. Blood preparation

3.2.2.1. Plasma samples

Capillaries were anti-coagulated with sodium citrate. 100 μl blood were drawn from the retro-orbital plexus of anesthetized mice and collected in tubes containing 100 μl sodium citrate. Samples were centrifuged at 2800 rpm for 5 min at RT and the supernatant was again centrifuged at 2800 rpm for 5 min at RT. Platelet-poor plasma (PPP) was spun down at 14,000 rpm for 5 min at RT and supernatants were immediately used for experiments or frozen at -20 °C.

3.2.2.2. Washed blood

50 μl blood were drawn from the retro-orbital plexus of anesthetized mice using heparinized capillaries and collected in a tube containing 300 μl heparin in TBS (20 U/ml, pH 7.3). Ca^{2+}-free Tyrode's buffer (650 μl) was added to each sample and blood was centrifuged twice at 2800 rpm for 5 min at RT and resuspended in Ca^{2+}-free Tyrode's buffer. Finally, samples were resuspended in 750 μl Tyrode's buffer with 2 mM Ca^{2+}.

3.2.2.3. Washed platelets

Mice were bled under isoflurane anesthesia from the retro-orbital plexus with heparin-coated capillaries and 700 μl blood were collected in a reaction tube containing 300 μl heparin in TBS (20 U/ml, pH 7.3). Blood was centrifuged at 800 rpm for 7 min at RT (Eppendorf Centrifuge 5415 C). Supernatant and buffy coat were transferred into a new tube and again centrifuged at 800 rpm for 7 min at RT to obtain platelet-rich plasma (PRP). To prepare washed platelets, PRP was centrifuged at 2800 rpm for 5 min at RT and the platelet pellet was resuspended in 1 ml Ca^{2+}-free Tyrode's buffer containing PGI_2 (0.1 μg/ml) and apyrase (0.02 U/ml) and incubated for 10 min at 37°C. This washing step was repeated and the

platelet count was determined using a Sysmex KX-21N automated hematology analyzer (Sysmex Corporation, Kobe, Japan). After centrifugation, the pellet was resuspended in Ca^{2+}-free Tyrode's buffer containing apyrase (0.02 U/ml) to obtain the desired platelet concentration. Washed platelets were incubated for 30 min at 37°C prior to analysis.

3.2.2.4. Platelet lysates

Washed platelets ($1 \times 10^6/\mu l$) were lysed in lysis buffer containing 1% IGEPAL CA-360 and protease inhibitors for 20 min on ice. The samples were then centrifuged at 14,000 rpm for 10 min at 4°C and the supernatant was used for experiments.

3.2.3. Compound preparation

3.2.3.1. BI1002494

For *in vitro* assays, BI1002494 ($C_{23}H_{24}N_3O_5$)[226], kindly provided by Boehringer Ingelheim, was dissolved in DMSO and final DMSO concentration in the assays was less than 0.1%. The washed platelets were incubated at 37°C with BI1002494 10 min prior to the experiment. For animal experiments, BI1002494 was dissolved in water and applied by oral gavage 15 hours (h) and 1 h prior to blood taking (*ex vivo* aggregation experiments) or prior to the *in vivo* experiments (100 mg/kg b.i.d.). To assess the therapeutic function of the Syk inhibitor, BI1002494 was dissolved in water and applied by oral gavage directly after tMCAO (100 mg/kg), i.e. directly upon removal of the filament.

3.2.4. Biochemistry

3.2.4.1. Western blotting

4x Laemmli SDS sample buffer (with β-mercaptoethanol for reducing conditions) was added to platelet lysates and samples were boiled for 5 min at 95°C. Proteins were separated by sodium dodecyl sulfate polyacrylamide gel electrophoresis (SDS-PAGE) on a 12% separating gel with a 4% stacking gel. Samples were loaded onto the gel including a molecular weight marker, run in Laemmli running buffer and transferred onto a polyvinylidene difluoride (PVDF) membrane for 1 h using a semi-dry transfer system. To prevent unspecific antibody binding, membranes were blocked in 5% fat-free dry milk or 5% BSA dissolved in washing buffer for 2 h at RT or o/n at 4°C. Membranes were then incubated with primary antibodies o/n at 4°C. Membranes were washed with washing buffer 3x 15 min at RT and incubated with HRP-conjugated secondary antibodies for 1 h at RT. After three washing steps, membranes were developed using ECL detection substrate with autoradiography films. To re-probe a membrane, blots were incubated in stripping buffer for 30 min at RT,

washed thoroughly in washing buffer, blocked and subsequently probed with antibodies. PLCγ2 levels were used as loading control.

3.2.5. *In vitro* analyses of platelet function

3.2.5.1. Determination of blood parameters

To determine blood parameters, 50 μl blood were drawn from the retro-orbital plexus of anesthetized mice using heparinized capillaries and collected into a tube containing 300 μl heparin in TBS (20 U/ml, pH 7.3). Blood cell counts and parameters were determined using a Sysmex KX-21N automated hematology analyzer (Sysmex Corporation, Kobe, Japan).

3.2.5.2. Determination of platelet count, size and surface protein expression

To measure platelet count, size and surface protein expression, 50 μl blood were drawn from the retro-orbital plexus of anesthetized mice using heparinized capillaries and collected in a tube containing 300 μl heparin in TBS (20 U/ml, pH 7.3). Blood was diluted 1:20 with Ca^{2+}-free Tyrode's buffer or 1x PBS and stained with saturating amounts of fluorophore-conjugated antibodies for 15 min at RT. The reaction was stopped by the addition of 500 μl 1x PBS and samples were analyzed on a FACSCalibur (BD Biosciences, Heidelberg, Germany).

3.2.5.3. Determination of platelet activation responses

To measure platelet activation responses, 50 μl washed blood were activated with the respective agonist (10-fold concentrated) in the presence of saturating amounts of a 1:1 mixture of PE-coupled 4H5 (anti-activated αIIbβ3) and FITC-coupled 5C8 (anti-P-selectin) antibodies. Samples were incubated for 7 min at 37 ºC and additionally for 7 min at RT. The reaction was stopped by the addition of 500 μl 1x PBS and samples were analyzed on a FACSCalibur (BD Biosciences, Heidelberg, Germany).

3.2.5.4. Aggregometry

Washed platelets (50 μl with 5 x 10^5 platelets/μl) were diluted into 110 μl Tyrode's buffer containing 2 mM Ca^{2+} and 100 μg/ml human fibrinogen. Alternatively, heparinized PRP was diluted into Tyrode's buffer containing 2 mM Ca^{2+} and used for investigation of aggregation. Agonists were added at indicated concentrations to the continuously stirring (1000 rpm) platelet suspension. Light transmission was recorded on a Fibrintimer 4-channel aggregometer (APACT Laborgeräte und Analysensysteme, DiaSys Deutschland, Flacht,

Germany) for 10 min and expressed in arbitrary units with buffer representing 100% transmission and washed platelet suspension or PRP representing 0% transmission. For platelet activation using thrombin, washed platelets were diluted in fibrinogen-free Tyrode's buffer containing 2 mM Ca^{2+}.

3.2.5.5. Platelet adhesion on fibrinogen under static conditions

Glass coverslips (24 x 60 mm) were coated with 100 µg/ml human fibrinogen diluted in sterile 1x PBS o/n at 4 °C under humid conditions. Coverslips were blocked with sterile filtered 1% BSA in PBS for 2 h at RT and rinsed with Tyrode's buffer containing 2 mM Ca^{2+}. Washed platelets (50 µl with 3 x 10^5 platelets/µl for early time points and 30 µl with 3 x 10^5 platelets/µl for late time points) were left unstimulated or were stimulated with thrombin (0.01 U/ml f.c.) and/or second wave inhibitors (indomethacin (1.4 µM f.c.) and apyrase (2 U/ml f.c.)) and were allowed to spread for the indicated time points at RT. Platelets were fixed with 4% PFA in PBS for 5 min at RT and visualized with a Zeiss Axiovert 200 inverted microscope (100x oil objective, Zeiss, Oberkochen, Germany) using differential interference contrast (DIC) microscopy. Representative images were taken and evaluated according to different platelet spreading stages using ImageJ software (NIH, Bethesda, MD, USA).

3.2.5.6. Clot retraction

700 µl blood were drawn from the retro-orbital plexus of anesthetized mice using non-heparinized capillaries and collected in a tube containing 70 µl sodium citrate. Platelets were washed and PPP and erythrocytes were collected. The platelet concentration in the suspension was adjusted to 3 x 10^5 platelets/µl using PPP. 1.5 µl of erythrocytes (to contrast the clot) and 20 mM $CaCl_2$ were added to 250 µl of the platelet suspension. To induce clot retraction, the samples were stimulated with 4 U/ml thrombin. Clot retraction was monitored at 37°C under non-stirring conditions. Images were taken every 15 min and after 4 h the residual fluid was measured.

3.2.5.7. Platelet adhesion on collagen under flow conditions

Glass coverslips (24 x 60 mm) were coated with 200 µg/ml fibrillar type I collagen (Horm) o/n at 37 °C and blocked with sterile filtered 1% BSA in PBS for 1 h at RT. They were rinsed with Tyrode's buffer containing 2 mM Ca^{2+} and gently fixed in a transparent flow chamber with a slit depth of 50 µm. Heparinized whole blood (700 µl blood in 300 µl heparin in TBS) was diluted with Tyrode's buffer containing 2 mM Ca^{2+} (800 µl heparinized blood and 400 µl buffer). Platelets were labeled with a DyLight 488 conjugated anti-GPIX antibody derivative

(0.2 μg/ml) for 5 min at 37 °C and blood was filled into a 1 ml syringe, which was connected to the flow chamber. Perfusion was accomplished using a pulse-free pump under high shear stress equivalent to a wall shear rate of 1000 s^{-1} for 4 min. Microscopic phase-contrast images were recorded in real-time during perfusion. Thereafter, coverslips were washed by a 2 min perfusion with Tyrode's buffer containing 2 mM Ca^{2+} at the same shear rate. Phase-contrast and fluorescence images were obtained from at least seven different collagen-containing microscopic fields for each sample using a Zeiss Axiovert 200 inverted microscope (40x objective, Zeiss Oberkochen, Germany) and analyzed offline using Metavue software (Visitron, Puchheim, Germany).

3.2.6. *In vivo* analyses of platelet function

3.2.6.1. Platelet depletion

Thrombocytopenia was induced by intravenous injection of rat anti-GPIbα (anti-CD42b) antibodies (2.0 μg/g body weight). Peripheral platelet counts were determined directly before the experiments using a Sysmex KX-21N automated hematology analyzer (Sysmex Corporation, Kobe, Japan) or by flow cytometry.

3.2.6.2. Tail bleeding time

Mice were anesthetized by intraperitoneal injection of medetomidine (0.5 μg/g), midazolam (5 μg/g) and fentanyl (0.05 μg/g) and 1 mm of the tail tip was removed using a scalpel. Tail bleeding was monitored by gently absorbing blood on filter paper at 20 s intervals without interfering with the wound site. Bleeding was determined to have ceased when no blood was observed on the paper. Experiments were stopped manually after 20 min by cauterization to prevent excessive blood loss and anesthesia was antagonized by intraperitoneal injection of atipamezole (2.5 μg/g), flumazenil (0.05 μg/g) and naloxone (1.2 μg/g).

3.2.6.3. Thrombus formation in FeCl$_3$-injured mesenteric arterioles

Mice (4 to 5 weeks old, 15–18 g) were anesthetized by intraperitoneal injection of medetomidine (0.5 μg/g), midazolam (5 μg/g) and fentanyl (0.05 μg/g) and were intravenously injected with 1.5 μg of a DyLight 488-conjugated anti-GPIX antibody derivative to label platelets *in vivo.* The mesentery was then gently exteriorized through a midline abdominal incision. Mesenterial arterioles with a diameter between 35-60 μm were visualized with a Zeiss Axiovert 200 inverted microscope (10x objective, Zeiss, Oberkochen, Germany). The microscope was equipped with a 100 W HBO fluorescent lamp and a CoolSNAP-EZ

camera. Injury was induced by topical application of a 3 mm^2 filter paper saturated with 20% FeCl$_3$. Adhesion and aggregation of fluorescently labeled platelets in mesenterial arterioles was monitored until complete vessel occlusion occurred for at least 1 min or for a maximum of 40 min. Digital images were recorded and analyzed offline using Metavue software (Visitron, Puchheim, Germany). Experiments were conducted by Ina Thielmann.

3.2.6.4. Mechanical injury of the abdominal aorta

Mice (8 to 12 weeks old) were anesthetized by intraperitoneal injection of medetomidine (0.5 μg/g), midazolam (5 μg/g) and fentanyl (0.05 μg/g) and a longitudinal incision was used to open the abdominal cavity to expose the abdominal aorta. An ultrasonic flow probe (0.5PSB699; Transonic Systems, New York, USA) was placed around the abdominal aorta and thrombus formation was induced by a single firm compression with forceps. Blood flow was monitored until complete blood vessel occlusion occurred for at least 5 min or for a maximum of 30 min. Experiments were conducted by Ina Thielmann and Sarah Beck.

3.2.6.5. Transient middle cerebral artery occlusion (tMCAO)

Focal cerebral ischemia was induced in 8 to 12 week old mice by a transient middle cerebral artery occlusion (tMCAO) as previously described.[227] Inhalation anesthesia was induced by 2% isoflurane in a 70% N$_2$/30% O$_2$ mixture and a servo-controlled heating device was used to record and maintain body temperature during the surgical procedure. The duration of the surgical procedure per animal was kept below 15 min. A silicon rubber–coated 6.0 nylon monofilament (6021PK10, Doccol, Redlands, CA, USA) was advanced through the right common carotid artery and the internal carotid artery up to the origin of the middle cerebral artery (MCA) causing an MCA occlusion. After an occlusion time of 60 min, the filament was removed allowing reperfusion. Animals were sacrificed 24 h after reperfusion and brains were checked for intracerebral hemorrhages. The extent of the infarction was quantitatively assessed on 2,3,5-triphenyltetrazolium chloride (TTC, 2% (w/v) solution) stained brain sections. Global neurological outcome and motor function were evaluated by the Bederson score[228] and the grip test,[229] respectively. Planimetric measurements of infarcted areas (ImageJ software, NIH, Bethesda, MD, USA) corrected for brain edema and assessment of functional outcome were performed in a blinded fashion. Experiments were carried out by Dr. Peter Kraft from the Department of Neurology, University of Würzburg according to the recommendations in mechanism-driven basic stroke research.[230]

3.2.6.6. Multiphoton intravital microscopy of the brain vasculature

Mice (8 to 12 weeks old) were anesthetized by intraperitoneal injection of medetomidine (0.5 μg/g), midazolam (5 μg/g) and fentanyl (0.05 μg/g). A 1-cm incision was made along the midline to expose the frontoparietal skull. The external layer of the compact bone and most of the spongy bone were removed from a small part of the skull using a high-speed microdrill, creating a thinned skull window. The scalp was sutured and the mouse was left to recover for at least 24 h. On the day of imaging, the mouse was anesthetized and subsequently placed on a customized metal stage equipped with a stereotactic holder to immobilize its head. Images were acquired with a fluorescence microscope equipped with a 20x water objective with a numerical aperture of 0.95 and a TriM Scope II multiphoton system (LaVision BioTec), controlled by ImSpector Pro-V380 software (LaVision BioTec). Emission was detected with HQ535/50-nm and ET605/70-nm filters. A tunable broad-band Ti:Sa laser (Chameleon, Coherent) was used at 760 nm to capture Alexa Fluor 488 and tetramethylrhodamine dextran fluorescence. ImageJ software (NIH) was used to generate movies.

3.2.7. Megakaryocyte analyses

3.2.7.1. Immunofluorescence staining of whole femora cryo-sections

Femora and sterna of mice (6 to 12 weeks old) were isolated and fixed in 4% PFA for 2-4 h at 4°C and subsequently transferred into 10% sucrose/PBS and dehydrated using a graded sucrose series (incubation in 10% sucrose/PBS, followed by 20% sucrose/PBS and 30% sucrose/PBS for 24 h at 4°C). Samples were either embedded in Cryo-Gel, frozen and cryo-sections were produced using a CryoJane tape transfer system (Leica Biosystems, Wetzlar, Germany) or embedded in Tissue-Tek medium, snapfrozen in liquid nitrogen and cryo-sections were produced as described previously.[231] MKs were stained with anti-CD41-FITC antibodies, anti-β1-tubulin antibodies or anti-GPIX antibody derivatives. CD105 was used as an endothelial cell marker. Nuclei were stained with Hoechst 33258 or DAPI-containing mounting medium. Staining with antibodies and secondary reagents was performed for 30 min at RT. Sections were analyzed by confocal microscopy (Leica TCS-SP5, Leica Microsystems, Wetzlar, Germany) and processed with Leica LAS AF software and ImageJ software (NIH). MK number and density was measured in every visual field. Three femur sections from three separate animals were examined and 20 MKs per section were quantified with regards to area and shortest distance to sinusoids.

3.2.7.2. Multiphoton intravital microscopy of the bone marrow

Mice (8 to 12 weeks old) were anesthetized by intraperitoneal injection of medetomidine (0.5 μg/g), midazolam (5 μg/g) and fentanyl (0.05 μg/g). A 1-cm incision was made along the midline to expose the frontoparietal skull, while carefully avoiding damage to the bone tissue. The mouse was placed on a customized metal stage equipped with a stereotactic holder to immobilize its head. BM vasculature was visualized by injection of tetramethylrhodamine dextran (8 μg/g body weight) and anti-CD105 Alexa Fluor 546/Alexa Fluor 594 (0.4 μg/g body weight). Platelets and MKs were antibody stained with anti-GPIX (CD42a) Alexa Fluor 488 (0.6 μg/g body weight). Images were acquired with a fluorescence microscope equipped with a 20x water objective with a numerical aperture of 0.95 and a TriM Scope II multiphoton system (LaVision BioTec), controlled by ImSpector Pro-V380 software (LaVision BioTec). Emission was detected with HQ535/50-nm and ET605/70-nm filters. A tunable broad-band Ti:Sa laser (Chameleon, Coherent) was used at 760 nm to capture Alexa Fluor 488 and Alexa Fluor 546/Alexa Fluor 594/tetramethylrhodamine dextran fluorescence. ImageJ software (NIH) was used to generate movies.

3.2.7.3. Light-sheet fluorescence microscopy of the bone marrow

Platelets were antibody stained with an anti-GPIX Alexa Fluor 750 antibody derivative (0.6 μg/g body weight). BM vasculature was stained with an anti-CD105 Alexa Fluor 647 antibody (0.4 μg/g body weight). After 25 min, the mice were sacrificed and transcardially perfused with ice-cold PBS to wash out the blood and ice-cold 4% PFA to fix the tissues. Sterna and femora were harvested and stored in 4% PFA for 30 min. The samples were washed in PBS and decalcified in 10% EDTA for 96 h at 4°C on a shaker. The samples were then washed in PBS, followed by dehydration in a graded methanol series (50%, 70%, 95%, 100% for 30 min each) at RT and stored at 4°C overnight. The methanol was replaced stepwise by a clearing solution consisting of 1 part benzyl alcohol in 2 parts benzyl benzoate (BABB). After incubation in the clearing solution for at least 2h at RT, tissue specimens became optically transparent and were used for LSFM imaging on the following day.

3.2.7.4. Image analysis of the light-sheet fluorescence microscopy stacks

Multicolor LSFM stacks were processed and analyzed by FIJI[232] and Bitplane Imaris® 7.7.2 (Bitplane AG, Zurich, Switzerland). Data visualization and analysis was performed in three major steps: (i) image preprocessing, (ii) segmentation, (iii) data extraction. Step (i) was performed using either Imaris or FIJI, steps (ii) and (iii) were exclusively performed using Bitplane Imaris® 7.7.2, particularly the ImarisCell module. Statistical analysis of object positions, numbers and volumes (MK, vessel, bone marrow), edge-to-edge distance MK to

vessel and available vessel interspace were performed using Microsoft Excel (ver. 2013, Microsoft Corporation, Redmond, WA, USA), Origin (ver. 8.6, OriginLab Corporation, Northampton, MA, USA) and SPSS statistics (ver.23, IBM, Ehningen, Germany). Multi-photon microscopy images of 37 MKs were corrected for noise and converted to binary images using FIJI. Cell tracking of binary images was performed with the *active contours* module of Icy software (www.icy.bioimageanalysis.org, Institut Pasteur, France). Cell trajectories were analyzed using Matlab (Mathworks, USA) and *msdanalyzer* class.[233] Image processing was performed by Oğuzhan Angay and Patrick Schmithausen.

3.2.7.5. Computer simulations

Simulations were performed with a self-written algorithm in Matlab software (Mathworks, USA) using volume image stacks of mouse sterna acquired by LSFM and processed with Bitplane Imaris® 7.7.2 software (see above). Thus, the modeled MKs and vasculature perfectly reflected the spatial physiological situation. For random simulation (SimR), MKs were randomly placed in the 3D intervascular space. For vessel associated random simulation (SimVA), 60% of MKs from a pool of 30 different MKs were randomly placed at the vessels with minimal cross-volume of 1 voxel. Subsequently, the remaining MKs were placed into the intervascular space without vessel contact. The MK-vessel distances were calculated by using vessel distance transformation maps. For both types of simulations, the number and size distribution of MKs in the pool were matched to the experimentally estimated values. The presented results are mean ± standard deviation (SD) from at least five independent experiments per group, if not stated otherwise. Computational modeling was performed by Mari Gorelashvili.

3.2.8. Statistical analyses

Results are shown as mean ± SD from three individual experiments per group, unless indicated otherwise. Statistical analysis was conducted using the Student's t-test, apart from the Fischer's exact test which was applied to assess variance between non-occluded vessels in models of arterial thrombosis or in tail bleeding assays and the Mann-Whitney U test which was used for analysis of Bederson score and grip test after tMCAO. Differences between more than two groups were analyzed with one-way ANOVA with Dunnett's T3 as post-hoc test using SPSS 21. P-values <0.05 were considered statistically significant with: not significant (ns), $p > 0.05$; *, $p < 0.05$; **, $p < 0.01$; ***, $p < 0.001$.

4. Results

4.1. Multiphoton intravital microscopic analyses of thrombopoiesis and proplatelet formation

Recent developments in imaging methods allow the observation of dynamic cellular events *in vivo* using MP-IVM.[57,59] Megakaryopoiesis and thrombopoiesis have been studied intensively, but the exact mechanisms that control platelet generation from MKs remain poorly understood, mainly due to the inaccessibility of MKs in their natural BM environment. Therefore, MP-IVM is a helpful tool to study thrombopoiesis and proplatelet formation *in vivo*.

4.1.1. Establishment of multiphoton intravital microscopy of the murine bone marrow and brain

The flat bones forming the calvaria of the murine skull contain BM, which is macroscopically visible. Imaging of the BM in the frontoparietal skull without surgical manipulation of the bone is achievable, since the thin layer of bone covering the BM cavities is sufficiently transparent.[196] In order to study thrombopoiesis by MP-IVM, an *in vivo* imaging protocol had to be established first. Crucial steps in the establishment of the MP-IVM protocol involved the immobilization of the mouse, thinning of the skull for transcranial imaging, characterization of fluorescent markers and reporter mice and visualization of dynamic processes using one laser.

For the *in vivo* imaging set-up, several methods were tested, including rings from agarose and plastic to spread the skin of the skull in combination with a stereotactic holder,[234] but the metal plate skull holder provided the best result in terms of stable fixation. The mouse was placed on a customized plate equipped with a skull holder to immobilize its head, thereby allowing imaging of the BM without movement artefacts. The skull holder was fixed onto the mouse's skull and the region of interest was exposed by a circular hole in the metal plate, the imaging window (Figure 8).

To visualize the cortical blood vessels and the mouse brain *in vivo*, a thinned skull cranial window was used. This transcranial imaging method allows the visualization of fluorescently labeled blood vessels, neurons, microglia and astrocytes.[234] The procedure involves thinning of the skull by removing the external layer of the compact bone and the spongy bone, leading to an optically transparent cranium.
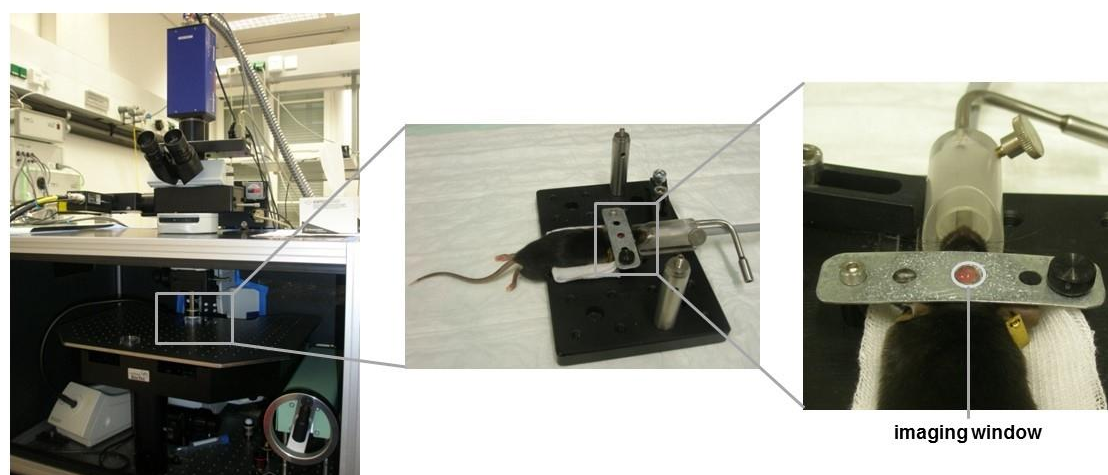
Figure 8. *In vivo* imaging set-up to study thrombopoiesis by multiphoton intravital microscopy. For *in vivo* visualization of the bone marrow (BM) or the brain by multiphoton intravital microscopy (MP-IVM, left panel), the mouse was placed on a customized plate equipped with a skull holder to immobilize its head (middle panel). The skull holder was fixed onto the mouse's skull and the region of interest was exposed by the imaging window (right panel).
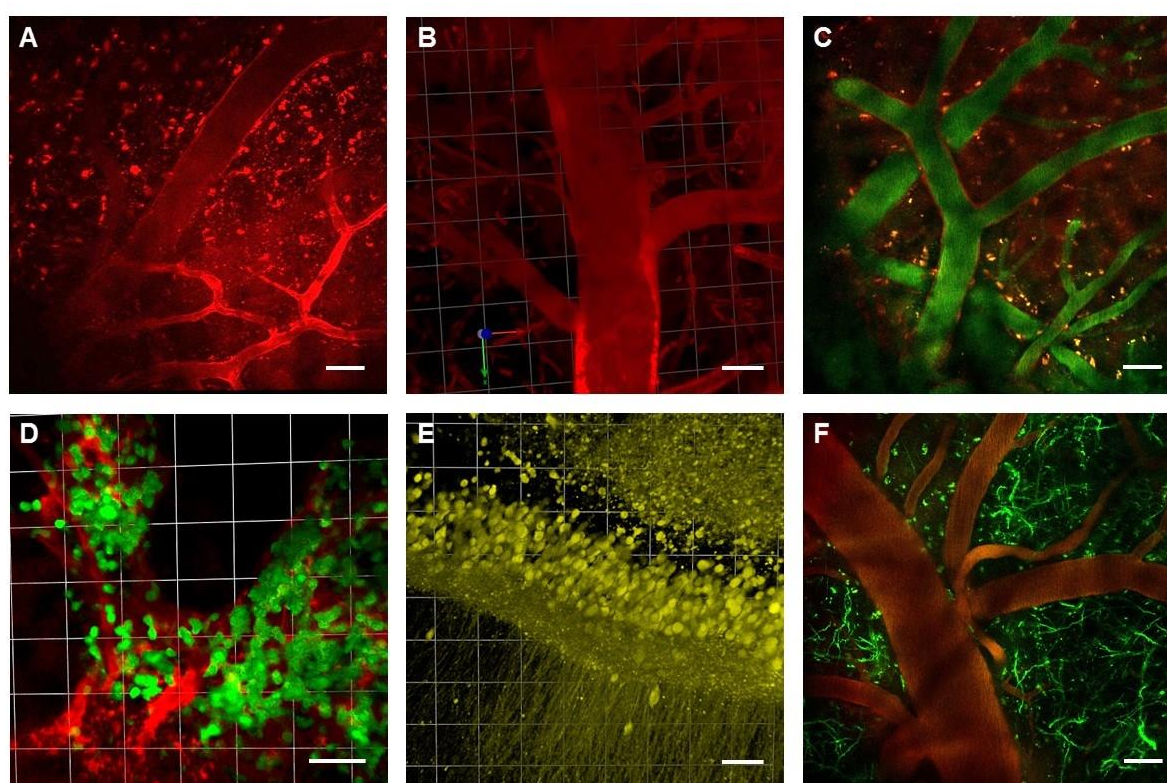

Figure 9. Characterization of fluorescent markers and reporter mice. (A) Staining of the endothelium in the brain of *Flk1-mCherry*^{+/-} mice (red). **(B)** Tetramethylrhodamine dextran marks the plasma of the meningeal blood vessels (red). **(C)** Transcranial imaging of the *Tie2-Cre/R26-tdRFP*^{+/-} mice showed a strong staining of the endothelial lining (red), whereas FITC-BSA provided intraluminal staining (green). **(D)** Macrophages and neutrophil granulocytes (green) are clearly visible in *Lys-eGFP*[+/ -] mice. Blood vessels were stained with tetramethylrhodamine dextran (red). **(E)** *Thy1-eGFP*^{+/-} mice are used to visualize neurons *ex vivo* (yellow) in a brain slice or **(F)** *in vivo* (green). Blood vessels were stained with tetramethylrhodamine dextran (red). Scale bar 50 μm.

Upon mouse preparation, several plasma and endothelial markers were tested to visualize and characterize the vascular anatomy in the BM and the brain. Tetramethylrhodamine dextran and FITC-BSA provided an intense intraluminal staining and only minimal extravasation of the substances was observed (Figure 9B,C,D,F). An anti-endoglin antibody was used for staining of the endothelium (Figure 12, Video 1). In addition, a number of reporter mouse lines were analyzed. Reporter mice are transgenic mice, that express fluorescent proteins under the control of a specific promoter to ensure that only the desired cell type expresses the fluorescent protein. They can be used for visualizing these specific cells *in vivo*.[235] The *Flk1-mCherry*[+/- 221] and *Tie2-Cre/R26-tdRFP*[+/- 222] mice showed a strong staining of the endothelial lining (Figure 9A,C). Besides reporter mice for endothelial cells, reporters for macrophages and neutrophil/granulocytes (*Lys-eGFP*[+/- 224]), neurons (*Thy1-eGFP*[+/- 225]) and MKs and platelets (*CD41-YFP*[223]) were analyzed using MP-IVM (Figure 9D-F, Figure 11A).
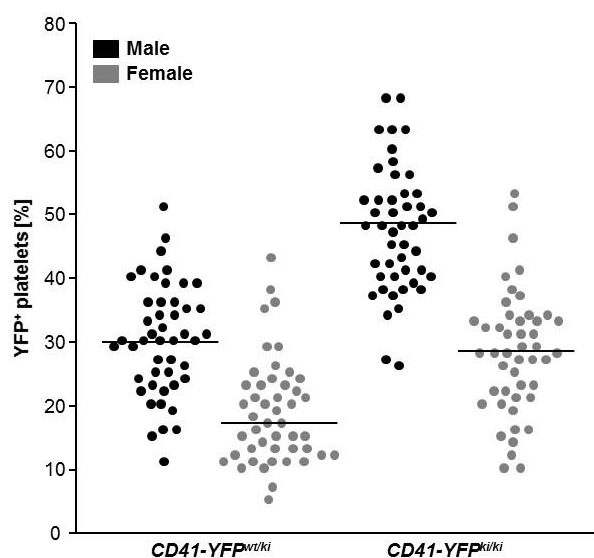

Figure 10. A subset of platelets is YFP-positive in *CD41-YFP* mice. The percentage of YFP-positive platelets in whole blood was measured by flow cytometry in *CD41-YFP*[wt/ki] and *CD41-YFP*[ki/ki] mice. Each symbol represents one animal. The lines represent the median value.

The *CD41-YFP* mouse line was developed to allow *in vivo* imaging of megakaryopoiesis.[223] The mice expressing yellow fluorescent protein (YFP) in MKs and platelets specifically were generated by insertion of the gene encoding YFP (*eyfp*) by homologous recombination into embryonic stem cells at the transcriptional start site of the *GpIIb* locus. To analyze the YFP expression in platelets, the percentage of YFP-positive platelets in whole blood was measured by flow cytometry (Figure 10). In both *CD41-YFP*[wt /ki] and *CD41-YFP*[ki/ki] mice, only a subset of the platelets was YFP-positive, confirming previous data by Zhang *et al.*.[223] Large variations between individual animals were observed and the proportion of YFP-labeled platelets was gender-dependent. The male *CD41-YFP*[wt/ki] mice had a median value of 30% YFP-positive platelets, whereas the female heterozygous mice only contained 17% YFP-positive platelets. The lower percentages of YFP-positive platelets in female mice were also found in the *CD41-YFP*[ki/ki] mice, although the proportion of YFP-labeled platelets was higher

compared to the *CD41-YFP^wt/ki* mice with 48% and 28% in male and female mice, respectively. The YFP-positive platelets from the *CD41-YFP^wt/ki* mice did not have a reduced life span (data not shown). In the *CD41-YFP^ki/ki* mice, a bleeding phenotype was observed, probably due to the lack of the αIIbβ3 receptor complex. YFP-positive platelets were also detected *in vivo* by MP-IVM of the BM (Figure 11A). Since only a subset of the MKs and platelets was YFP-labeled, Thpo treatment or platelet depletion were required to enhance megakaryopoiesis and thereby increase the number of labeled MKs within the BM. To improve cell labeling without the necessity to use Thpo treatment or platelet depletion, other staining methods using fluorophore-conjugated antibodies were tested. *In vivo* labeling targeting the MK- and platelet-specific vWF receptor subunit CD42a (GPIX), and not CD41 (GPIIb) as anti-CD41 antibodies cause thrombocytopenia[210], was used to stain the entire MK population in the BM. The optimal staining was achieved using Alexa 488-labeled anti-GPIX antibody derivatives, leading to the visualization of MKs in the BM and single platelets within the circulation *in vivo* (Figure 11B,C). In addition, using the Alexa 488-labeled anti-GPIX antibody derivatives, platelet thrombus formation in the meningeal vessels *in vivo* could also be observed (Figure 11D).
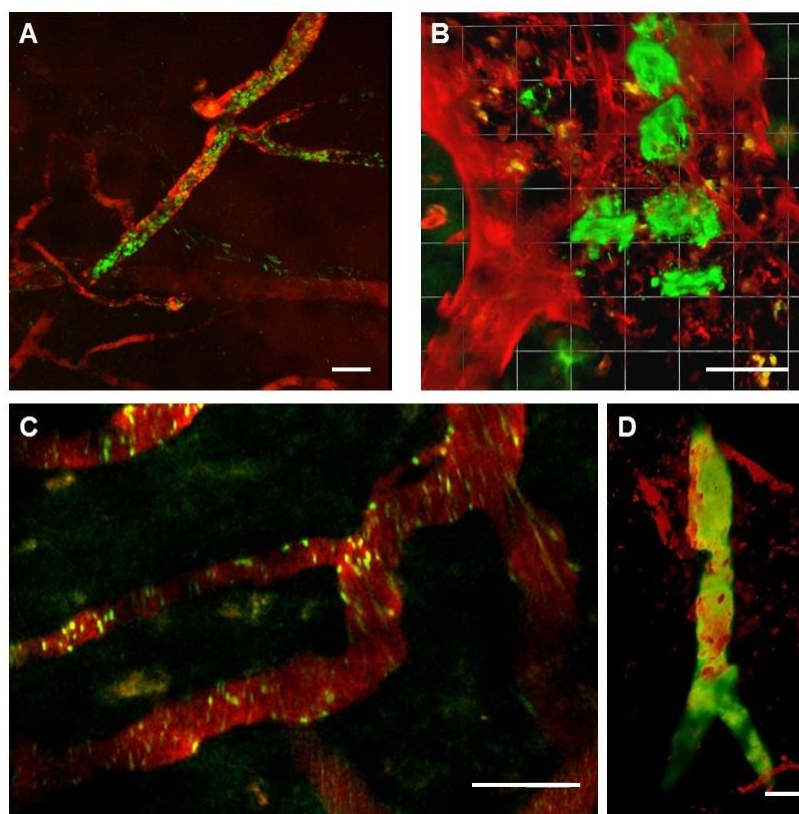

Figure 11. MP-IVM of megakaryocytes within the bone marrow and of platelets in the circulation. (A) YFP-positive platelet aggregates (green) in *CD41-YFP^wt/ki* mice were detected *in vivo*. **(B)** Megakaryocytes (MK, green) were labeled using Alexa 488-labeled anti-GPIX antibody derivatives. **(C)** Single platelets (anti-GPIX, green) were visualized in the cortical blood vessels. **(D)** 3D reconstruction of a thrombus (anti-GPIX, green) in a meningeal vessel. Blood vessels were stained with tetramethylrhodamine dextran (red). Scale bar 50 μm.

Since the MP-IVM was equipped with one Ti:Sa laser and dynamic cellular processes were to be observed, a fixed excitation wavelength needed to be used to excite different fluorescent molecules at the same time to obtain dual-color fluorescence.[236] Several combinations of fluorescent proteins and reporter mice were tested to achieve optimal imaging of different cell types while using one excitation wavelength. For the visualization of MKs/platelets and blood vessels at the same time, a combination of anti-GPIX-Alexa 488 antibody derivatives and tetramethylrhodamine dextran provided the best result. In addition, to stain the endothelial lining, anti-endoglin-Alexa 594 was used. Consequently, an imaging method was established to monitor the dynamic process of proplatelet formation in blood vessels within the BM of the murine skull in real-time and *in vivo*. MKs extending proplatelet-like protrusions into the microvessels of the BM, which were sheared off in the blood stream, were identified *in vivo* (Figure 12, Video 1).
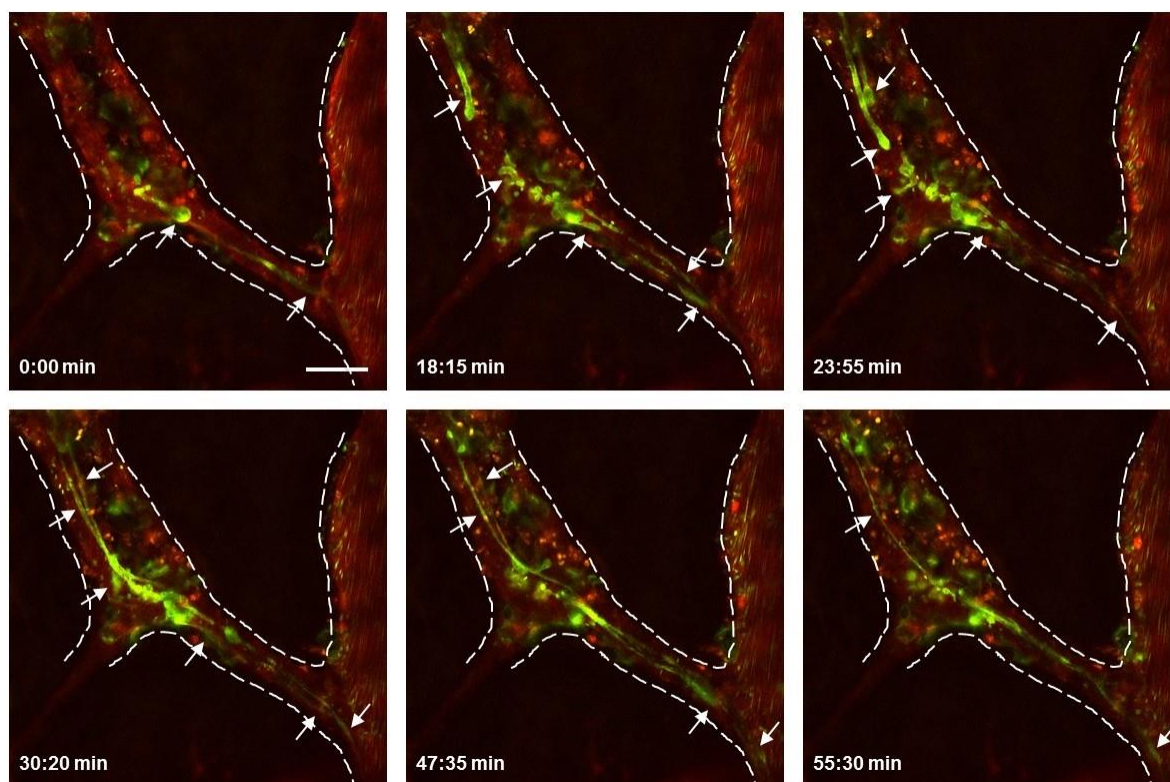

Figure 12. *In vivo* proplatelet formation in the murine bone marrow. Proplatelet formation by MKs can be observed by MP-IVM. The MKs/platelets were stained using anti-GPIX-Alexa 488 antibody derivatives (green). The blood vessels were labeled with tetramethylrhodamine dextran (lumen, red) and anti-endoglin-Alexa 594 (endothelium, red). The white dashed lines represent the outline of the blood vessels. Scale bar 50 μm.

4.1.2. The role of Profilin1, TRPM7 and RhoA in thrombopoiesis *in vivo*

Platelets are constantly produced by their BM precursors *in vivo* and MP-IVM allows real-time visualization of proplatelet formation in the BM of living animals. However, the mechanisms that control platelet generation and the release from BM MKs remain poorly understood. It is known that proplatelet formation requires substantial cytoskeletal rearrangements. Therefore, the role of three proteins involved in these cytoskeletal rearrangements, Profilin1, TRPM7 and RhoA, was studied in thrombopoiesis *in vivo*.

4.1.2.1. Profilin1-deficiency leads to premature platelet release into the bone marrow

Wiskott–Aldrich syndrome (WAS) is a X-linked disease caused by mutations in the *WAS* gene and is characterized by immunodeficiency, eczema and microthrombocytopenia.[237] Platelets from WAS patients display defective microtubule reorganization.[217] Profilin1 is a key regulator of actin turnover, but also interacts with other proteins, including the WAS protein (WASp)/WASp-interacting protein (WIP) complex. MK and platelet-specific Profilin1-deficiency mimics the MK and platelet phenotype of WAS patients.[217] MP-IVM of *Pfn1*$^{fl/fl, Pf4-cre+/-}$ (*Pfn1*$^{-/-}$) mice revealed that the majority of the *Pfn1*$^{-/-}$ MKs released platelets prematurely into the BM compartment next to the sinusoids (arrowheads in Figure 13B, Video 3). The premature platelet release was, however, not caused by defective proplatelet formation, as proplatelets were observed in both Wt and *Pfn1*$^{-/-}$ mice (indicated by arrows in Figure 13A,B, Video 2,3). These results suggest that the microthrombocytopenia in *Pfn1*$^{-/-}$ mice is caused by, besides accelerated platelet clearing by macrophages[217], the premature platelet release into the BM, revealing Profilin1 as a key regulator of thrombopoiesis.
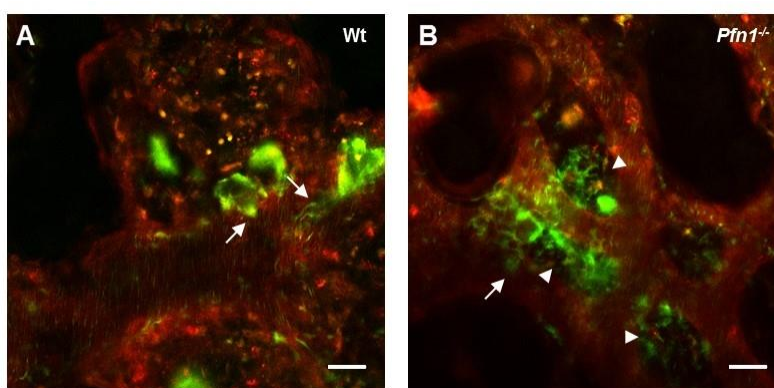

Figure 13. Premature platelet release into the bone marrow in *Pfn1*$^{-/-}$ mice. (A,B) MP-IVM of BM MKs in the murine skull revealed unaltered proplatelet formation into the BM sinusoids (arrows), but also prematurely released platelets in Pfn1-deficient mice (arrowheads). MKs and platelets were stained with anti-GPIX-Alexa 488 (green) and blood vessels were stained with tetramethylrhodamine dextran (lumen, red) and anti-endoglin-Alexa 594 (endothelium, red). Scale bar 25 μm. (Bender, Stritt *et al.*, *Nat Commun.* 2014)[217]

4.1.2.2. TRPM7-deficiency causes impaired proplatelet formation

Mg^{2+} plays a pivotal role in platelet function. The TRPM7 channel is a ubiquitously expressed, constitutively active ion channel, which is highly selective for divalent cations, such as Mg^{2+}, Ca^{2+} and Zn^{2+}. TRPM7 plays an essential role in Mg^{2+} homeostasis, cell motility, proliferation and differentiation and is critical for early embryonic development.[77] A human genetic variant in *TRPM7* caused macrothrombocytopenia.[238] This phenotype was strongly resembled by the *Trpm7$^{fl/fl, Pf4-cre+/-}$* (*Trpm7$^{-/-}$*) mice, where impaired channel function of TRPM7 in MKs also resulted in macrothrombocytopenia. *Trpm7$^{-/-}$* mice were analyzed by MP-IVM and decreased proplatelet formation *in vivo* was observed compared to Wt mice (Figure 14A, Video 4). Furthermore, MKs in *Trpm7$^{-/-}$* mice formed short and bulky proplatelet protrusions that remained attached to the MK cell body during the observation period (arrowhead in Figure 14B, Video 5). The impaired proplatelet formation was mainly caused by cytoskeletal alterations due to increased actomyosin contractility and could be rescued by either Mg^{2+} supplementation or chemical inhibition of NMMIIA activity.[238] These findings reveal that the regulation of Mg^{2+} homeostasis in MKs by TRPM7 plays a critical role in thrombopoiesis.
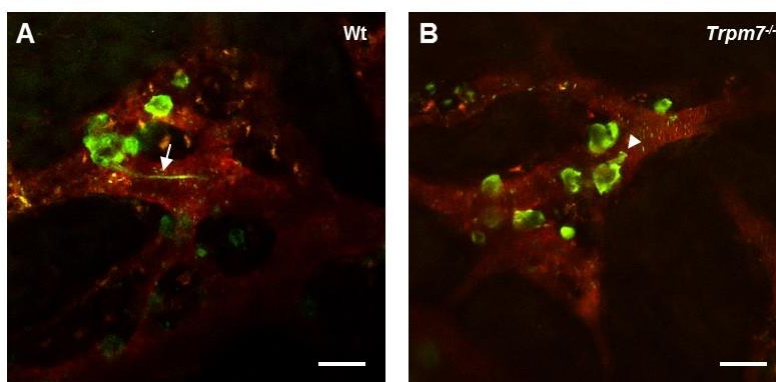

Figure 14. Impaired proplatelet formation in the bone marrow of *Trpm7$^{-/-}$* mice. (A) Normal proplatelet formation by MKs in the BM of Wt mice was observed by MP-IVM (arrow). **(B)** MKs in *Trpm7$^{-/-}$* mice formed short and bulky proplatelet protrusions *in vivo* (arrowhead). MKs and platelets were stained with anti-GPIX-Alexa 488 (green) and blood vessels were stained with tetramethylrhodamine dextran (lumen, red) and anti-endoglin-Alexa 594 (endothelium, red). Scale bar 50 μm. (Stritt *et al.*, *Nat Commun.* 2016)[238]

4.1.2.3. RhoA-deficiency induces megakaryocyte mislocalization and transmigration

Small GTPases of the Rho family are known to be critical regulators of cytoskeletal rearrangements in platelets.[108,109] Studies in MK and platelet-specific RhoA-deficient (RhoA$^{fl/fl, Pf4-cre+/-}$ (*RhoA$^{-/-}$*)) mice showed that RhoA signaling is essential for platelet shape change and the observed macrothrombocytopenia suggests that RhoA is necessary for platelet production.[111] In cryo-sections of the femoral BM of *RhoA$^{-/-}$* mice, a mislocalization of the MKs was observed and on average 30% of the MKs were detected inside the BM sinusoids. The remaining MKs were mostly found in direct contact with the BM sinusoids (Dütting *et al.*, unpublished). MP-IVM was used for dynamic visualization of MK localization and proplatelet formation in the BM of *RhoA$^{-/-}$* mice (Figure 15, Video 6,7). MKs in Wt mice were found near the sinusoids or in close sinusoidal contact and released long proplatelets into the blood vessel (arrows in Figure 15A, Video 6). In sharp contrast, MKs in *RhoA$^{-/-}$* mice were able to completely transmigrate from the BM into the sinusoidal vascular bed (arrowheads in Figure 15B, Video 7) or were stably present inside the BM sinusoid for up to 50 min (star in Figure 15B). These observations indicate that RhoA negatively regulates MK localization towards BM vascular sinusoids and acts as a central regulator of thrombopoiesis by inhibiting MK transmigration.
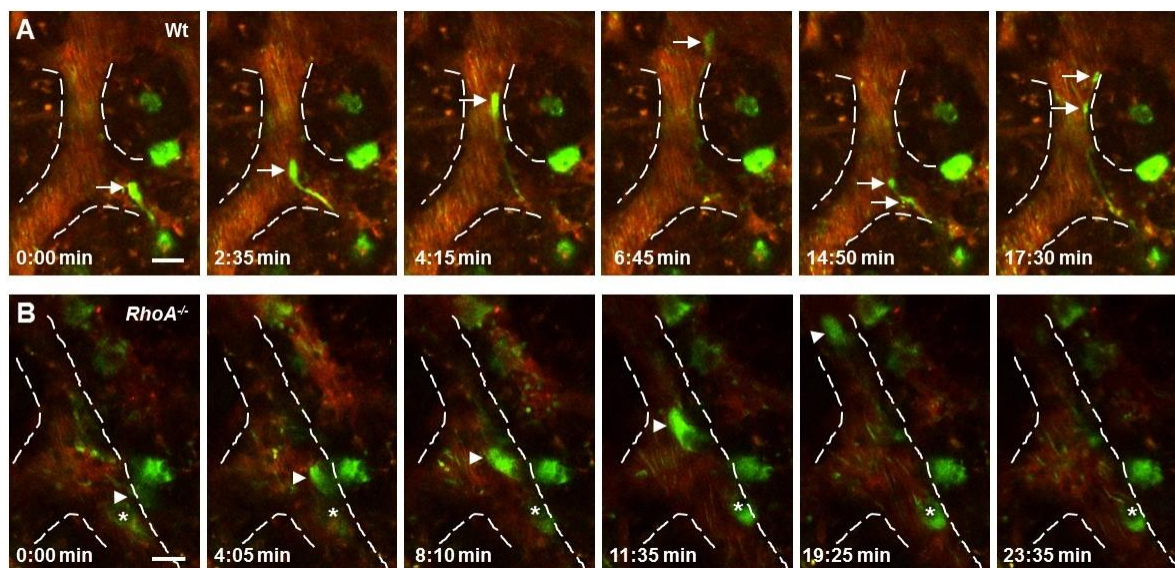

Figure 15. Megakaryocyte mislocalization and transmigration in *RhoA$^{-/-}$* mice. (A) MP-IVM of BM MKs in the murine skull of Wt mice revealed unaltered proplatelet formation into the BM sinusoids (arrows). **(B)** MKs in *RhoA$^{-/-}$* mice transmigrated into the sinusoidal vascular bed (arrowheads) or adhered to the vessel wall inside the BM sinusoid (star). MKs and platelets were stained with anti-GPIX-Alexa 488 (green) and blood vessels were stained with tetramethylrhodamine dextran (red). The white dashed lines represent the outline of the blood vessels. Scale bar 25 μm.

4.2. Thrombopoiesis is spatially regulated by the bone marrow vasculature

Currently, it is thought that blood cell precursors migrate from the endosteal niche towards the vessel sinusoids during maturation.[18,39,45,239,240] Yet, this concept is much less supported by direct evidence, but mostly based on evaluation of cell populations present at distinct spatiotemporal niches. The exact location of MK maturation, the functional significance of MK migration towards the vascular niche for thrombopoiesis and the exact mechanisms of platelet generation from MKs still remain ill-defined.

4.2.1. Megakaryocytes in the bone marrow are largely sessile

In contrast to the current concept of megakarypoiesis, Junt *et al.* reported that MKs are overall sessile in the BM when compared to lymphocytes and they are mostly found in close proximity to blood vessels.[57] To study MK migration in the BM under steady-state conditions, mouse skull BM was analyzed by MP-IVM and single MKs were tracked over time (Figure 16). MKs were sessile with an instantaneous velocity of 0.39 ± 1.16 μm/s (median $\pm$ SD) and displayed either a vibrating movement or shifted their center of mass during proplatelet formation at BM sinusoids, which is in line with the previous study by Junt *et al.*[57] MK mobility was assessed by analyzing MK tracks based on an anomalous diffusion model. The mean squared displacement (MSD = $<r^2(t)> = 4Dt^\alpha$) of the MKs was calculated for different time scales t as the MSD can be directly linked to the (time scale dependent) diffusion coefficient D and the anomalous diffusion exponent α. For MK migration, low values (median $\pm$ SD) for MSD (0.14 ± 0.69 μm^2) and α (0.42 ± 0.29) were found, indicating a slow and subdiffusion-like movement in a highly crowded environment (Figure 16C), demonstrating hindered-diffusion-like movement of MKs due to random trapping in the BM.
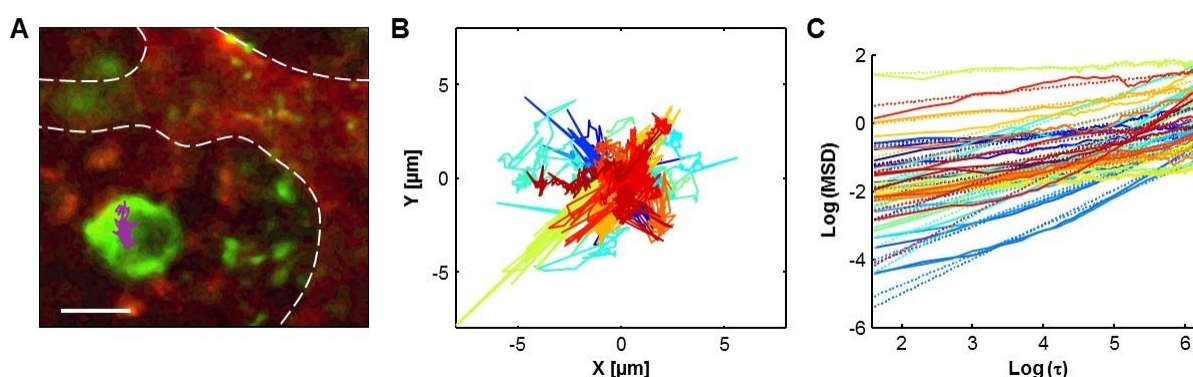

Figure 16. Cell tracking reveals a minimal displacement of megakaryocytes *in vivo*. (A) One representative track (magenta on the green MK) is displayed with 5x magnification. Scale bar 20 μm. **(B)** MK tracking traces. **(C)** Mean squared displacement analysis of individual MKs for different time scales. The slopes of fitted lines represent the corresponding alpha coefficients. Each color represents one MK.

4.2.2. The majority of megakaryocytes is in direct contact with the vasculature

Since MP-IVM only has a limited field of view and most studies on megakarypoiesis and thrombopoisesis have been performed on BM of the long bones, especially femur, tibia and sternum, immunohistochemical analyses of cryo-sections[231] of murine femora (Figure 17A) and sterna (Figure 17B) were performed in addition. Under steady-state conditions, a homogeneous distribution of CD41 (GPIIb) positive cells, a highly expressed early marker for the MK lineage, was found.[41] Surprisingly, MKs were found even in close contact to endosteal zones (indicated by dark regions surrounding the BM, Figure 17A,B). MK diameters were comparable in sternum and femur (22.19 ± 0.14 μm vs. 22.57 ± 1.44 μm) and in both, the majority of MKs ($68.2 \pm 6.9\%$ vs. $73.1 \pm 5.2\%$) was found in direct contact with the vessel, which is in agreement with previous studies.[57,58] Complementary cryo-sections confirmed that more than 95% of all CD41-positive MKs were positive for CD42a and both groups showed identical MK diameters and percentage of vessel-association. The MK-specific tubulin isoform $\beta1$[241] was used as a marker for mature MKs (Figure 17C). As expected, double-positive MKs were larger than $\beta1$-tubulin-negative CD41-positive cells (23.53 ± 6.23 μm vs. 20.19 ± 4.24 μm, Figure 17D). Surprisingly, however, this was not accompanied by altered MK distribution, as the majority of both $\beta1$-tubulin negative and positive cells were in direct contact with the vessel (66.9 ± 4.5 vs. $73.9 \pm 4.9\%$; Figure 17E) and the vessel distant MKs were distributed similarly throughout the BM (Figure 17F).

4.2.3. Establishment of light-sheet fluorescence microscopy of the murine bone marrow

MP-IVM revealed that MKs in the BM are largely sessile and the analysis of cryo-sections of bones showed that the majority of MKs is localized in close contact with the sinusoid. These methods allow studies on megakaryopoiesis and thrombopoiesis in the BM with sufficient resolution, however, they only cover a small field of view, have a limited penetration depth and provide restricted 3D information. Facing the opaque and dense bone tissue, quantitative imaging of the MKs in their intact 3D environment would be challenging, but of great interest, since little is known on the architecture of the BM and the overall MK distribution. Therefore, LSFM of intact, murine bones was established. Crucial steps in the establishment of the LSFM protocol were cell staining, tissue fixation and dehydration, optical clearing, visualization of the samples by optical sectioning using LSFM, semi-automated image processing and quantitative data analysis (Figure 18).
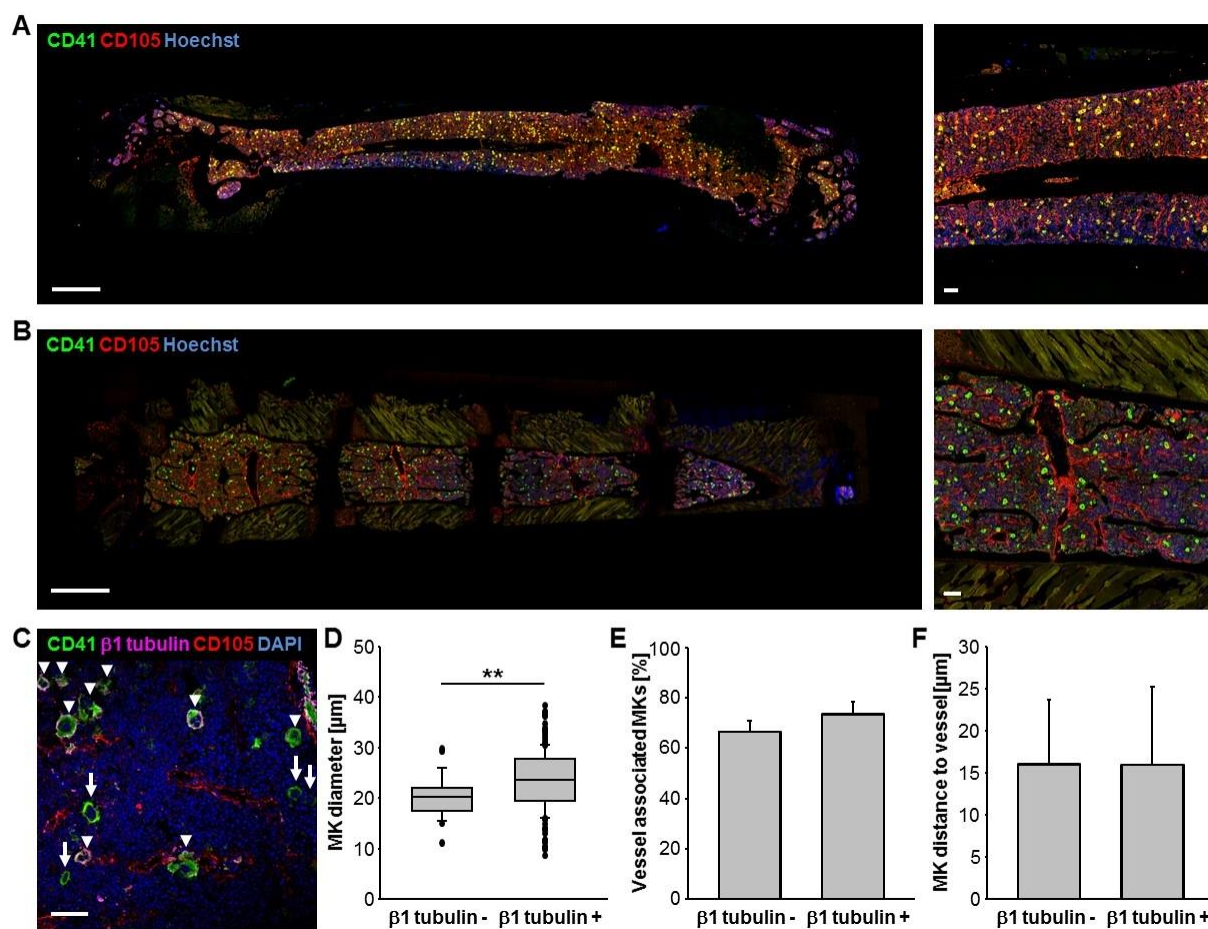
Figure 17. Homogeneous distribution of megakaryocytes in the bone marrow. MKs (CD41^{+}, green) in cryo-sections of whole-length femur **(A)** and sternum **(B)** showing vessels (CD105^{+}, red) and nuclei (Hoechst33258, blue). Scale bar 1 mm. Right panels display a higher magnification (scale bar 100 μm). **(C)** MKs were counter-stained for β1-tubulin (magenta, indicated with arrowheads - in contrast to β1[-] MKs which are indicated with arrows). Scale bar 20 μm. These mature MKs were increased in size **(D)**, but their distribution was similar between β1-tubulin negative and positive cells as depicted by the percentage of vessel-associated MKs **(E)** and the MK-vessel distance of non-vessel associated MKs **(F)**. Bar graphs represent mean ± SD. **, $p < 0.01$.
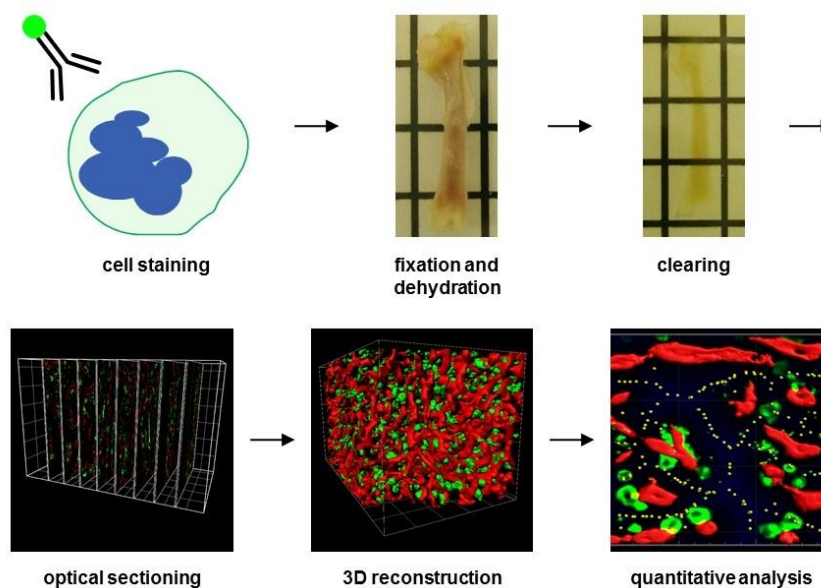
Figure 18. Establisment of light-sheet fluorescence microscopy of the murine bone marrow. For the 3D visualization of the BM of intact murine bones with a cellular resolution and without cutting artefacts, a protocol was established. This protocol involves cell staining, tissue fixation and dehydration, optical clearing, visualization of the samples by optical sectioning using light-sheet fluorescence microscopy (LSFM), semi-automated image processing and quantitative data analysis.

First, cell labeling protocols for the visualization of MKs and blood vessels had to be established. *Ex vivo* and *in vivo* staining protocols were tested, but to avoid staining artefacts due to insufficient antibody penetration *in situ*, *in vivo* labeling of MKs by anti-GPIX antibody derivatives was used (Figure 19).

Several fluorescent conjugates were tested, including Alexa 488, Alexa 546, Alexa 647 and Alexa 750 (Figure 19A,B). The optimal MK staining was achieved using Alexa 750-labeled anti-GPIX antibody derivatives, since excitation of the near-infrared fluorophore led to a low autofluorescence signal and a high signal-to-noise ratio (Figure 19C,D). For staining of the endothelium, Alexa 647-labeled anti-endoglin antibodies were used (Figure 19C,D).

LSFM uses a thin sheet of light to illuminate and optically section the tissue specimen. The tissue has to be transparent to allow penetration of the laser light sheet. To obtain optically transparent samples, a clearing protocol for complete and intact bones had to be established (Figure 20). Only clearing protocols for soft tissues, but not for bones were available and, therefore, different tissue clearing methods had to be tested.[203-205,242] The first step towards tissue clearing was transcardial perfusion of the mice with ice-cold PBS to wash out the blood and ice-cold 4% PFA to fix the tissues. The bones were perfusion-fixed to protect the structure of the tissue. To ensure optimal clearing and reduce scattering effects during the measurements, adherent tissues, such as muscles and connective tissue had to be removed. Upon harvesting of the sterna and femora, the bones were decalcified using EDTA and were dehydrated using either ethanol, methanol (MeOH) or tetrahydrofuran (THF), which

was stepwise replaced by a clearing solution (DBE or BABB). After incubation in the clearing solution, tissue specimens became optically transparent. Dehydration with MeOH followed by clearing with BABB provided the best result compared to bone clearing using THF and DBE (Figure 20).
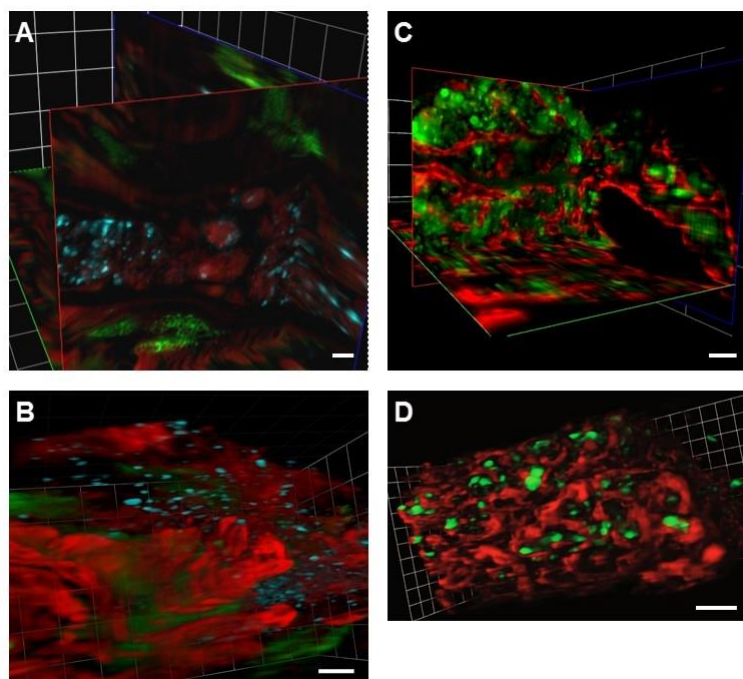

Figure 19. *In vivo* cell labeling for LSFM. 3D reconstructions of the sternum including MKs, which were stained *in vivo* by anti-GPXI antibodies labeled with either Alexa 647 (cyan, **A,B**) or Alexa 750 (green, **C,D**). The endothelium was labeled with anti-endoglin-Alexa 647 (red, **C,D**). Autofluorescence of the tissue was shown in red and green (**A,B**). Scale bar 100 μm.

Initially, a LSFM prototype with 3-color detection was successfully used to map immune processes in intact tissues at cellular resolution[242] and to visualize the BM in intact bones (Figure 21A). However, during the time of this thesis, the LSFM prototype has been further developed by implementing 4-color detection, new sCMOS cameras and a filterwheel. As a result, resolution, contrast and imaging speed of larger images were enhanced, whereas photobleaching effects were further reduced, improving the image quality dramatically (Figure 21B).
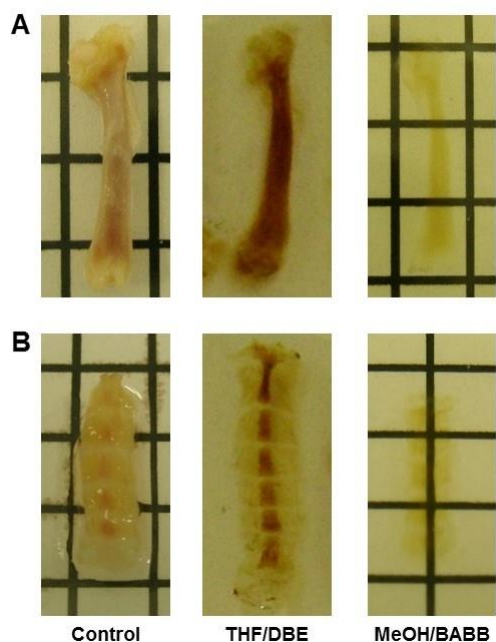
Figure 20. Optical clearing of bone tissue. Femur **(A)** and sternum **(B)** before (left panel) and after clearing (middle and right panel) using the combination of either tetrahydrofuran (THF) and dibenzyl ether (DBE) or methanol (MeOH) and benzyl alcohol benzyl benzoate (BABB).

To finally obtain quantitive data including MK number, volume and localization, the multicolor LSFM stacks were processed and analyzed by FIJI[232] and Bitplane Imaris® 7.7.2 (Figure 21, Video 8). Image processing was performed by Oğuzhan Angay and Patrick Schmithausen. Data visualization and analysis was performed in three major steps: image preprocessing, segmentation and data extraction. Image preprocessing involved the removal of noise and crosstalk, contrast enhancement, the removal of debris and background subtraction (Figure 21B,C), leading to minimized noise and reduced unspecific signals. Next, MKs and vessels were identified automatically and segmented based on morphology, fluorescence intensity and size. Segmentation of MKs, proplatelets and vessels allowed for their recognition as individual objects (Figure 21D,E,J). Objects were exported to iso-surfaces (Figure 21D,E,K,L) to allow the generation of distance transformation maps to perform vessel interspace analyses (Figure 22D) to obtain quantitive data for further statistical analyses. Since MKs are labeled by antibody staining of the cell surface, the unstained lumen of the MK had to be filled with artificial "soma" (Figure 21F-I). Furthermore, due to size and morphological differences of MKs, sequential segmentation was performed using two MK populations: MKs with a spherical cell diameter ≥ 20 μm (green, Figure 21K) and MKs with a spherical cell diameter of 10 μm (purple, Figure 21K).

By combining cell staining, optical tissue clearing, microscope optimization and semi-automated image processing, a method for the 3D visualization of the BM of intact murine bones with a cellular resolution and without cutting artefacts was, for the first time, established (Figure 21L).
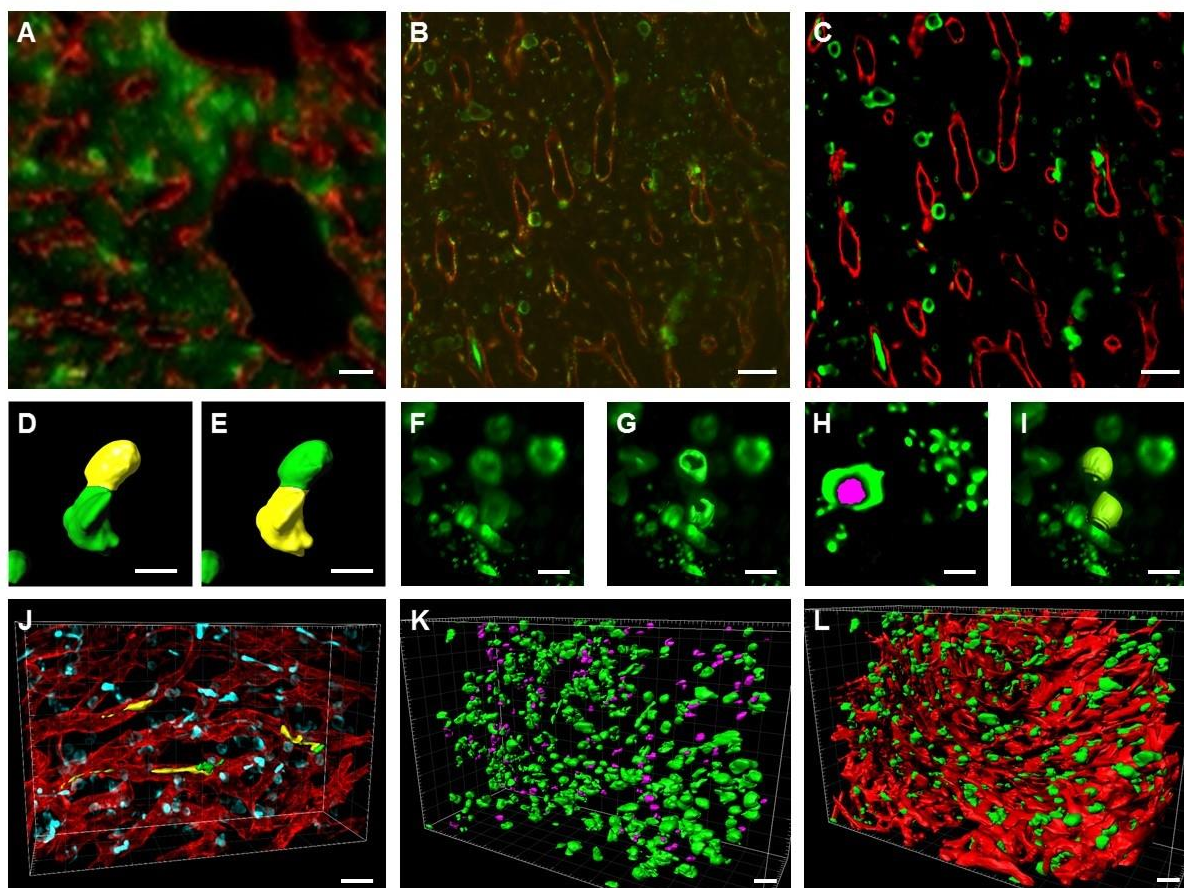
Figure 21. LSFM image processing and analysis. Imaging of the BM in intact bones **(A)** was improved by optimization of the microscope design **(B)**. **(C)** Image preprocessing involved the removal of noise and crosstalk, contrast enhancement and background subtraction. Segmentation of MKs (green and yellow, **D,E**), proplatelets (yellow, **J**) and vessels (red, **J**) allowed for their recognition as individual objects. **(F-I)** The unstained lumen of the MK had to be filled with artificial "soma". **(K)** Sequential segmentation was performed using two MK populations. **(L)** 3D visualization of the BM of intact murine bones with a cellular resolution showing MKs (green) and blood vessels (red) was achieved. Scale bar A-C, J-L 50 μm. Scale bar D-I 20 μm.

4.2.4. Megakaryocytes are homogenously distributed throughout the bone marrow

The femur comprises the epiphysis and diaphysis and stacks were recorded in the diaphysis, the shaft of the long bone (Figure 20A). The sternum consists of several segments containing BM and stacks were recorded per BM segment (Figure 20B). Optical sectioning of the sternum segments revealed a big central vessel in each BM segment. Femora contained a central vessel along the inter-epiphyseal axis. The sinusoids in femora appeared more aligned and structurally organized along the bone axis compared to the sinusoids in sterna. LSFM imaging of the cleared intact femora (Figure 22A) and sterna (Figure 22B) transversally allowed visualization of MKs with a resolution (<2 μm) that was sufficient to identify proplatelets (Figure 22C). The 3D reconstructions of LSFM data enabled the analysis of 30-fold more MKs per bone sample compared to conventional cryo-sections and revealed a surprisingly dense blood vessel network with an average maximal vessel-to-vessel

distance of only 43.18 ± 12.72 µm (Figure 22D). Given that the mean MK-diameter was 20.36 ± 8.19 µm (Figure 22E), the spatial distribution of MKs was highly restricted by the vasculature. Consequently $79.3 \pm 5.1\%$ of all MKs localized adjacent to the blood vessels (Figure 22G), values which are higher than those obtained with cryo-sections.
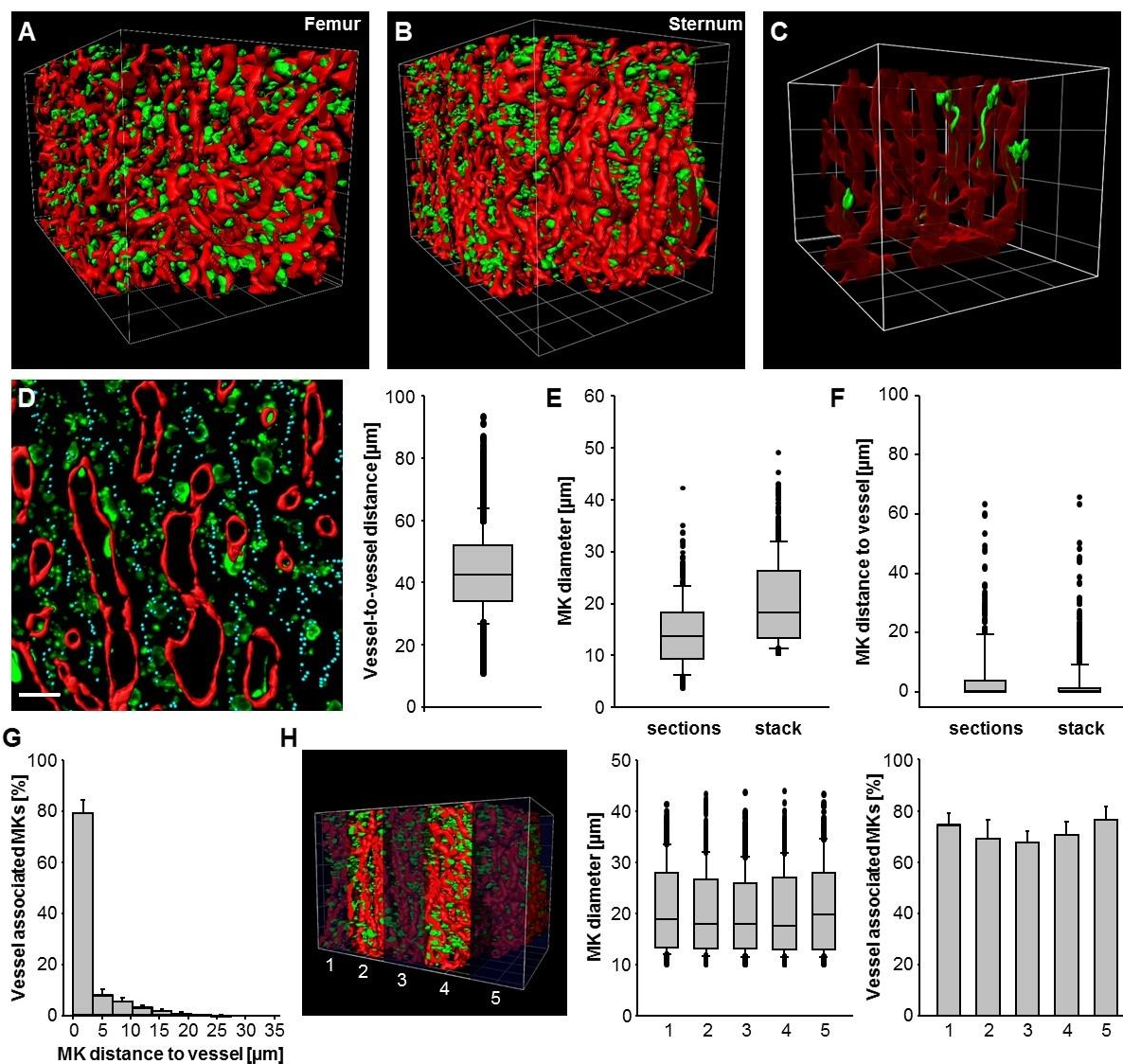

Figure 22. Dense blood vessel network and homogeneous distribution of megakaryocytes in reconstructed bone marrow using LSFM. 3D reconstructions of the BM of femur **(A)** and sternum **(B)** with MKs (green) and blood vessels (red). **(C)** These reconstructions enable visualization of proplatelets in intact BM. **(D)** Reconstruction of sternal BM revealed a dense blood vessel network with limited space for MKs shown by vessel-to-vessel distances and average MK diameter **(E)**. Cyan dots represent the middle between two adjacent vessels. Scale bar 50 µm. **(E,F)** Comparison of the MK diameter and MK-vessel distance in cryo-sections and LSFM stacks. **(G)** Most MKs are localized adjacent to sinusoids and **(H)** MK distribution was homogeneous throughout the whole sternum as shown by the percentage of vessel associated MKs and the MK-vessel distance in five different sections of the reconstructed BM. Bar graphs represent mean ± SD; grid size 100 µm.

This is presumably due to the additional structural 3D information, which enables the detection of vessels surrounding each MK in all possible directions and minimizes the underestimation of MK diameters (Figure 22E) and MK-to-vessel contacts (Figure 22F) due to cutting artefacts. Analysis of five equally sized substacks of the sternum did not reveal differences in any analyzed MK parameter (Figure 22H), confirming the conception of a homogeneous MK distribution throughout the complete BM of the entire and intact bone.

4.2.5. Platelet depletion or CXCR4 blockade do not affect megakaryocyte localization

To determine the effects of increased platelet consumption on MK distribution, bones were analyzed upon platelet depletion with anti-CD42b (GPIbα) antibodies that cause rapid Fc-independent platelet clearance (Figure 23A).[210] Interestingly, despite the severe thrombocytopenia in the treated animals (Figure 23B), MK migration and destruction were not observed and the main MK parameters remained grossly unaltered, with only a mild elevation in MK volume at day 3 after platelet depletion, resulting in an increased fraction of vessel-associated MKs (Figure 23C-E). This indicates that even upon high platelet demand, the MK distribution remains overall unaltered, which stands in clear contrast to the current concept that immature MKs migrate towards the vessels.

The chemokine receptor CXCR4 has been shown to modulate MK migration *in vitro* and to contribute to platelet production, especially in the absence of the Thpo-c-Mpl axis.[18,49] Therefore, CXCR4 in wildtype mice was blocked using 5 mg/kg AMD3100 (AMD/Plerixafor), a CXCR4 antagonist, and the effects on MK localization were determined after 24 h. Treatment with AMD3100 resulted in elevated HSC counts (Sca-1^{+}, c-kit[+], Lin^{-} cells) in the peripheral blood after 24 h (not shown), confirming previous results.[243] However, CXCR4 blockade did not modulate MK localization or volume (Figure 23F-H). Similar results were obtained in mice receiving the CXCR4 ligand SDF1 (16 μg/kg) 24 hours before analysis (Figure 23F-H), indicating that despite the relevance of the SDF1-CXCR4 for HSC mobilization,[244] it appears to be negligible for MK (re)localization.

4.2.6. Computational modeling implies a vessel-biased megakaryocyte distribution

High MK numbers and their limited capability of (chemotactic) migration led to the hypothesis that MKs are randomly distributed throughout the BM. To test this hypothesis, computational modeling was performed to identify possible 3D MK distributions matching the data obtained by LSFM. Computational modeling was performed by Mari Gorelashvili. For modeling, the virtual MKs were randomly placed into the intervascular space, with the 3D vasculature serving as a space-restricting scaffold (Figure 24A).
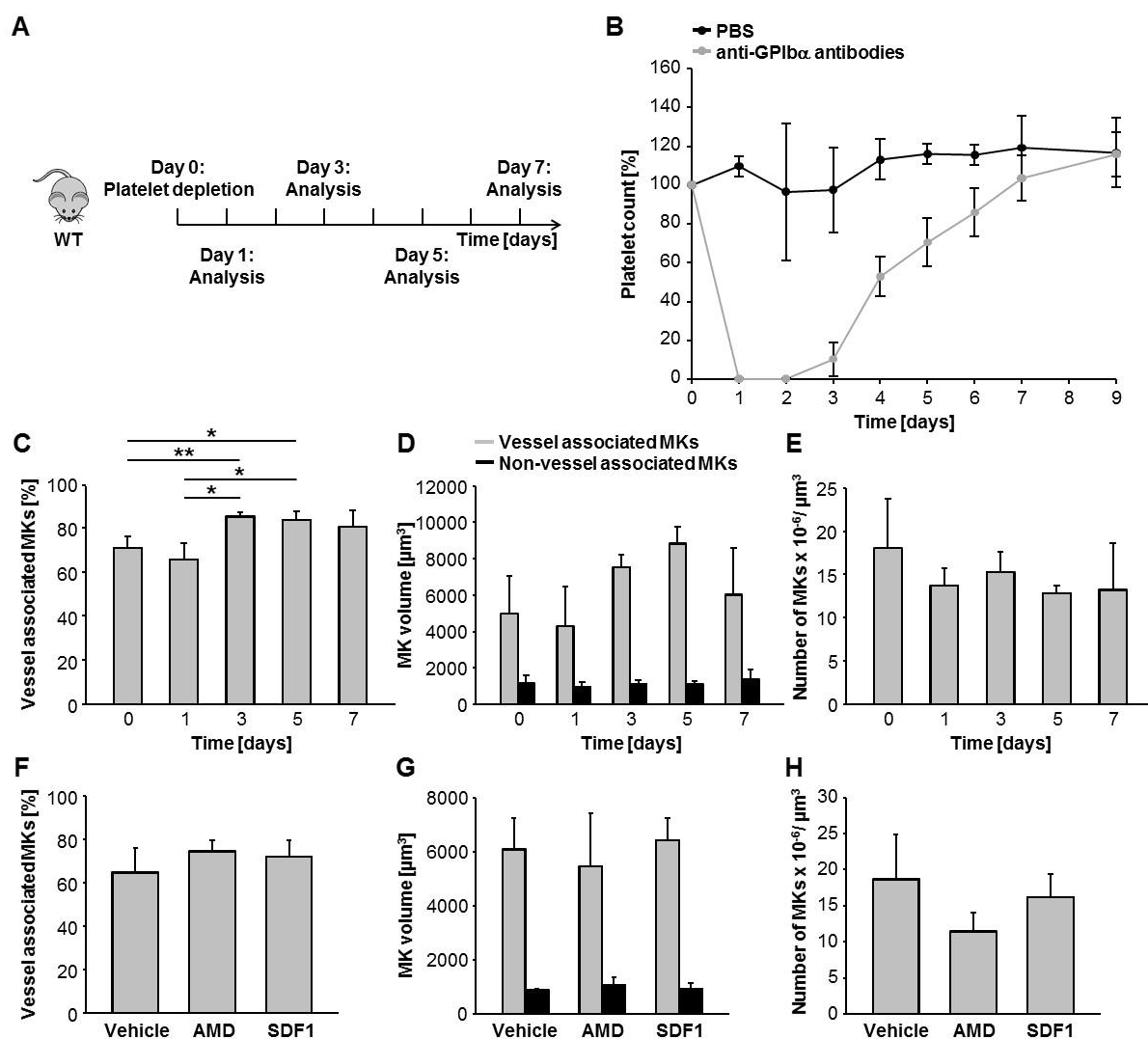
Figure 23. Dysregulated platelet homeostasis does not affect megakaryocyte distribution or migration within the bone marrow. (A) Platelets were depleted using anti-CD42b (GPIbα) antibodies and analysis of sterna was performed on day 1, 3, 5 and 7 after depletion. Day 0 (PBS) served as control. **(B)** Mice displayed severe, but reversible thrombocytopenia. **(C)** Increase in vessel associated MKs upon platelet depletion correlates with an increase in MK-volume of vessel associated (grey bars) but not of non-vessel associated MKs (black bars, **D**). **(E)** MK numbers remain unaltered. Treatment with AMD3100 (AMD) or SDF1 did not modify MK localization **(F)**, MK volume **(G)** or MK numbers **(F)**. Bar graphs represent mean ± SD. *, $p < 0.05$; **, $p < 0.01$.

Since LSFM-derived MKs and vessel isosurfaces were exclusively used, the morphology and size of the modeled MKs and vasculature perfectly reflected the spatial physiological situation. Furthermore, a clear distinction was made between vessel-associated MKs (light green) and non-vessel associated MKs (dark green) in the simulation. The first simulation, a random simulation (SimR) of total MK distribution in the BM, did not reflect the measured results (actual data). Instead, it predicted significantly larger total MK-vessel distances (Figure 24B) and a lower percentage of vessel associated MKs, indicating a non-random, but vessel-biased MK distribution for the LSFM data. The single data stack used for the actual data to compare to the simulation data, displayed 60% of the MKs in association with the

vessels. Therefore, for the next simulation (SimVA), a vast percentage of the MKs (60%) were vessel-associated and the remaining 40% of the MKs were randomly distributed within the intervascular space. When only taking the non-vessel associated MKs into account (dark green in Figure 24), the SimVA, and not the SimR, fully reflects the actual 3D imaging data (Figure 24B). These results indicate that MK localization is vessel-biased, but the non-vessel associated MKs are distributed within the BM in a random fashion. The current concept of megakaryopoiesis involves MK migration and, in that situation, a non-random distribution of non-vessel associated MKs would be expected. In addition, MK localization did not correlate with MK volume of non-vessel associated MKs, pointing towards a random distribution of immature and mature MKs throughout the BM and thereby confirming the absence of MK migration.
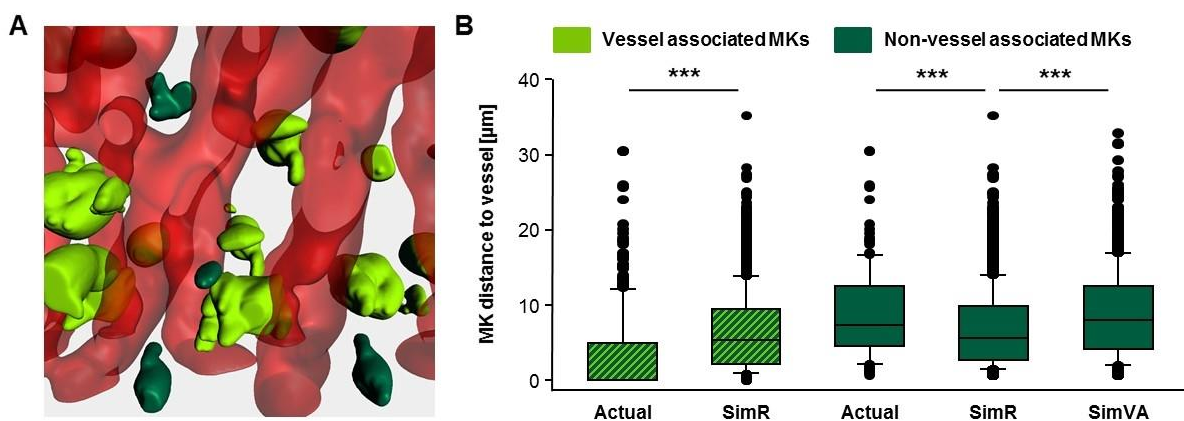

Figure 24. Megakaryocytes display a vessel-biased random distribution. (A) Computational modeling was performed using the 3D vasculature (red) as a space-restricting scaffold. LSFM-derived MK and vessel isosurfaces were used to reflect the spatial physiological situation. Vessel associated MKs are depicted in light green and non-vessel associated MKs in dark green. **(B)** A random MK distribution (SimR) and a vessel-biased random MK distribution (SimVA) were simulated by placing the virtual MKs randomly into the intervascular space with a vast percentage of vessel-associated MKs in SimVA. The MK-vessel distances were measured and revealed a vessel-biased random MK distribution. ***, p<0.001.

4.2.7. Light-sheet fluorescence microscopy as a tool to study thrombopoiesis

LSFM allows the 3D visualization of intact murine bones, but also the quantitative structural analysis of BM components. MP-IVM already revealed that the majority of the *Pfn1*^{-/-} MKs released platelets prematurely into the BM (Figure 13B, Video 3) and therefore *Pfn1*^{-/-} mice were analyzed using LSFM. It was confirmed that MKs of *Pfn1*^{-/-} mice showed increased fragmentation and platelets were prematurely released into the BM compartment (Figure 25A,B). These results demonstrate the potential of LFSM for studying animal models of human disease.

Since a mislocalization of the MKs of *RhoA*$^{-/-}$ mice was observed using cryo-sections and MP-IVM (Dütting *et al.*, unpublished, Figure 15B, Video 7), the overall MK distribution in the intact murine BM was assessed using LSFM. In Wt mice, on average, 10% of the MK volume was present inside the sinusoidal vascular bed, mainly represented by proplatelets, whereas in *RhoA*$^{-/-}$ mice 50% of the MK volume was found intrasinusoidal (Figure 25C,D), demonstrating a global defect in MK localization in *RhoA*$^{-/-}$ mice.
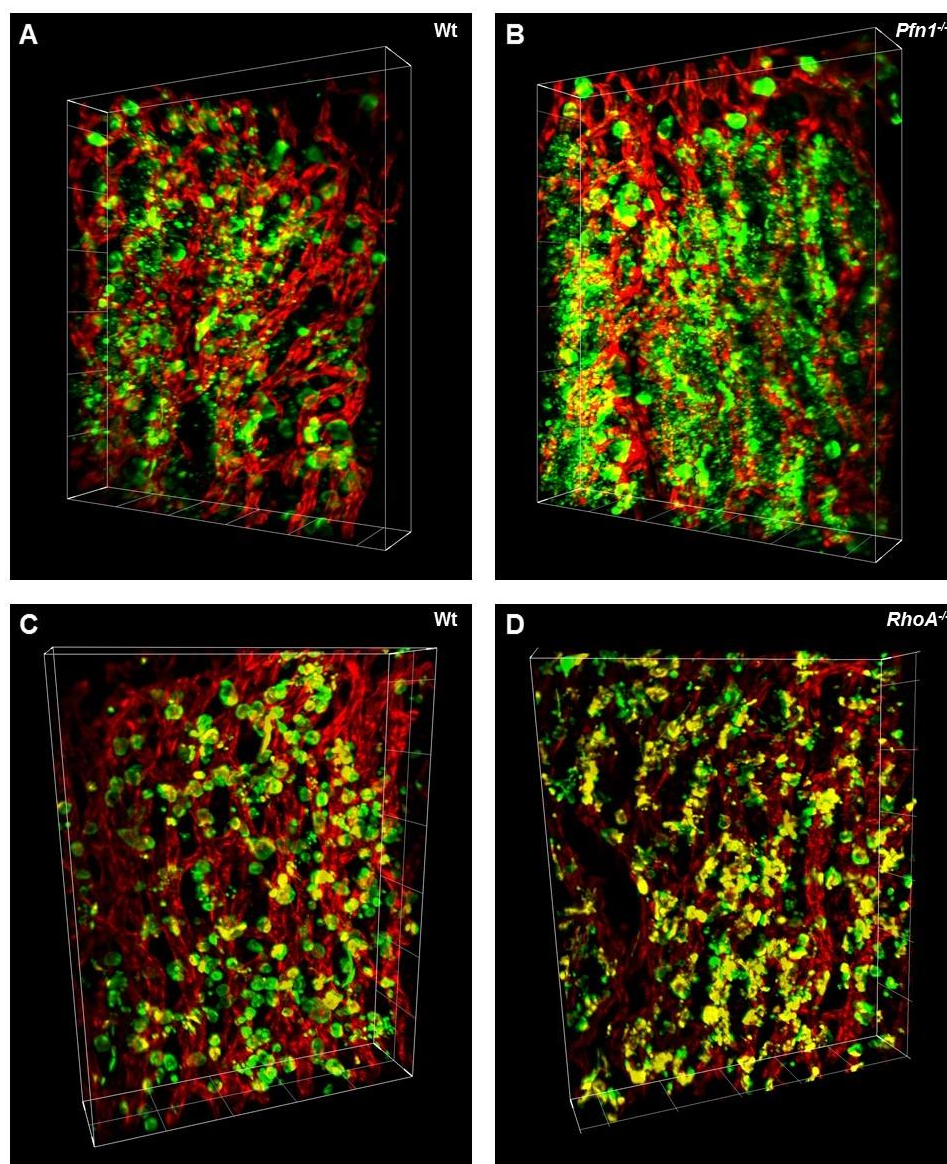
Figure 25. LSFM as a tool to study thrombopoiesis. The BM of **(A)** Wt and **(B)** *Pfn1*$^{-/-}$ mice was analyzed, revealing increased fragmentation and premature platelet release into the BM compartment. The BM of **(C)** Wt and **(D)** *RhoA*$^{-/-}$ mice was analyzed, showing a mislocalization of the MKs in the BM. The LSFM data confirmed data obtained by MP-IVM, thereby demonstrating the potential of LFSM for studying animal models of human disease. MKs are labeled green and blood vessels are labeled red. Yellow indicates the overlap of MKs and blood vessels, representing the intrasinusoidal part of the MK. Grid size 100 μm.

4.3. Syk deficiency or inhibition protect mice from arterial thrombosis and thrombo-inflammatory brain infarction

Syk is an essential signaling mediator downstream of immune cell receptors, but also of GPVI and CLEC-2 in platelets.[179-181] Due to its central role in immunological processes, several Syk inhibitors have been developed and clinically used in the treatment of for example allergy,[143] B cell malignancies,[138] heparin-induced thrombocytopenia[145] and autoimmune diseases.[139,144] However, definite evidence for a role of Syk in hemostasis, arterial thrombosis and ischemic stroke is limited.

4.3.1. (hem)ITAM signaling is abolished in *Syk*$^{-/-}$ platelets

To investigate the role of Syk in platelet biology, mice deficient for Syk in platelets and MKs, *Syk*$^{fl/fl, Pf4-cre+/-}$ mice, were analyzed (further referred to as *Syk*$^{-/-}$ mice). *Syk*$^{-/-}$ mice were generated by intercrossing mice containing the Syk gene flanked by loxP sites (*Syk*$^{fl/fl}$) with *Pf4-cre*$^{+/-}$ mice. *Syk*$^{fl/fl, Pf4-cre-/-}$ mice were used as controls and are further referred to as wildtype (Wt) mice. Conditional knockout mice were used for the analysis, since constitutive Syk-deficient mice die perinatally.[170] *Syk*$^{-/-}$ mice were born at normal Mendelian ratios and the absence of Syk in platelet lysates was confirmed by Western Blot analysis (Figure 26A). *Syk*$^{-/-}$ mice displayed normal basal blood parameters, platelet counts and size (Table 1). Flow cytometric analysis showed unaltered expression levels of prominent platelet surface receptors in *Syk*$^{-/-}$ platelets (Table 1). The effect of Syk deficiency on platelet activation was measured by flow cytometric analyses of agonist-induced activation of the major platelet integrin αIIbβ3 (JON-A/PE binding) and degranulation-dependent P-selectin surface exposure (Figure 26B). In response to GPCR agonists, such as ADP, the TxA$_2$ analog U46619 and thrombin, platelet integrin activation and degranulation were unaltered, whereas responses to GPVI and CLEC-2 agonists, including CRP, CVX and rhodocytin were abolished.

In addition, platelet aggregation of *Syk*$^{-/-}$ platelets (washed platelet and PRP) was analyzed in response to various agonists (Figure 27A,B). The lack of functional Syk resulted in severely defective aggregation in response to GPVI (collagen, CRP) or CLEC-2 (rhodocytin) agonists. However, *Syk*$^{-/-}$ platelets showed unaltered aggregation upon stimulation with ADP, thrombin and U46619. To determine the effect of Syk deficiency on platelet adhesion and aggregation under flow conditions, thrombus formation *ex vivo* was analyzed by a flow adhesion assay (Figure 27C).

	Wt	*Syk*^{-/-}
Platelets (nl^{-1})	1097 ± 69	1134 ± 136
Mean platelet volume (fl)	5.4 ± 0.1	5.4 ± 0.1
GPIb	365 ± 42	347 ± 45
GPV	314 ± 15	301 ± 14
GPIX	428 ± 40	412 ± 37
CD9	943 ± 55	920 ± 32
CD84	32 ± 2	31 ± 2
GPVI	49 ± 5	55 ± 5
CLEC-2	143 ± 8	138 ± 6
α2	53 ± 3	53 ± 2
α5	20 ± 2	19 ± 2
β1	128 ± 20	132 ± 8
β3	177 ± 23	160 ± 20
αIIbβ3	539 ± 29	521 ± 25
White blood cells (nl^{-1})	6.0 ± 2.1	6.9 ± 2.1
Red blood cells (pl^{-1})	9.1 ± 0.7	8.6 ± 1.4
Hemoglobin (g dl^{-1})	14.8 ± 1.6	14.7 ± 2.5
Hematocrit (%)	47.8 ± 4.7	46.9 ± 8.2
Mean red blood cell volume (fl)	54.2 ± 1.6	54.6 ± 1.0

Table 1. Analysis of basal blood parameters and surface expression of glycoproteins on platelets of Wt and *Syk*^{-/-} mice. Basal blood parameters were analyzed on a Sysmex KX-21N automated hematology analyzer. Diluted whole blood was stained with saturating amounts of fluorophore-labeled antibodies and platelets were analyzed by flow cytometry to determine the expression of prominent platelet surface receptors. Results represent mean fluorescence intensities (MFI) ± SD if not stated otherwise. (van Eeuwijk, Stegner *et al.*, *Arterioscler Thromb Vasc Biol.* 2016)[245]

Therefore, heparinized whole blood of Wt and *Syk*^{-/-} mice was perfused over a collagen-coated surface at a shear rate of 1000 s^{-1}. Wt platelets adhered to the collagen surface and recruited additional platelets from the flowing blood, leading to the formation of stable, 3D thrombi that finally covered approximately 50% of the total surface area. In sharp contrast, thrombus formation was abolished when perfusing heparinized whole blood from Syk-deficient mice and only a few, single platelets adhered to the immobilized collagen. These results confirm that Syk is required for (hem)ITAM signaling downstream of GPVI and CLEC-2 in platelets.
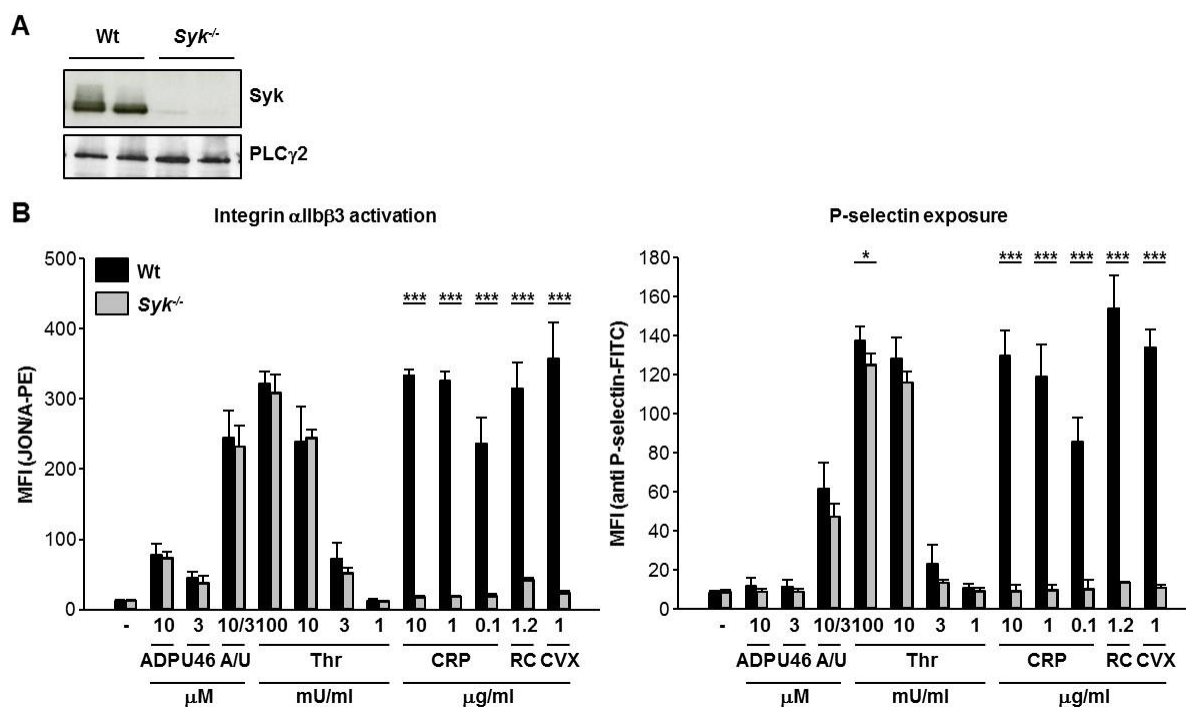
Figure 26. Abolished (hem)ITAM signaling in the absence of Syk. (A) Western blot analysis demonstrating the absence of Syk in *Syk*^{-/-} platelets. PLCγ2 expression was used as loading control. **(B)** Flow cytometric analysis of αIIbβ3 integrin activation (JON/A-PE, left panel) and degranulation-dependent P-selectin exposure (right panel) in response to the indicated agonists of Wt (black bars) and *Syk*^{-/-} (grey bars) platelets. Results represent mean fluorescence intensities (MFI) ± SD. ADP, adenosine diphosphate; U46, U46619; A/U, ADP/U46; Thr, thrombin; CRP, collagen-related peptide; RC, rhodocytin; CVX, convulxin. *, p<0.05; ***, p<0.001. (van Eeuwijk, Stegner *et al.*, *Arterioscler Thromb Vasc Biol.* 2016)[245]

4.3.2. Murine Syk is dispensable for integrin-dependent outside-in signaling

Syk has been proposed to contribute to outside-in signaling of integrin αIIbβ3 for platelet adhesion and cytoskeletal remodeling.[179-181] To test this hypothesis, Wt and *Syk*^{-/-} platelets were allowed to spread on fibrinogen (Figure 28), a process dependent on outside-in signaling. The Syk-deficient platelets were treated with indomethacin and apyrase to inhibit the effect of the second wave mediators TxA$_2$ and ADP. Under these conditions, *Syk*^{-/-} platelets spread on fibrinogen to a similar extent and with similar kinetics as Wt platelets (Figure 28A). Spreading of Wt and *Syk*^{-/-} platelets with thrombin stimulation was also comparable (Figure 28B). The integrin αIIbβ3 also plays a critical role in regulating clot retraction by platelets.[152] Upon ligand binding, clot retraction is mediated by the αIIbβ3 integrin and the cytoskeleton to consolidate thrombus formation *in vivo*. To investigate whether the loss of Syk alters clot retraction, clot formation was induced in PRP of Wt and *Syk*^{-/-} mice (Figure 28C). Clot retraction was monitored over time and started as early as 20 minutes after the start of the experiment. No differences were observed in clot retraction of Wt and *Syk*^{-/-} samples and the excess serum levels extruded during clot retraction were similar between Wt and *Syk*^{-/-} (95 ± 2.0% versus 94 ± 5.2% of the initial PRP volume).

Together, these results indicate that Syk is dispensable for integrin-dependent spreading of mouse platelets on fibrinogen and for clot retraction.
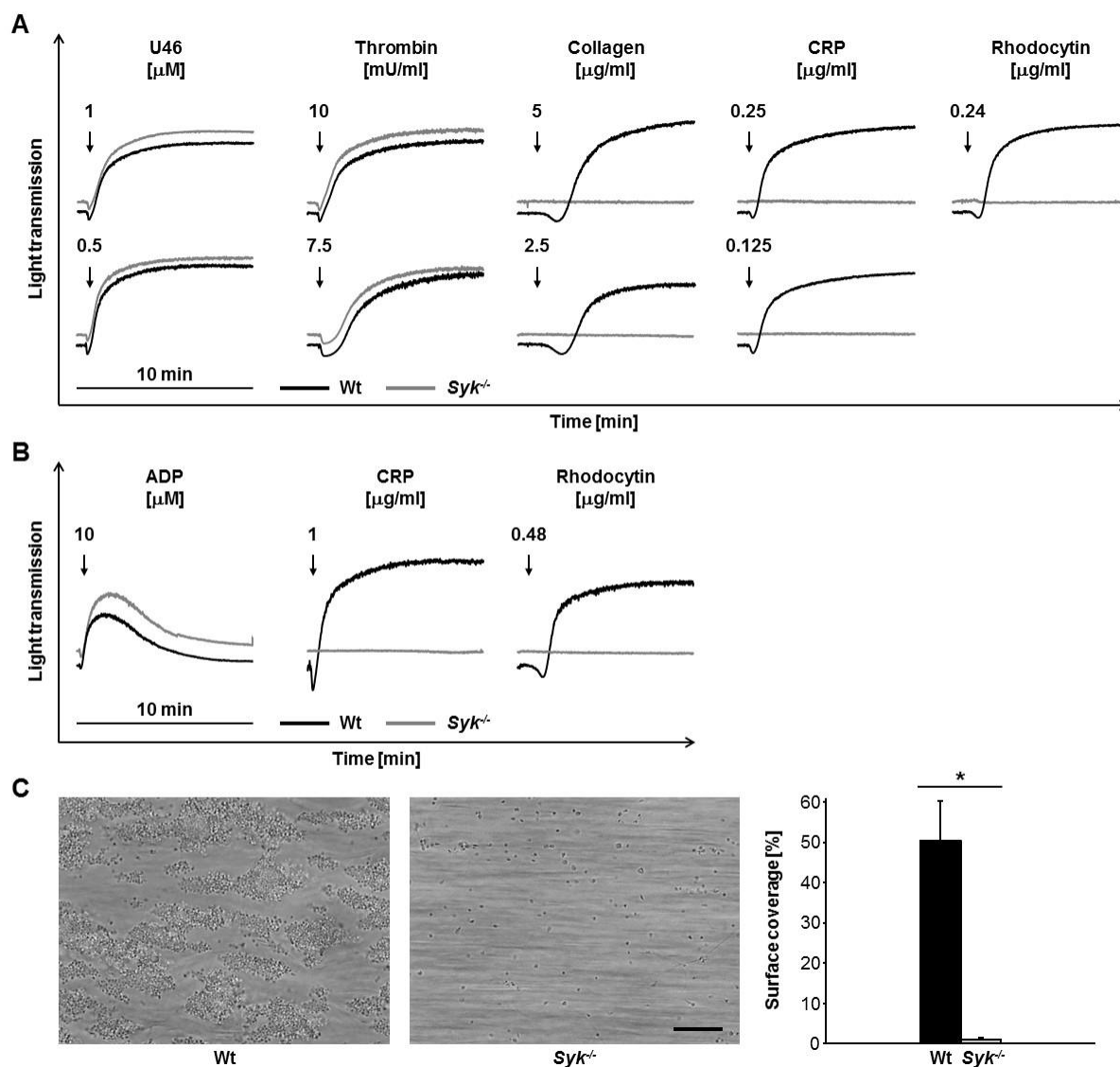
Figure 27. Abolished aggregation response of *Syk^{-/-}* platelets. (A) Washed platelets and **(B)** platelet-rich plasma (PRP) of Wt (black line) and *Syk^{-/-}* (grey line) mice were stimulated with the indicated agonists and light transmission was recorded on a Born aggregometer. Representative aggregation curves of 3 individual experiments are shown. **(C)** Heparinized whole blood of Wt (black bar) and *Syk^{-/-}* mice (grey bar) was perfused over immobilized fibrillar collagen at a shear rate of 1000 s^{-1} and surface coverage was determined. Representative phase-contrast images are depicted. Scale bar 25 μm. Bar graphs represent mean ± SD. U46, U46619; CRP, collagen-related peptide; ADP, adenosine diphosphate. *, p<0.05. (van Eeuwijk, Stegner *et al.*, *Arterioscler Thromb Vasc Biol.* 2016)[245]
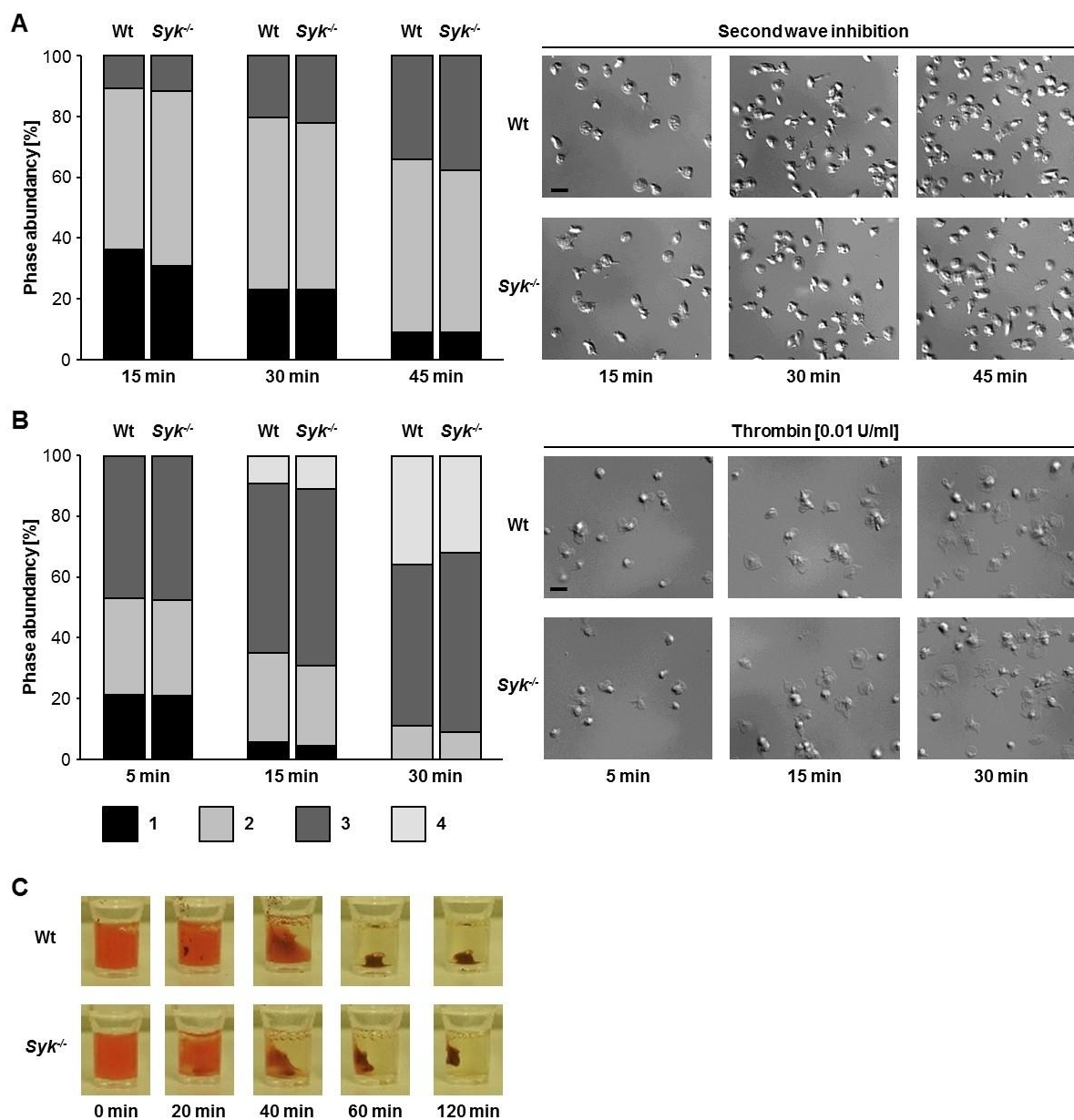
Figure 28. Platelet spreading is unaffected by Syk-deficiency. Washed platelets from Wt and *Syk*^{-/-} mice were allowed to adhere to immobilized human fibrinogen (100 μg/ml) in the presence of either **(A)** the second wave inhibitors indomethacin (1.4 μM) and apyrase (1 U/ml) or **(B)** thrombin (0.01 U/ml). Images were taken at the indicated time points and representative images are shown. Results indicate percentage of phase abundancy with (1), round platelets; (2), only filopodia; (3), filopodia and lamellipodia; (4), full platelet spreading. Scale bar 5 μm. **(C)** Clot formation was induced in PRP of Wt and *Syk*^{-/-} mice by 4 U/ml thrombin and clot retraction was monitored over time. Images were taken at the indicated time points and representative images are shown. (van Eeuwijk, Stegner *et al.*, *Arterioscler Thromb Vasc Biol.* 2016)[245]

4.3.3. Syk deficiency results in moderately prolonged tail bleeding times and impaired arterial thrombus formation

Since only limited evidence exists on the role of Syk in hemostasis and thrombosis, several *in vivo* analyses were performed. To investigate the role of Syk in hemostasis, tail bleeding times were measured (Figure 29A). Bleeding times after amputation of the tail tip were moderately prolonged in *Syk^-/-* mice compared to their respective controls. The hemostatic defect was, however, not as dramatic as upon downregulation of both GPVI and CLEC-2 from the platelet surface by antibody treatment, where no hemostatic function is present.[133]
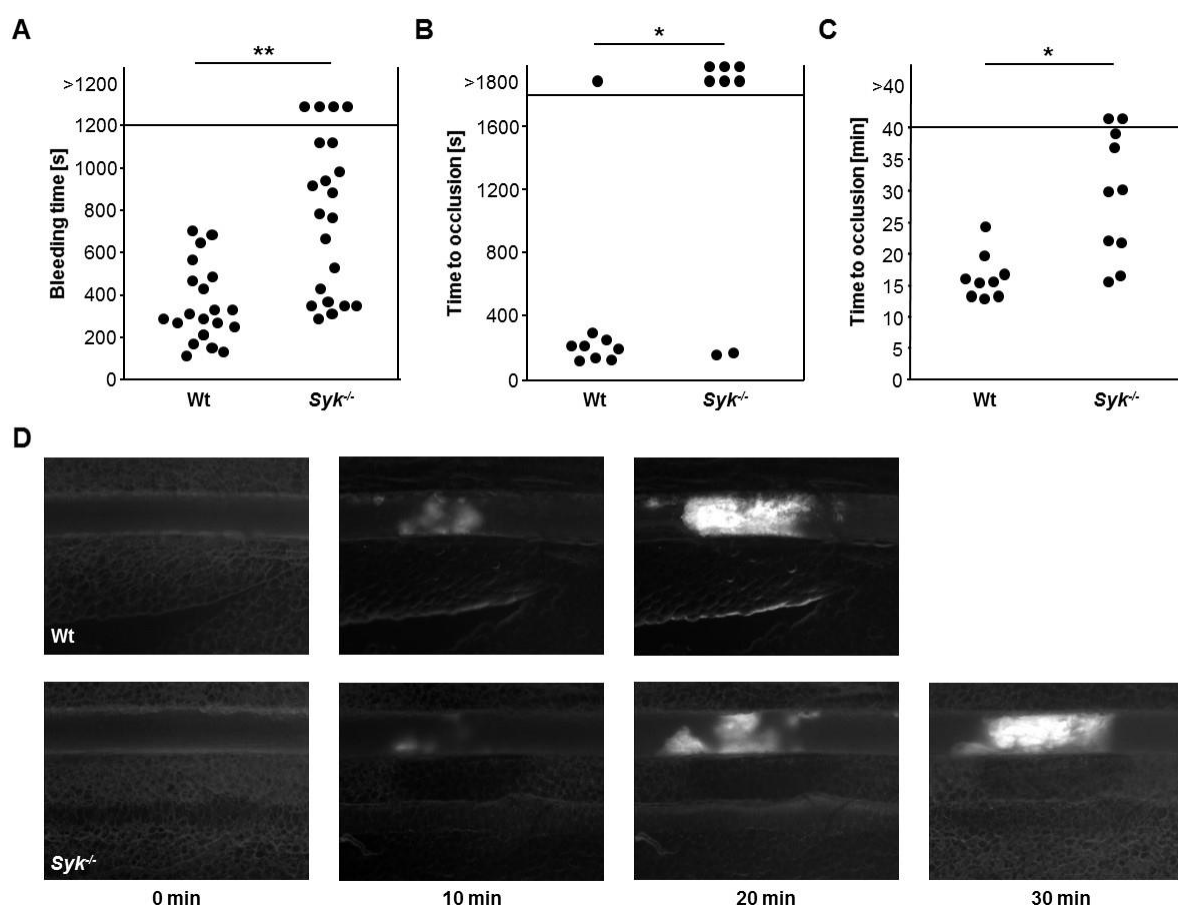
Figure 29. Syk-deficiency leads to a mild hemostatic defect, but protects from arterial thrombosis. (A) Tail bleeding times of Wt and *Syk^-/-* mice. Each symbol represents one animal. **(B)** In an aorta occlusion model, the blood flow of Wt and *Syk^-/-* mice was monitored for 30 min or until complete occlusion occurred. Time to stable vessel occlusion is depicted. Each symbol represents one animal. **(C)** In a chemical injury model, the blood flow of Wt and *Syk^-/-* mice in the mesenteric arterioles was monitored for 40 min or until complete occlusion occurred. Time to stable vessel occlusion is depicted. Each symbol represents one animal. **(D)** Images of thrombus formation in the mesenteric arterioles were taken at the indicated time points and representative images are shown. *, $p<0.05$; **, $p<0.01$. (van Eeuwijk, Stegner *et al.*, *Arterioscler Thromb Vasc Biol.* 2016)[245]

To study thrombus formation *in vivo*, Wt and *Syk*^{−/−} mice were subjected to two different models of arterial thrombosis. These experiments were performed by Ina Thielmann. Mesenteric arterioles of mice were chemically injured by topical application of 20% $FeCl_3$ and subsequently thrombus formation was monitored by intravital fluorescence microscopy (Figure 29C,D). The loss of functional Syk led to delayed or absent occlusive thrombus formation *in vivo*. To determine if Syk deficiency affects thrombus formation in bigger vessels with a different shear rate, mice were subjected to another *in vivo* model. Upon mechanical injury of the abdominal aorta, occlusive thrombus formation in *Syk*^{−/−} mice was abrogated, confirming an important role for Syk in arterial thrombosis (Figure 29B).

4.3.4. Syk deficiency protects from thrombo-inflammatory brain infarction

To assess the role of platelet Syk in brain infarction following focal cerebral ischemia, mice were subjected to 60-minute transient middle cerebral artery occlusion (tMCAO) and infarct volume and neurological deficits were assessed after 24 hours (Figure 30). This experiment was performed by Peter Kraft (Department of Neurology, University of Würzburg). Strikingly, the infarct volumes in *Syk*^{−/−} mice were significantly reduced compared to Wt mice (Figure 30A,B) and the Bederson score assessing global neurological function was significantly improved (Figure 30D). The grip test also showed an improved outcome (Figure 30C). Remarkably, no intracerebral hemorrhages were observed in these animals by systematic microscopical inspection (data not shown). Thus, Syk deficiency in platelets provides protection against cerebral infarct progression, indicating that Syk might be an attractive anti-thrombotic or anti-thrombo-inflammatory target.
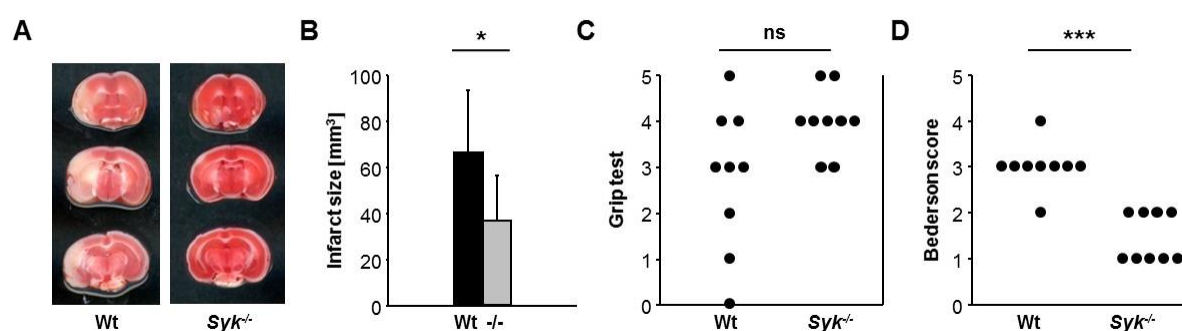
Figure 30. Syk-deficiency protects from ischemic stroke. (A) Mice were subjected to 60 min of transient middle cerebral artery occlusion (tMCAO). Representative images of three coronal sections stained with 2,3,5-triphenyltetrazoliumchloride (TTC) 24 h after tMCAO. **(B)** Brain infarct volumes of Wt (black bar) and *Syk*^{−/−} (grey bar) mice were measured by planimetry. Bar graphs represent mean ± SD. **(C)** Grip test and **(D)** Bederson score determined 24 h after tMCAO. Each symbol represents one animal. ns, p>0.05; *, p<0.05; ***, p<0.001. (van Eeuwijk, Stegner *et al.*, *Arterioscler Thromb Vasc Biol.* 2016)[245]

4.3.5. Syk inhibition abolishes (hem)ITAM signaling

Platelet inhibition is commonly used in secondary stroke prevention.[246] In acute stroke, however, revascularization by recombinant tissue plasminogen activator (rt-PA) or mechanical thrombectomy are the only therapeutic means[246,247] with limited efficacy.[248] Addition of conventional anti-platelet agents such as acetylsalicylic acid (ASA) led to bleeding complications.[249] In order to improve functional outcome in acute stroke, novel anti-thrombotic strategies preserving physiological hemostasis are eagerly awaited.

To determine if Syk could be an anti-thrombotic or anti-thrombo-inflammatory target, several commercially available Syk inhibitors were tested, but, in our laboratory, the anti-platelet efficacy *in vivo* was limited (data not shown). Therefore, the novel and highly selective oral ATP-competitive Syk inhibitor, BI1002494 was used.[226] C57BL/6JRj mice were obtained from Janvier Labs and treated with either the vehicle or the inhibitor.
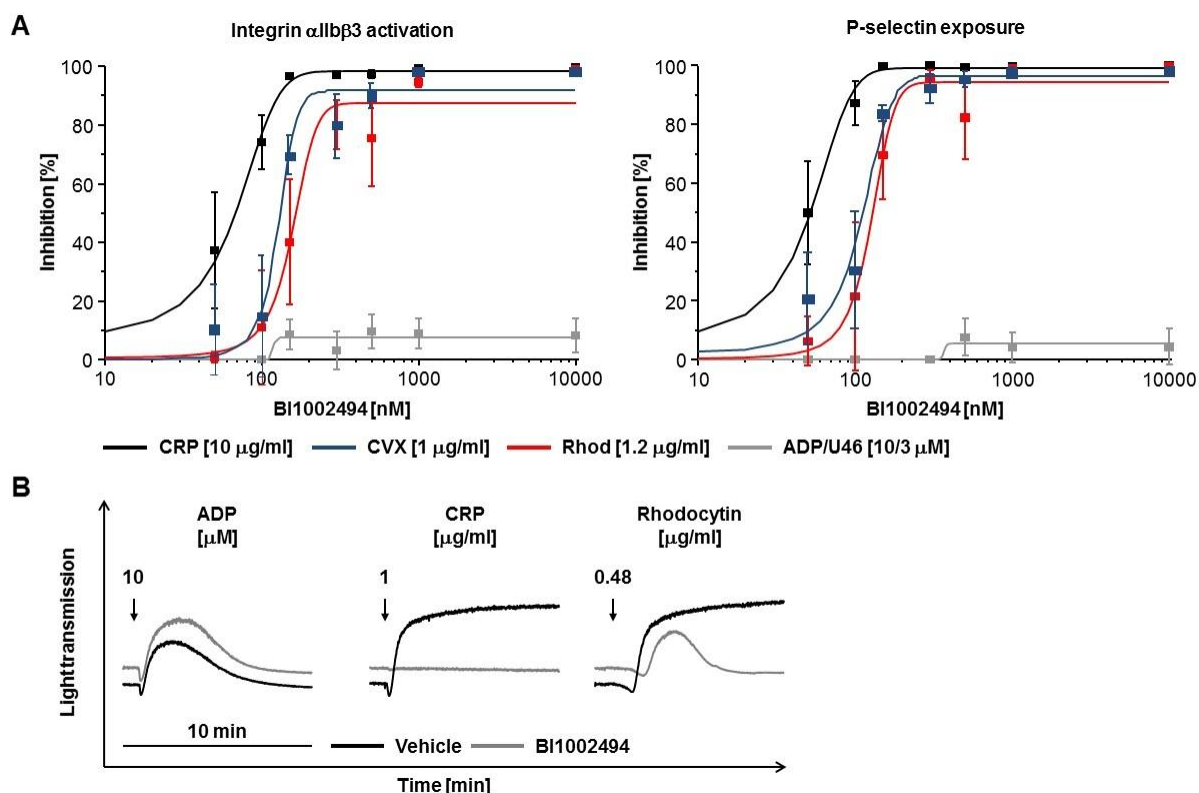
Figure 31. Pharmacological inhibition of Syk abolishes (hem)ITAM signaling. (A) Dose-response curves showing flow cytometric analysis of αIIbβ3 integrin activation (JON/A-PE, left panel) and degranulation-dependent P-selectin exposure (right panel) of wildtype platelets in response to the indicated agonists and the indicated concentrations of BI1002494. Results represent percentage of inhibition ± SD compared to vehicle-treated platelets. **(B)** Platelet-rich plasma (PRP) of vehicle-treated (black line) and BI1002494-treated (grey line) mice was stimulated with the indicated agonists and light transmission was recorded on a Born aggregometer. Representative aggregation curves of 3 individual experiments are shown. CRP, collagen-related peptide; CVX; convulxin; Rhod, rhodocytin; ADP, adenosine diphosphate; U46, U46619. (van Eeuwijk, Stegner *et al.*, *Arterioscler Thromb Vasc Biol.* 2016)[245]

The effect of Syk inhibition on platelet activation was measured by flow cytometric analyses of agonist-induced activation of the major platelet integrin αIIbβ3 (JON-A/PE binding) and degranulation-dependent P-selectin surface exposure (Figure 31A). In response to ADP and U46619, no effects on platelet integrin activation and degranulation via GPCR signaling were observed with any of the tested inhibitor concentrations, whereas responses to GPVI and CLEC-2 agonists, including CRP, CVX and rhodocytin were abolished. *In vitro* incubation of Wt platelets with 150 nM BI1002494 abrogated CRP responses, while a concentration of 500 nM of the inhibitor was required to abolish CVX and rhodocytin responses.

Oral administration of BI1002494 (100 mg/kg b.i.d.) in mice resulted in plasma concentrations greater than 980 nM over a 24-hour time period.[226] Subsequent *ex vivo* analysis of PRP showed abolished GPVI-induced platelet aggregation, while aggregation responses to rhodocytin were reduced, but not abolished (Figure 31B). In contrast, PRP from inhibitor-treated mice showed unaltered aggregation upon stimulation with ADP. These results show that BI1002494 is a suitable inhibitor for *in vivo* blockade of platelet (hem)ITAM signaling.

4.3.6. Human platelets require Syk for integrin-dependent outside-in signaling

To determine the effect of BI1002494 on outside-in signaling of integrin αIIbβ3, thrombin-stimulated Wt and BI1002494-treated mouse platelets were allowed to spread on fibrinogen (Figure 32A). Inhibitor-treated platelets spread on a fibrinogen-coated surface to a similar extent and with similar kinetics as Wt platelets. Interestingly and in contrast to mouse platelets, outside-in signaling of integrin αIIbβ3 in human platelets was impaired upon inhibitor treatment (Figure 32B), revealing a requirement of Syk for integrin-dependent outside-in signaling in human platelets.

4.3.7. Syk inhibition protects from arterial thrombosis and cerebral infarct progression, without affecting hemostasis

To investigate if Syk inhibition would alter hemostasis, mice were treated with BI1002494 (100 mg/kg b.i.d.) and tail bleeding times were determined (Figure 33A). Bleeding times after amputation of the tail tip were unaltered in inhibitor-treated mice compared to vehicle-treated controls. To study thrombus formation *in vivo*, vehicle-treated and BI1002494-treated mice were subjected to mechanical injury of the aorta (Figure 33B). The experiment was performed by Sarah Beck. Inhibitor-treated mice were completely protected from vessel occlusion compared to their respective controls.
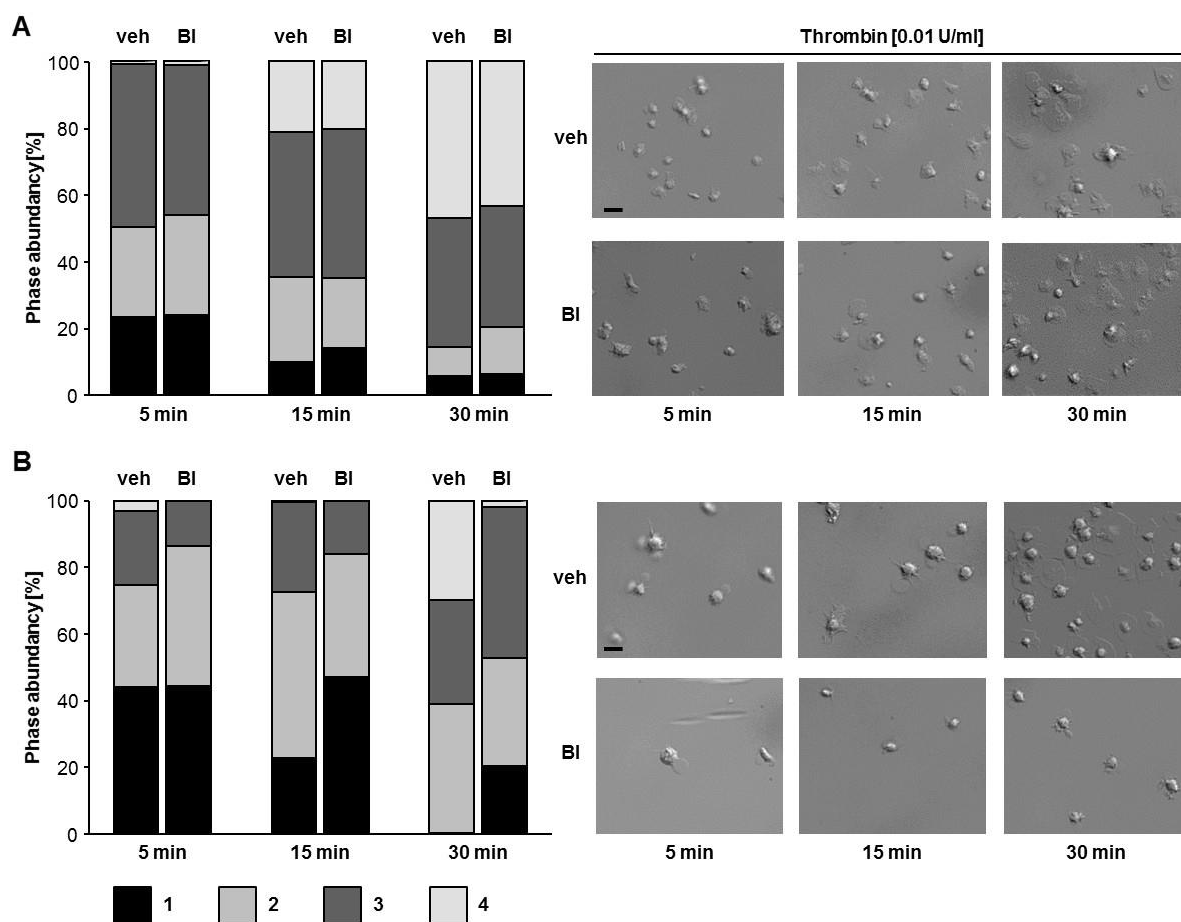
Figure 32. Syk inhibition impairs spreading of human platelets. Vehicle-treated (veh) and BI1002494-treated (BI) washed **(A)** mouse and **(B)** human platelets were allowed to adhere to immobilized human fibrinogen (100 µg/ml). Mouse platelets were stimulated with thrombin (0.01 U/ml). Images were taken at the indicated time points and representative images are shown. Results indicate percentage of phase abundancy with (1), round platelets; (2), only filopodia; (3), filopodia and lamellipodia; (4), full platelet spreading. Scale bar 5 µm. (van Eeuwijk, Stegner *et al.*, *Arterioscler Thromb Vasc Biol.* 2016)[245]

To assess the effect of the Syk inhibitor on ischemic stroke, Wt mice were pretreated with BI1002494 and subsequently subjected to 60-minute tMCAO (Figure 34A). The experiment was performed by Peter Kraft. Similar to *Syk*$^{-/-}$ mice, these animals displayed markedly reduced infarct sizes and improved motor function 24 hours after tMCAO without evidence of major intracerebral bleeding (Figure 34A-C). The neurological function also showed an improved outcome (Figure 34D). To determine if the Syk inhibitor could be used therapeutically, i.e. when given after the occurrence of ischemic stroke, mice were treated with the inhibitor directly after tMCAO (directly upon removal of the filament) (Figure 34E-H). Strikingly, also under these conditions, inhibitor-treated mice had reduced infarct sizes and a better motor function as compared to the vehicle-treated controls (Figure 34E-G). A tendency towards a generally improved neurological outcome was also observed (Figure 34H). Together, these results indicate that Syk inhibition might be effective in preventing cerebral

reperfusion injury and could serve as an anti-thrombotic therapy or anti-inflammatory therapy.
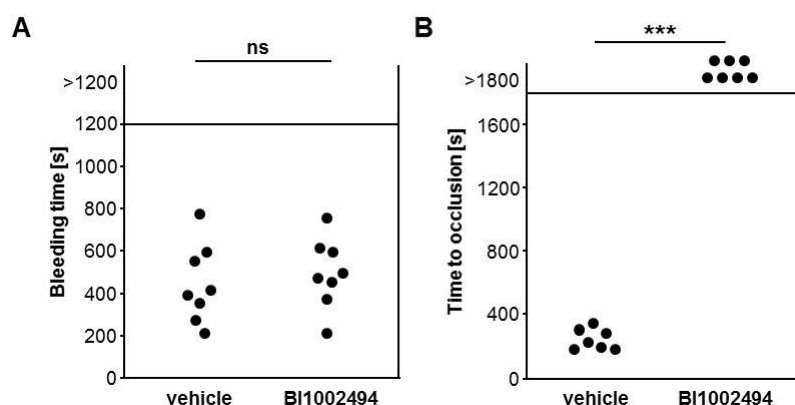

Figure 33. Pharmacological inhibition of Syk protects from occlusive thrombus formation. (A) Tail bleeding times of vehicle-treated and BI1002494-treated mice. Each symbol represents one animal. **(B)** In an aorta occlusion model, the blood flow of vehicle-treated and BI1002494-treated mice was monitored for 30 min or until complete occlusion occurred. Time to stable vessel occlusion is depicted. Each symbol represents one animal. ns, p>0.05; ***, p<0.001. (van Eeuwijk, Stegner *et al.*, *Arterioscler Thromb Vasc Biol*. 2016)[245]
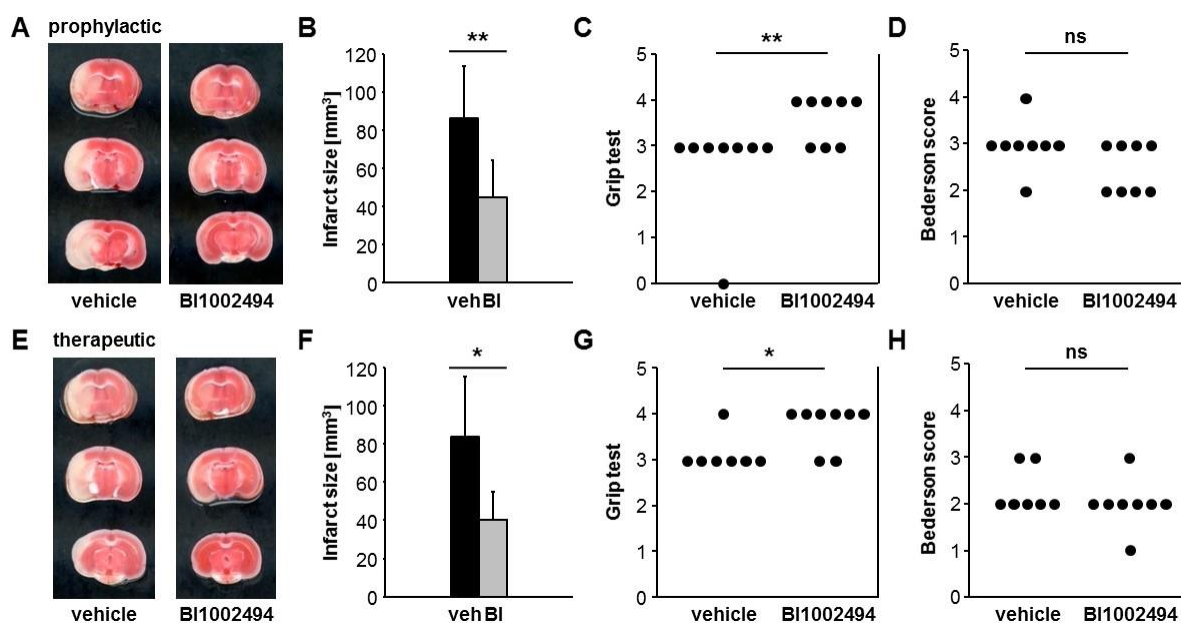
Figure 34. Pharmacological inhibition of Syk protects from ischemic stroke. (A) Vehicle-treated and prophylactic BI1002494-treated mice were subjected to 60 min of transient middle cerebral artery occlusion (tMCAO). Representative images of three coronal sections stained with TTC 24 h after tMCAO. **(B)** Brain infarct volumes of vehicle-treated (black bar) and prophylactic BI1002494-treated (grey bar) mice were measured by planimetry. Bar graphs represent mean ± SD. **(C)** Grip test and **(D)** Bederson score determined 24 h after tMCAO. Each symbol represents one animal. **(E)** Vehicle-treated and therapeutic BI1002494-treated mice were subjected to 60 min of transient middle cerebral artery occlusion (tMCAO). Representative images of three coronal sections stained with TTC 24 h after tMCAO. **(F)** Brain infarct volumes of vehicle-treated (black bar) and therapeutic BI1002494-treated (grey bar) mice were measured by planimetry. Bar graphs represent mean ± SD. **(G)** Grip test and **(H)** Bederson score determined 24 h after tMCAO. Each symbol represents one animal. ns, p>0.05; *, p<0.05; **, p<0.01. (van Eeuwijk, Stegner *et al.*, *Arterioscler Thromb Vasc Biol*. 2016)[245]

4.4. Thrombus formation *in vivo* can occur independently of Syk kinase function

Syk and Zap-70 are both spleen tyrosine kinase family members, which phosphorylate key adapter proteins and PLCγ isoforms. Both kinases display partly overlapping expression patterns, but the intrinsic kinase activity of Zap-70 is lower. In contrast to Syk, which is highly expressed by hematopoietic cells, Zap-70 expression is largely confined to T cells and natural killer cells. In mouse platelets, Zap-70 is not expressed, but Syk is present in the (hem)ITAM signaling pathways mediating signal transduction by GPVI and CLEC-2.

	Wt	*Syk^ki*
Platelets (nl^{-1})	840 ± 181	636 ± 108
Mean platelet volume (fl)	5.3 ± 0.2	5.6 ± 0.5
GPIb	395 ± 17	408 ± 29
GPV	291 ± 11	302 ± 11
GPIX	414 ± 14	433 ± 14
CD9	892 ± 56	891 ± 45
CD84	35 ± 2	33 ± 4
GPVI	53 ± 4	55 ± 3
CLEC-2	135 ± 8	126 ± 11
α2	58 ± 5	59 ± 5
α5	17 ± 2	16 ± 2
β1	132 ± 6	128 ± 9
β3	181 ± 19	157 ± 11
αIIbβ3	588 ± 38	540 ± 34
White blood cells (nl^{-1})	9.6 ± 3.2	8.4 ± 1.7
Red blood cells (pl^{-1})	8.5 ± 1.0	9.2 ± 1.9
Hemoglobin ($g\, dl^{-1}$)	13.5 ± 1.5	15.0 ± 3.1
Hematocrit (%)	44.1 ± 3.4	48.9 ± 13.0
Mean red blood cell volume (fl)	51.9 ± 1.8	52.7 ± 3.2

Table 2. Analysis of basal blood parameters and surface expression of glycoproteins on platelets of Wt and *Syk^ki* mice. Basal blood parameters were analyzed on a Sysmex KX-21N automated hematology analyzer. Diluted whole blood was stained with saturating amounts of fluorophore-labeled antibodies and platelets were analyzed by flow cytometry to determine the expression of prominent platelet surface receptors. Results represent mean fluorescence intensities (MFI) ± SD if not stated otherwise.

To assess if the two kinases exhibit interchangeable functions *in vivo*, the group of Friedemann Kiefer generated mice, which express Zap-70 under the control of intrinsic Syk promoter elements ($Syk^{Zap70/Zap70}$ mice, further referred to as Syk^{ki} mice), thereby disrupting wildtype Syk expression. $Syk^{+/+}$ mice, further referred to as Wt mice, were used as controls.[220]

4.4.1. *Syk^{ki}* mice die perinatally

To determine the consequence of the kinase replacement for platelet activation, Syk^{ki} mice were analyzed. Initially, Syk^{ki} mice were born at normal Mendelian ratios and the mice were vital and fertile. However, at a later stage, upon several rounds of animal mating, Syk^{ki} mice were born at submendelian ratios due to perinatal lethality. Backcrossing of the mice with either C57BL/6J or 129/Sv mice did not improve the birth ratios. Therefore, fetal liver chimeric mice and BM chimeric mice were generated and used for analysis.
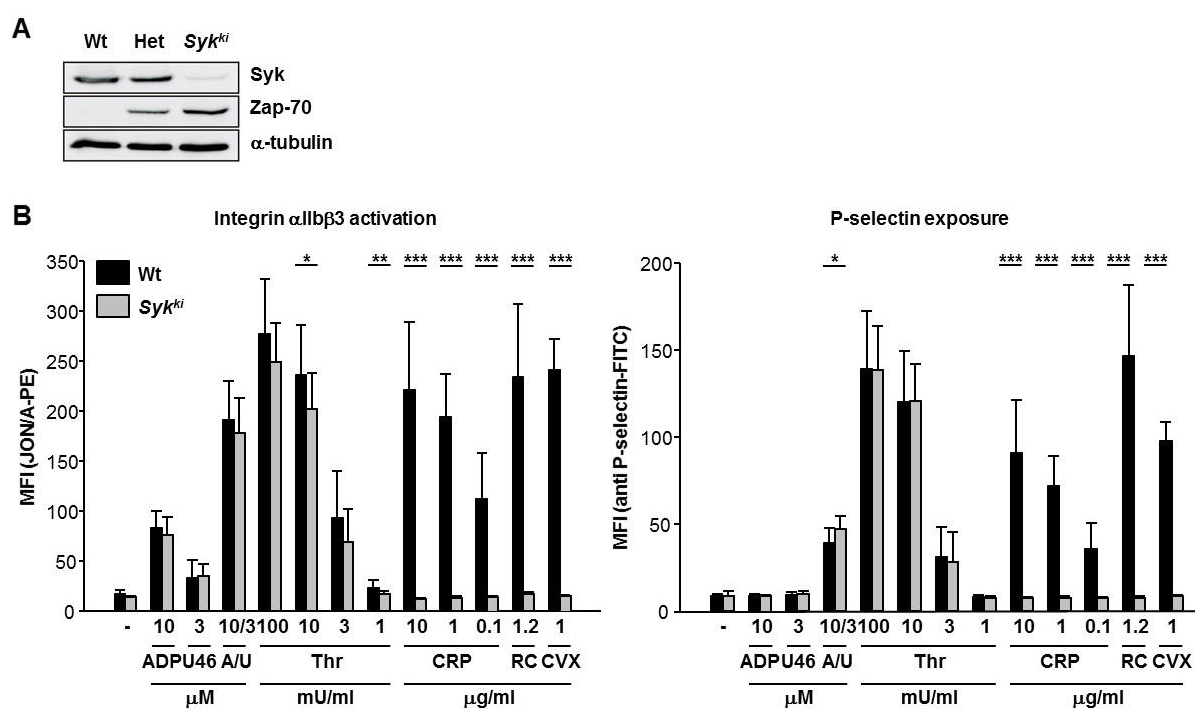
Figure 35. Abolished (hem)ITAM signaling in *Syk^{ki}* platelets. (A) Western blot analysis demonstrating the absence of Syk and the presence of Zap-70 in *Syk^{ki}* platelets. α-tubulin expression was used as loading control. **(B)** Flow cytometric analysis of $\alpha IIb\beta 3$ integrin activation (JON/A-PE, left panel) and degranulation-dependent P-selectin exposure (right panel) in response to the indicated agonists of Wt (black bars) and *Syk^{ki}* (grey bars) platelets. Results represent mean fluorescence intensities (MFI) ± SD. ADP, adenosine diphosphate; U46, U46619; A/U, ADP/U46; Thr, thrombin; CRP, collagen-related peptide; RC, rhodocytin; CVX, convulxin. *, $p<0.05$; **, $p<0.01$; ***, $p<0.001$.

4.4.2. (hem)ITAM signaling is abolished in *Syk^{ki}* platelets

The presence of Zap-70 and the absence of Syk in platelet lysates were confirmed by Western Blot analysis (Figure 35A). *Syk^{ki}* mice displayed normal basal blood parameters, platelet counts and size (Table 2). Flow cytometric analysis showed unaltered expression levels of prominent platelet surface receptors in *Syk^{ki}* platelets (Table 2). The impact of the kinase exchange on platelet activation was measured by flow cytometric analyses of agonist-induced activation of the major platelet integrin αIIbβ3 (JON-A/PE binding) and degranulation-dependent P-selectin surface exposure (Figure 35B). In response to GPCR agonists, such as ADP, U46619 and thrombin, platelet integrin activation and degranulation were unaltered. However, αIIbβ3 activation and degranulation in response to the GPVI and CLEC-2 agonists CRP, CVX and rhodocytin failed to exceed resting state levels, indicating an abrogated GPVI and CLEC-2 signaling.
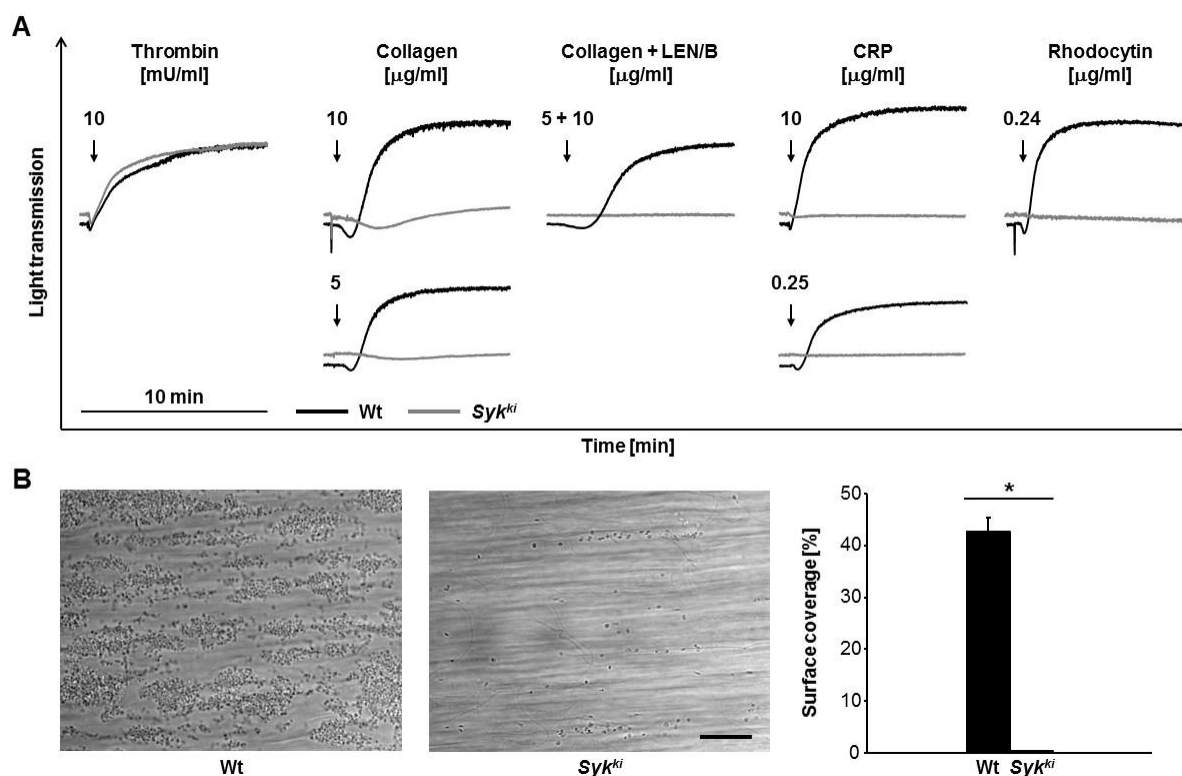
Figure 36. Abolished aggregation response of *Syk^{ki}* platelets. (A) Washed platelets of Wt (black line) and *Syk^{ki}* (grey line) mice were stimulated with the indicated agonists and light transmission was recorded on a Born aggregometer. Representative aggregation curves of 3 individual experiments are shown. **(B)** Heparinized whole blood of Wt (black bar) and *Syk^{ki}* mice (grey bar) was perfused over immobilized fibrillar collagen at a shear rate of 1000 s^{-1} and surface coverage was determined. Representative phase-contrast images are depicted. Scale bar 25 μm. Bar graphs represent mean ± SD. CRP, collagen-related peptide. *, p<0.05.

Furthermore, platelet activation *in vitro* in response to different agonists was analyzed by aggregometry (Figure 36A). Replacing Syk by Zap-70 resulted in abrogated aggregation in response to CRP and rhodocytin. However, a delayed and weak residual aggregation of the

Syk^{ki} platelets was observed in response to collagen. Since platelet binding to collagen is mediated by integrin α2β1 besides GPVI, *Syk^{ki}* platelets were pre-treated with the anti-α2β1 antibody LEN/B (10 μg/ml) and stimulated with collagen. This resulted in a completely abolished aggregation response comparable to CRP stimulation of *Syk^{ki}* platelets. Upon stimulation with thrombin, *Syk^{ki}* platelets showed unaltered aggregation compared to Wt platelets. To determine the effect of the kinase replacement on platelet adhesion and aggregation under flow conditions, thrombus formation *ex vivo* was analyzed by a flow adhesion assay (Figure 36B). Therefore, heparinized whole blood of Wt and *Syk^{ki}* mice was perfused over a collagen-coated surface at a shear rate of 1000 s^{-1}. Wt platelets adhered to the collagen surface and recruited additional platelets from the flowing blood, leading to the formation of stable, 3D thrombi that finally covered approximately 40% of the total surface area. In sharp contrast, thrombus formation was abolished when perfusing heparinized whole blood from *Syk^{ki}* mice and only a few, single platelets adhered to the immobilized collagen. These results confirm that the Zap-70 kinase is insufficient in sustaining signaling downstream of (hem)ITAM-coupled receptors in platelets.

4.4.3. Integrin outside-in signaling is unaffected by the kinase exchange

To assess if the kinase exchange affects outside-in signaling of integrin αIIbβ3, thrombin-stimulated platelets from Wt and *Syk^{ki}* mice were allowed to spread on fibrinogen (Figure 37). Similar to Syk-deficient platelets, *Syk^{ki}* platelets showed unaltered spreading compared to Wt platelets. Also, spreading of unstimulated Wt and *Syk^{ki}* platelets was comparable (data not shown).
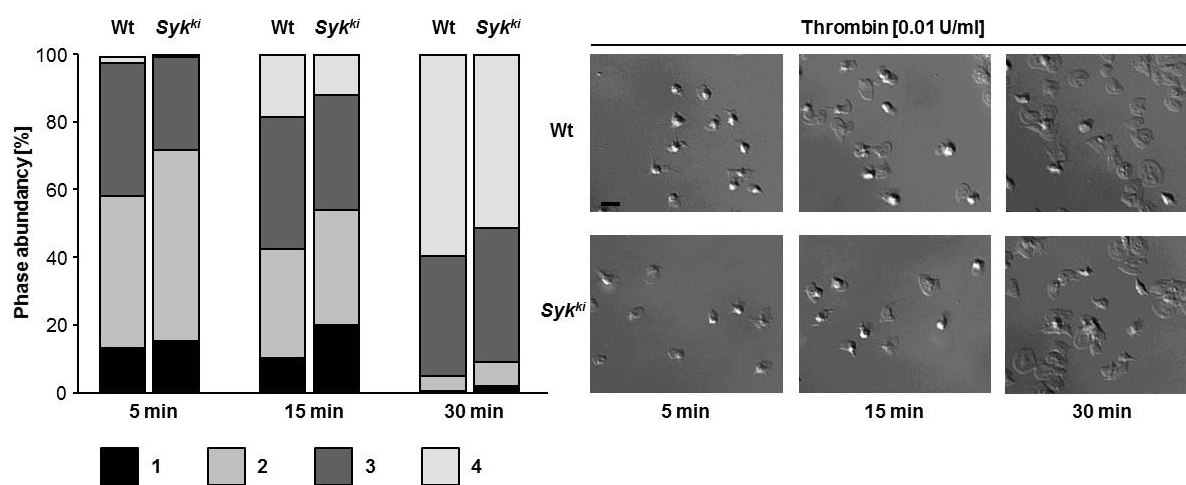
Figure 37. The kinase exchange does not affect platelet spreading. Washed platelets from Wt and *Syk^{ki}* mice were allowed to adhere to immobilized human fibrinogen (100 μg/ml) in the presence of thrombin (0.01 U/ml). Images were taken at the indicated time points and representative images are shown. Results indicate percentage of phase abundancy with (1), round platelets; (2), only filopodia; (3), filopodia and lamellipodia; (4), full platelet spreading. Scale bar 5 μm.

4.4.4. Zap-70 partially compensates for the loss of Syk *in vivo*

To determine if Zap-70 could functionally replace Syk *in vivo*, hemostatic and thrombotic assays were performed. To investigate the role of Zap-70 in hemostasis, tail bleeding times were measured (Figure 38A). Bleeding times after amputation of the tail tip were significantly increased in *Syk^{ki}* mice compared to their respective controls, which is in agreement with the results obtained in the Syk-deficient mice (see section 4.3.3).
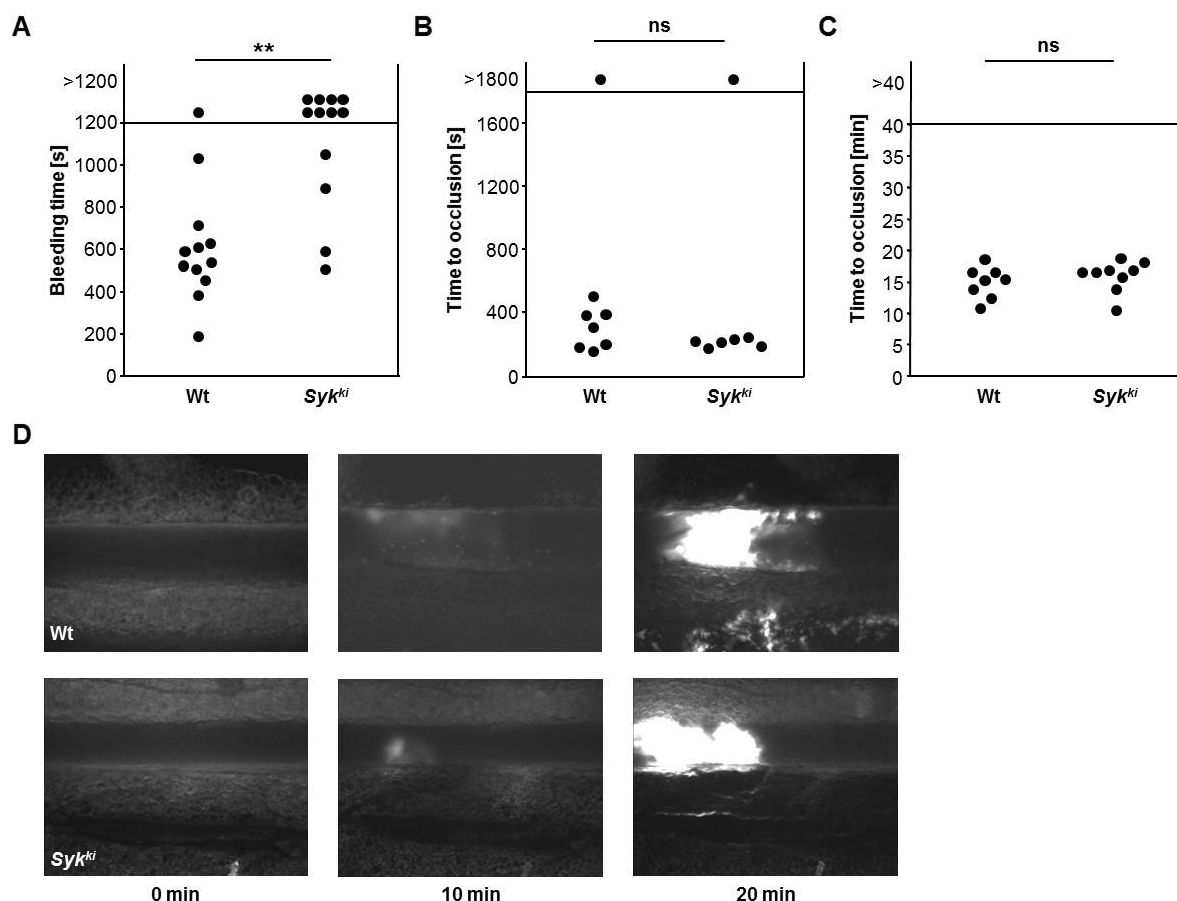
Figure 38. Zap-70 partially compensates for the loss of Syk *in vivo*. (A) Tail bleeding times of Wt and *Syk^{ki}* mice. Each symbol represents one animal. **(B)** In an aorta occlusion model, the blood flow of Wt and *Syk^{ki}* mice was monitored for 30 min or until complete occlusion occurred. Time to stable vessel occlusion is depicted. Each symbol represents one animal. **(C)** In a chemical injury model, the blood flow of Wt and *Syk^{ki}* mice in the mesenteric arterioles was monitored for 40 min or until complete occlusion occurred. Time to stable vessel occlusion is depicted. Each symbol represents one animal. **(D)** Images of thrombus formation in the mesenteric arterioles were taken at the indicated time points and representative images are shown. ns, $p > 0.05$; **, $p < 0.01$.

To study thrombus formation *in vivo*, Wt and *Syk^{ki}* mice were subjected to two different models of arterial thrombosis. The experiments were performed by Ina Thielmann. Mesenteric arterioles of mice were chemically injured by topical application of 20% $FeCl_3$ and subsequently thrombus formation was monitored by intravital fluorescence microscopy (Figure 38C,D). The loss of functional Syk, but the presence of Zap-70 surprisingly led to

unaltered occlusive thrombus formation *in vivo*. To determine if Zap-70 is also able to compensate for the loss of Syk during thrombus formation in bigger vessels with a different shear rate, mice were subjected to another *in vivo* model (Figure 38B). Upon mechanical injury of the abdominal aorta, occlusive thrombus formation in Syk^{ki} mice was again unaffected, in stark contrast to GPVI-, CLEC-2-, double-deficient or Syk-deficient mice. These results indicate that Zap-70 partially compensates for the loss of Syk *in vivo*.

5. Discussion

Over the past years, significant progress has been made in identifying the regulatory mechanisms of hematopoiesis, which was also facilitated by the development of new imaging methods. Blood platelets are produced by MKs, which originate from HSCs. Before MKs are able to produce platelets, they undergo maturation and during this process, they are thought to migrate from the endosteal niche towards the vascular niche within the BM.[18,39,45,239,240] However, the concept of MK maturation and migration is mainly based on the evaluation of cell populations present at distinct spatiotemporal niches. The exact location of MK maturation and the functional significance of MK migration towards the vascular niche for thrombopoiesis are unknown. In order to understand the regulatory mechanisms of megakaryopoiesis, it is important to determine the spatiotemporal organization of MKs within the BM and their interaction with the BM microenvironment. In addition, the exact mechanisms of platelet generation from MKs still remain ill-defined. *In vivo* studies already showed that sphingosine-1-phosphate and Thpo are critical factors stimulating thrombopoiesis via proplatelet formation.[18,36,58] This process also requires substantial cytoskeletal rearrangements.[40,60-62] Therefore, there is an increasing demand for further investigation of the contribution of critical regulators to platelet generation, such as proteins and receptors involved in the control of cytoskeletal dynamics.

Platelets play an essential role in hemostasis, as platelet activation and aggregation at sites of vascular injury are required to limit blood loss. The platelet activation process, however, needs to be tightly controlled, since excessive platelet aggregation under pathological conditions could lead to uncontrolled thrombus formation, causing life-threatening vessel occlusion and acute ischemic disease states, such as myocardial infarction and stroke. Therefore, platelet signaling has been studied intensively over the last decades. However, currently available treatment options are limited and potent anti-platelet agents often induce an increased risk of bleeding complications, thereby outweighing their therapeutic benefits. In order to improve functional outcome in acute ischemic disease states, novel anti-thrombotic strategies preserving physiological hemostasis are eagerly awaited. The (hem)ITAM-bearing receptors GPVI and CLEC-2 have been identified as critical regulators of platelet activation and have been proposed as promising new anti-thrombotic targets, due to their role in thrombosis and thrombo-inflammation.[98,117] Syk is an essential signaling mediator downstream of immune cell receptors, but also of GPVI and CLEC-2.[179-181] Since there is an increasing demand to identify the platelet activation mechanisms governing acute ischemic disease states, the role of Syk in hemostasis, arterial thrombosis and ischemic stroke was further investigated.

5.1. Profilin1, TRPM7 and RhoA are critical regulators of thrombopoiesis

MP-IVM is an insightful tool to study thrombopoiesis and proplatelet formation *in vivo* and in the first part of this thesis, the establishment of MP-IVM of the murine BM was described. By using a metal plate skull holder, the mouse's head was immobilized, allowing *in vivo* imaging of the BM without movement artefacts (Figure 8). Since the thin layer of bone covering the BM is sufficiently transparent, the BM can be studied without trauma-induced hemorrhage or inflammation. The same imaging set-up can be used to visualize the blood vessels of the brain or the brain tissue (Figure 9), although the use of a cranial window is then required. The procedure of a thinned skull cranial window involves the removal of the external layer of the compact bone, allowing transcranial imaging.[234,250] This minimally invasive method can be repeated multiple times and permits studying of the brain tissue in the same mice over short or long time intervals.[250,251] Using a thinned skull cranial window, side effects caused by skull removal are avoided and imaging can take place directly following the procedure. To minimize signal distortion and further increase penetration depth, an open skull cranial window can be used, where a part of the skull is replaced by a cover glass.[250,252] This procedure, however, can induce a severe inflammatory response possibly affecting the neuronal structures in the brain.[253] Furthermore, using an open skull cranial window, optimal imaging can only be achieved after a resting period of several days upon craniotomy.[254]

For imaging specific cell types or structures *in vivo*, reporter mice expressing fluorescent proteins or fluorophore-conjugated proteins/antibodies can be used. A fluorophore-conjugated anti-endoglin antibody and the *Flk1-mCherry*^{+/-} and *Tie2-Cre/R26-tdRFP*^{+/-} mice provided a strong staining of the endothelial lining and both tetramethylrhodamine dextran and FITC-BSA were successfully used for intraluminal vessel staining (Figure 9). To detect macrophages and neutrophil granulocytes, neurons and MKs and platelets, *Lys-eGFP*^{+/-}, *Thy1-eGFP*^{+/-} and *CD41-YFP* mice, respectively, were used (Figure 9, Figure 11). However, in *CD41-YFP* mice only a subset of the platelets was YFP-positive (Figure 10). In addition, male mice showed a higher proportion of YFP-labeled platelets compared to female mice, but it is unclear why. One possible explanation could be an increased turnover of the YFP-expressing platelets, but these platelets did not have a reduced life span (data not shown). Furthermore, the YFP signal of the platelets is not reduced in aged platelets (data not shown). Zhang *et al.* generated the *CD41-YFP* mouse line and suggest that perhaps, due to the insert, a repressor complex is recruited, targeting the *eyfp* gene, leading to the repression of YFP expression.[223] To improve labeling of MKs and platelets for MP-IVM, stainings using fluorophore-conjugated antibodies were performed. For *in vivo* labeling, anti-GPIX antibody derivatives were used as anti-CD41 antibodies induce thrombocytopenia,[210] resulting in the visualization of MKs within the BM and, to the best of our knowledge, first time detection of single platelets in the circulation (Figure 11). In the BM, the blood vessel lumen was

visualized using fluorophore-conjugated dextran or BSA. The endothelial cells were stained with anti-endoglin antibodies. Endoglin (CD105) is a co-receptor for TGF-β and is expressed on vascular endothelial cells and considered to be a suitable marker for sinusoidal vessels. It can also be found on the surface of several other cell types, such as BM stromal fibroblasts and macrophages, but it is not present on MKs.[255-257] Altogether, the combination of anti-GPIX antibody derivatives, tetramethylrhodamine dextran and anti-endoglin antibodies, enabled the observation of the dynamic process of proplatelet formation within the BM sinusoids of the murine skull *in vivo* (Figure 12, Video 1), thereby allowing studies on factors critical for platelet biogenesis.

Over the past years, technical improvements of the MP-IVM, such as the addition of a motorized stage and more sensitive photomultiplier tubes, enhanced microscope usability and increased image quality. Furthermore, due to the more sensitive detectors, a lower illumination intensity is now required. However, since the MP-IVM was only equipped with one functional Ti:Sa laser, the use of different fluorophore-conjugated antibodies for staining of different cell types during live imaging was limited. One excitation wavelength could be used to excite different fluorophores with similar excitation and emission spectra at the same time, leading to dual-color two-photon fluorescence.[236] Yet, the tunable Ti:Sa laser only emits light in the range from 690 to 1020 nm, suitable for excitation of green, yellow and orange fluorophores, but not for red fluorescent proteins, such as RFP or mCherry. The microscope is, in addition, equipped with an optical parametric oscillator (OPO), which converts an input laser wave with a fixed wavelength into a tunable range of longer wavelengths (1100 to 1600 nm), making the excitation of red and near-infrared fluorophores possible. By making use of the longer wavelengths provided by the OPO, the penetration depth was further increased and phototoxicity and photobleaching were reduced.[258] The Ti:Sa laser and the OPO can be used simultaneously, although a fixed wavelength of the Ti:Sa laser is required to be able to use the OPO, limiting the number of fluorescent dyes which can be excited concomitantly. With the recent addition of a second laser to our MP-IVM, the Ti:Sa laser can be used at any wavelength, providing a system where more than two colors with largely different excitation and emission spectra can be visualized to monitor dynamic cellular interactions in deep tissue *in vivo*.

Upon establishment of MP-IVM of the murine BM in our laboratory, the role of Profilin1, TRPM7 and RhoA was studied in thrombopoiesis *in vivo*. MP-IVM of Profilin1-deficient mice showed that the majority of the MKs released platelets prematurely into the BM compartment next to the sinusoids, but proplatelet formation was still observed (Figure 13, Video 2,3). A study by Bender *et al.*[217] revealed that *Pfn1*^{-/-} mice mimic the MK/platelet phenotype observed in WAS patients and identified Profilin1 as a negative regulator of microtubule stability and reorganization. It is suggested that WASp modulates Profilin1 function in MKs,

causing premature platelet release into the BM and accelerated platelet clearing by macrophages, ultimately leading to microthrombocytopenia in *Pfn1*^{-/-} mice and WAS patients.

In contrast to the *Pfn1*^{-/-} mice, *Trpm7*^{-/-} mice displayed a macrothrombocytopenia and, *in vivo*, impaired proplatelet formation was observed (Figure 14, Video 4,5). MKs from TRPM7-deficient mice formed short and bulky proplatelet protrusions that remained attached to the MK cell body. A recent report by Stritt *et al.*[238] demonstrated a regulatory role of TRPM7-mediated Mg^{2+} influx for NMMIIA activity and cytoskeletal rearrangements during thrombopoiesis in mice and humans. The cytoskeletal alterations caused by increased actomyosin contractility due to TRPM7-deficiency resulted in impaired proplatelet formation, but could be rescued by Mg^{2+} supplementation or chemical inhibition of NMMIIA activity.[238]

Like the *Trpm7*^{-/-} mice, RhoA-deficient mice displayed a macrothrombocytopenia. However, dynamic visualization of the *RhoA*^{-/-} MKs within the BM using MP-IVM revealed a mislocalization of these cells, with them being stably present inside the BM sinusoid (Figure 15, Video 6,7). Additionally, a high percentage of the MKs in these mice completely transmigrated from the BM into the sinusoidal vascular bed. Dütting *et al.* (unpublished) provided evidence that RhoA negatively regulates MK guidance and/or localization towards the BM sinusoids and thereby acts as a critical regulator of proplatelet formation by providing a stop-signal for MK transmigration. Together with Cdc42, RhoA appears to act in a regulatory circuit downstream of GPIbα to control transendothelial platelet generation.

Taken together, the process of platelet biogenesis, thrombopoiesis, is tightly regulated and Profilin1, TRPM7 and RhoA were identified as central players herein, by regulating microtubule organization, MK Mg^{2+} homeostasis and transmigration, respectively.

5.2. Thrombopoiesis is spatially regulated by the bone marrow vasculature

Upon final maturation of the MKs, cytoplasmic extensions, the proplatelets, pass the endothelial barrier and are shed into the circulation, where the final sizing into hundreds of virtually identical platelets from each single MK takes place.[40,57] To be able to release platelets, MKs have to reside at the sinusoidal blood vessel. According to the current concept of megakaryopoiesis, blood cell precursors migrate from the endosteal niche towards the vessel sinusoids during maturation (Figure 39).[18,39,45,239,240] In contrast to this concept, Junt *et al.* reported that MKs are overall sessile in the BM and mostly found in close proximity to blood vessels.[57] By tracking single MKs over time *in vivo*, MK migration was studied and it was confirmed that MKs were largely sessile, displaying either a vibrating movement or a shift in their center of mass during thrombopoiesis (Figure 16). Immunohistochemical analyses of cryo-sections of murine femora and sterna verified the observation by Junt *et al.* that the majority of the MKs is in direct contact with the vasculature independent of the

maturation state of these cells (Figure 17).[57] Since cryo-sections and MP-IVM provide only limited structural and 3D information when studying megakaryopoiesis and thrombopoiesis, LSFM of the murine BM was established and described in the second part of this thesis (Figure 18).

Since LSFM enables the visualization of large tissue specimens in 3D with a subcellular resolution, this technique can be positioned between microscopic imaging methods like confocal microscopy and macroscopic imaging systems such as magnetic resonance imaging (MRI). The method is based on optical sectioning and allows studying intact organs on a single-cell level. Cell staining was achieved by *in vivo* labeling using fluorophore-conjugated antibodies (Figure 19). *Ex vivo* staining would be preferred to exclude additional, negative effects of the antibodies *in vivo*. It would also provide the opportunity to analyze human samples by LSFM. Unfortunately, several *ex vivo* staining protocols were tested, but sufficient antibody penetration was not achieved. Multiple factors, including fixation and permeabilization of the tissue, the antibody concentration and the duration of the incubation steps, should be taken into account for optimization of the *ex vivo* staining protocol. In LSFM, fixed samples possess a high tissue autofluorescence, especially in the green channel, and to avoid this, red and near-infrared fluorescent conjugates were used for antibody labeling (Figure 19).

For optical sectioning, tissues need to be transparent and optimal clearing of murine bones was accomplished by dehydration with MeOH and clearing with BABB (Figure 20). Using this clearing protocol, only minimal tissue shrinkage was observed and samples were imaged with a high penetration depth and low scattering effects. However, dehydration and clearing of tissues expressing fluorescent proteins, such as GFP and YFP, degraded the fluorescent signal, thereby preventing its detection. The tissue damage is a result of the lipid-solubilizing components of the clearing solution, specifically the high concentrations of the organic solvents required for full tissue clearing.[206] Therefore, to reduce background fluorescence and to preserve fluorescent signals by enhancing fluorescence protein stability, new clearing agents based on aqueous solutions have recently been developed, such as CLARITY and Sca*l*eS.[206,207] These developments provide the opportunity to use reporter mice for LSFM studies in addition to or instead of immunohistochemical labeling.

To allow an accurate computational 3D reconstruction and subsequent quantitative analysis of the intact tissue, an image processing protocol was established (Figure 21). The image analysis involved image preprocessing, including noise removal and contrast enhancement, segmentation and data extraction. Developments in microscopic imaging techniques, like LSFM also require improved image analysis software. Current advances include stitching software to combine several images and deconvolution software for LSFM data sets to further enhance contrast and resolution, providing more accurate and detailed 3D

reconstructions. In addition to software improvements, technical enhancements of the LSFM, such as dual-sided illumination would increase the image quality.

Upon establishment of LSFM of the intact murine BM, sterna and femora of Wt mice were analyzed. Surprisingly, a homogeneous distribution of MKs within the BM was found (Figure 22). Furthermore, an extremely dense blood vessel network was observed, with, on average, 79% of the MKs localized in close proximity to the BM sinusoids (Figure 22G). To determine the effect of increased platelet consumption on MK distribution, mice were treated with anti-CD42b antibodies to induce rapid platelet clearance (Figure 23A-E). Interestingly, the MK distribution remained largely unaltered. In addition, when blocking the chemokine receptor CXCR4 using AMD3100 or when stimulating the receptor using SDF1, MK localization was not affected (Figure 23F-H). The vessel-biased MK distribution was also confirmed by computational modeling (Figure 24). Altogether, these data contradict the current concept of MK migration during terminal megakaryopoiesis and therefore argue for a revised model of megakaryopoiesis, with the majority of MKs residing directly at the sinusoids (Figure 39).

The current concept is primarily based on the seminal paper by Avecilla *et al.*, who studied the relevance of the chemokine receptor CXCR4 in megakaryopoiesis[18], and on *in vitro* data of migrating MKs.[48,49] As the recruitment of HSCs and other progenitor cells from the osteoblastic niche is also affected by the CXCR4-SDF1 signaling pathway[18,259], inhibition of CXCR4 could block the recruitment of HSCs. Therefore, it is possible that the study by Avecilla *et al.*[18], which had relatively long observation periods after SDF1 treatment, was confounded by effects acting rather indirectly on the spatiotemporal MK distribution. Moreover, as shown in this thesis, the dense BM vasculature restricts the extraluminal space, thereby omitting the need for MK migration, as growing MKs will inevitably reach the vessel at some point with minimal movement. Since the stem cell niche concept for HSCs was proposed in 1978 by Schofield,[8] major progress in identifying the localization and characterization of the distinct niches in the BM has been made. However, important questions still remain, concerning the different types of niches in the BM, the cellular complexity of the niche, the molecular pathways regulating the cellular interactions and the role of the endosteal niche, vascular niche and the perivascular microenvironments in normal physiology or under stress conditions. The vessel-biased localization of MKs, as shown by LSFM, enables a rapid response upon conditions of elevated platelet needs. MK precursor cells already reside in close proximity to the vasculature, allowing the rapid generation of new MKs upon elevated platelet demand.
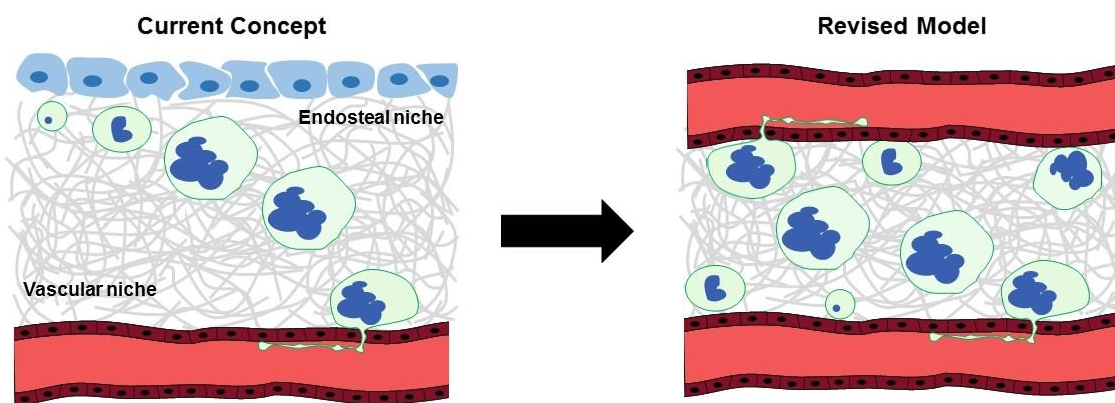
Figure 39. Revised model of megakaryopoiesis. The current concept of MK maturation involves the migration of MKs from the endosteal niche towards the vascular niche (left panel). Once the MKs have reached the vascular niche, proplatelets pass the endothelial barrier, releasing platelets into the bloodstream. The proposed revised model shows an extremely dense blood vessel network in which the MKs display a homogeneous, but vessel-biased distribution (right panel).

These results support the notion that the endosteal and vascular niches within the BM are not completely separable and that they should not be viewed as static microenvironments, but rather as dynamic environments capable of adapting to physiological requirements.[18,260] This is in agreement with previous studies indicating perivascular 'niches' for HSCs within the BM.[7,16,261] This concept is further supported by recent reports showing that distinct vascular niches mediate HSC quiescence[10] and non-dividing stem cells mainly localize at a perisinusoidal site.[11] In addition, the vessel-biased distribution of MKs might be supported by MK polarization (for example via 'directed growth'). This polarization could be triggered by mechanical cues, such as interactions with matrix proteins or endothelial cells expressing VCAM1[18] and VE-cadherin[18] or by environmental soluble factors, such as SDF1, FGF4 or sphingosine-1-phosphate,[18,58] thereby affecting platelet production rather than megakaryopoiesis. However, it could also be possible that two pools of MKs exist, one of which resides directly at the vessel to readily produce platelets ("on demand"), whereas a second, more quiescent pool of MKs, resides more distant from the vasculature. A similar concept has been proposed for HSCs,[16,262] which either reside directly at the blood vessels or at the endosteal niche.[7,11,16,261] Previous reports on MK-biased HSCs, where MKs appear to regulate HSC activity,[263] for example via CLEC-2 signaling,[264] and the fact that MK-secreted factors, like TGF-β1 and PF4 keep HSCs quiescent,[53,54] raise the intriguing possibility that MKs function as niche cells and regulate the HSCs pool in the BM. In addition, our data have translational implications. The vessel-biased MK distribution implies that promoting megakaryopoiesis (for example by differentiation-promoting chemokines) would be sufficient to rapidly enhance platelet production, as MKs do not need to migrate towards the vasculature. Besides the MK niche within the BM, MKs can also be found in the spleen and platelet production has also been described to occur within the capillary beds of the

lungs.[265,266] However, using MP-IVM, transmigration of whole MKs in Wt mice was never observed and in LSFM analyses, which allow assessment of much higher sample numbers, MKs were rarely detected within the vasculature (Dütting *et al.*, unpublished). Thus, it appears unlikely that the migration of BM-derived MKs into different organs would be a dominant phenomenon. The use of LSFM provided the possibility to examine the BM in a physiological context. By combining LSFM with other *in vitro* and *in vivo* imaging techniques, it could be possible to identify the key players in the regulation of megakaryopoiesis and thrombopoiesis and study the different BM niches in more detail.

5.3. Syk inhibition protects mice from arterial thrombosis and thrombo-inflammatory brain infarction

In the third part of this thesis, the role of Syk in hemostasis, arterial thrombosis and ischemic stroke was investigated. Syk is an essential signaling mediator downstream of GPVI and CLEC-2. The role of both (hem)ITAM receptors on platelets has been studied intensively using either genetically engineered knockout mice or antibody-induced receptor downregulation. *Gp6*^{-/-} mice and mice depleted of platelet GPVI by JAQ1 treatment showed inhibition of platelet aggregation in response to collagen and CRP.[98,134,267] *In vivo*, GPVI deficiency revealed only moderately increased tail bleeding times, indicating a minor role of GPVI in hemostasis.[98,134] In sharp contrast, a prominent role for GPVI in arterial thrombus formation exists, as the absence of GPVI on the platelet surface results in a long-term antithrombotic protection.[98,134,268] CLEC-2 deficiency on platelets induced by treatment with INU1 resulted in abolished aggregation in response to rhodocytin.[160] In addition, defective thrombus formation *in vivo* and prolonged tail bleeding times were observed in CLEC-2 deficient mice.[160] Since both receptors can be easily immunodepleted from the circulating platelets *in vivo* and are considered potential targets for effective and safe antithrombotic therapy, Bender *et al.* studied the combined loss of GPVI and CLEC-2, to assess possible redundant functions of the two receptors.[133] Interestingly, the combined deficiency of GPVI and CLEC-2 resulted in a severe hemostatic defect and virtually abolished thrombus formation,[133] indicating partially redundant functions of the receptors in hemostasis and pathological thrombus formation. It also showed that concomitant lack of GPVI and CLEC-2 possibly may be an effective, but not necessarily safe antithrombotic therapy. Since Syk is located downstream of the (hem)ITAM receptors, its function in hemostasis and arterial thrombosis was studied, using a conditional knock-out approach and a newly developed Syk inhibitor, BI1002494. It was shown that either the absence or the inhibition of Syk led to abolished (hem)ITAM signaling in platelets (Figure 26, Figure 31), resulting in defective aggregation responses under stirring conditions (Figure 27, Figure 31) and flow conditions (Figure 27). These results were not surprising, considering that similar observations were

previously reported for platelets from GPVI/CLEC-2 double-deficient animals.[133] *In vivo*, a mild hemostatic defect was observed in the *Syk⁻/⁻* mice and they were protected from arterial thrombosis (Figure 29). Pharmacological inhibition of Syk protected from occlusive thrombus formation without affecting hemostasis (Figure 33). BI1002494 dose-dependently abolished (hem)ITAM signaling in platelets, wherein CRP-induced platelet activation appeared to be more sensitive towards inhibition than CVX or rhodocytin-induced platelet activation. CVX activates platelets through the GPVI/FcR γ-chain receptor complex and subsequent signaling is mediated solely via Syk. A report by Asazuma *et al.* showed that CVX is a significantly stronger agonist than CRP or collagen, presumably due to greater GPVI cross-linking abilities.[269] Therefore, different clustering capacities and/or variation in receptor binding sites of the different agonists might contribute to the observed different sensitivities towards inhibition. Similar agonist and signaling pathway-dependent differences in BI1002494 efficacy were observed in various immune cells.[226] Furthermore, GPVI and CLEC-2 signaling differ in the sequential order of SFKs and Syk,[116] which could explain the different potencies of BI1002494 for inhibiting GPVI and CLEC-2 signaling, respectively, and thereby the unaltered tail bleeding times in inhibitor-treated mice compared to the slightly prolonged bleeding times in Syk-deficient mice. Also, given previous reports that simultaneous targeting of GPVI and CLEC-2 severely compromised hemostasis,[133] whereas in Syk-deficient mice only a mild hemostatic defect was observed, this could point towards signaling-independent functions of the two (hem)ITAM receptors in hemostasis. The unaltered bleeding times in BI1002494-treated mice are in line with observations made with other Syk inhibitors, such as fostamatinib[149] or PRT060318[145,183] and strongly suggest that Syk inhibition might be a safe anti-thrombotic regimen. However, as with all preclinical studies, differences between animal studies and the human situation need to be considered.

Besides its function downstream of GPVI and CLEC-2, Syk has been proposed to contribute to integrin-dependent outside-in signaling. Hence, clot retraction experiments were performed, showing no differences between Wt and *Syk⁻/⁻* mice (Figure 28). In addition, platelets were allowed to spread on a fibrinogen coated surface, but spreading of Syk-deficient platelets was comparable to spreading of Wt platelets (Figure 28). A similar result was obtained upon treatment of mouse platelets with BI1002494 (Figure 32).

Interestingly, spreading of BI1002494-treated human platelets was impaired (Figure 32). One notable difference between human and mouse platelets is the expression of FcγRIIA, which is present on human, but not on mouse platelets. FcγRIIA signals through an ITAM in its cytoplasmic tail and is critically involved in immune-mediated thrombocytopenia and thrombosis, but also enhances platelet integrin outside-in signaling via Syk.[81] This receptor expression difference is the most likely explanation for the observed differences between human and mouse platelet spreading upon inhibitor treatment.

While these studies indicate that short-term inhibition of Syk is well-tolerated, a longer treatment should be carefully considered. It is known that mice deficient in proteins involved in the CLEC-2 signaling pathway, such as SLP-76[270] and PLCγ2,[271] exhibit impaired blood-lymphatic vessel separation during development, resulting in blood-filled lymphatics. Platelets are important regulators during this developmental separation process, by interacting with podoplanin expressed on the lymphatic endothelial cells via CLEC-2.[149] This phenotype was also observed in GPVI/CLEC-2 double-deficient animals, although the defect was more severe compared to the CLEC-2 deficient mice.[133] Blood-lymphatic mixing or blood-filled lymph nodes were not observed in the Syk-deficient mice used for these studies. However, Syk-deficiency could result in a blood-lymphatic mixing phenotype[158,175,270] or defective integrity of high endothelial venules,[148] indicating that chronic Syk inhibition might have a similar effect in mice and possibly humans.

Since Syk deficiency and inhibition protected mice from arterial thrombosis and because a possible significance of Syk-mediated signaling in the pathogenesis of ischemic stroke has not been established to date, the role of Syk in ischemia reperfusion injury was determined. Ischemic stroke is primarily caused by thromboembolic occlusion of a brain vessel, inducing ischemia and infarction of the brain parenchyma.[272] Ischemia reperfusion injury paradoxically often occurs upon recanalization of previously occluded cerebral arteries in the setting of acute stroke. The tMCAO model is a well-established model to study this process and clinically reflects successful thrombectomy. Although the exact mechanisms by which platelets contribute to infarction of the brain are still poorly understood, ischemic stroke has been recognized as a complex disease. Over the past years, central players in reperfusion injury have been identified, including platelets, T cells,[273] blood coagulation,[274] and neuronal calcium homeostasis.[275] It has also become evident that interfering with early platelet adhesion and activation mechanisms involving GPIb, vWF and GPVI decrease infarct development, whereas blockade of platelet aggregation via αIIbβ3 in the setting of acute stroke leads to intracranial hemorrhage.[97,272] The therapeutic setting, in which mice were treated with BI1002494 directly upon removal of the filament, would reflect a clinical situation where a patient undergoes successful thrombectomy with additional treatment with an anti-platelet agent. In the Syk-deficient mice, the neurological outcome was significantly improved compared to Wt mice, whereas only a tendency towards a better motor function was observed (Figure 30). In contrast, the inhibitor-treated mice showed a significantly improved motor function, both in a prophylactic and in a therapeutic setting (Figure 34). However, a clear reduction of infarct sizes was observed for both Syk-deficient and inhibitor-treated mice compared to Wt mice. This was reflected by the improved outcomes in the neurological and motor function tests, providing direct evidence that pharmacological Syk inhibition might be a safe therapeutic strategy to limit infarct progression in acute stroke. Nevertheless, these data

were obtained using mouse models and when translating the results to a clinical situation, other risk factors, besides dysregulated platelet function, such as atherosclerosis, diabetes, hypertension and obesity have to be taken into account.

5.4. Thrombus formation *in vivo* can occur independently of Syk kinase function

Syk and Zap-70 are both spleen tyrosine kinase family members and display partly overlapping expression patterns. In the fourth part of this thesis, it was investigated whether the two kinases exhibit interchangeable functions *in vivo*. Therefore, *Syk^{ki}* mice, which express Zap-70 under the control of intrinsic Syk promoter elements were analyzed. For the analysis, fetal liver and BM chimeric mice were used, as, in contrast to the published report by Königsberger *et al.*[220], *Syk^{ki}* mice showed perinatal lethality in our laboratory. However, the results in the initial study were comparable to the data obtained with chimeric animals, making these mice a suitable tool to study the differential kinase fitness *in vivo*. The perinatal lethality is probably caused by the disruption of Syk expression, leading to a defect in the separation of the lymphatic vasculature from the blood vasculature, resulting in the appearance of blood-filled lymphatic vessels. A similar phenotype is found in mice deficient in Syk.[158,170,270] This assumption is further supported by the observation that *Syk^{ki}* chimeric animals develop blood-filled lymphatic vessels. However, these animals also presented with cloudy and bloody ascites, possibly due to an inflammatory response, indicating a more severe phenotype due to the absence of Syk/presence of Zap-70 in other cell types besides platelets.

In vitro analyses of *Syk^{ki}* platelets showed abolished (hem)ITAM signaling in response to CRP, CVX and rhodocytin (Figure 35), which is comparable to *Syk$^{-/-}$* platelets. Interestingly, platelet aggregation responses were abrogated in response to CRP and rhodocytin, but not upon stimulation with collagen, where a delayed and weak residual aggregation was observed (Figure 36). Pre-treatment of *Syk^{ki}* platelets with the anti-$\alpha2\beta1$ antibody LEN/B and stimulation with collagen resulted in a completely abolished aggregation. In addition, *Syk^{ki}* platelet adhesion to collagen and subsequent aggregate formation under flow conditions was strongly impaired (Figure 36). The integrin $\alpha2\beta1$ mainly mediates platelet adhesion, whereas GPVI is the central and indispensable activating collagen receptor on the platelet surface.[94,117] A previous report has shown that collagen-induced aggregation is GPVI- and $\alpha2\beta1$-dependent, whereas platelet adhesion to fibrillar collagen under shear stress is GPVI-, but not entirely $\alpha2\beta1$-dependent.[95] It can be assumed that, upon collagen stimulation of *Syk^{ki}* platelets, Zap-70 is not able to completely sustain signaling downstream of GPVI, but due to the adhesion of $\alpha2\beta1$ to collagen, a minor aggregation response is still observed. However,

under flow conditions, platelets are not able to adhere, resulting in a phenotype comparable to *Gp6*^{-/-} and *Syk*^{-/-} mice.[95] As CVX and CRP solely bind to GPVI, the residual aggregation response of the *Syk*[ki] platelets is only observed upon collagen stimulation.

Syk[ki] platelets spread normally on a fibrinogen-coated surface (Figure 37). Similar observations were made for *Syk*^{-/-} platelets (Figure 28) or murine platelets treated with BI1002494 (Figure 32A), indicating that either Zap-70 compensated for the loss of Syk in the integrin-dependent outside-in signaling pathway or, more likely, both Syk and Zap-70 are dispensable for murine platelet spreading.

To determine whether Zap-70 could functionally replace Syk *in vivo*, the role of Zap-70 in hemostasis and arterial thrombosis was analyzed. Tail bleeding times were prolonged in *Syk*[ki] mice (Figure 38), but the hemostatic defect was similar to the *Syk*^{-/-} mice (Figure 29) and not as severe as in the GPVI/CLEC-2 double-deficient animals.[133] Remarkably, a striking difference between the *Syk*^{-/-} mice and *Syk*[ki] mice was observed concerning occlusive thrombus formation *in vivo*. Whereas *Syk*^{-/-} mice were protected from arterial thrombosis (Figure 29), the presence of Zap-70 led to unaltered occlusive thrombus formation (Figure 38). It might be possible that the minimal (hem)ITAM signaling observed in *Syk*[ki] platelets, due to partial signal transduction via Zap-70, is sufficient for arterial thrombus formation *in vivo*. This process could be slower than the classical (hem)ITAM signaling pathway and probably requires the activation of other receptors, such as the GPCRs. These findings indicate that Zap-70 partially compensates for the loss of Syk *in vivo*, but not *in vitro*. Moreover, hemostatic function seems to be more Syk-dependent than arterial thrombus formation. In contrast to Syk, Zap-70 has a much lower intrinsic kinase activity[162] and is not able to phosphorylate the ITAM residues in the receptors itself, probably due to conformational restraints. Consequently, Zap-70 has a greater dependency on SFKs for its activation and ability to phosphorylate and promote the activation of MAPK p38.[167,189] From a report by Lorenz *et al.*, it is known that INU1-induced CLEC-2 receptor downregulation occurs through SFK-dependent receptor internalization *in vitro* and *in vivo*, whereas the associated antibody-induced thrombocytopenia is Syk-dependent.[161] These results suggest that either the hemITAM of CLEC-2 can be phosphorylated by SFKs or that INU1 induces activation of SFKs without hemITAM phosphorylation, thereby contributing to CLEC-2 internalization via a currently unknown mechanism. As Zap-70 strongly depends on SFKs, it might be possible that in the absence of functional Syk, but in the presence of Zap-70, the SFKs mediate downstream signaling of the (hem)ITAM receptors, possibly playing a role in arterial thrombus formation *in vivo*.

5.5. Concluding remarks and future prospects

The findings summarized in this thesis shed new light on megakaryopoiesis and thrombopoiesis. MP-IVM and LSFM were established in our laboratory and the use of both imaging techniques helped us to better understand the mechanisms underlying the thrombocytopenia in mice lacking Profilin1, TRPM7 or RhoA. In addition, it was found that thrombopoiesis is spatially regulated by the BM vasculature and for MKs to produce platelets, no migration towards the vasculare niche is required, contradicting the current concept of megakaryopoiesis. Without the recent developments in imaging methods it would not have been possible to visualize these processes. Although it was shown that the murine BM contains an extremely dense blood vessel network with the majority of MKs residing directly at the sinusoids, further investigations are required to determine the exact location of MK maturation, the cellular interactions within the different BM microenvironments and the regulatory mechanisms of megakaryopoiesis and thrombopoiesis.

In addition, the results presented here showed that Syk deficiency and inhibition protect mice from arterial thrombosis and thrombo-inflammatory brain infarction, without affecting hemostatic function, revealing Syk as a potential anti-thrombotic target. However, the role of GPVI and CLEC-2 is not restricted to their involvement in thrombosis and primary hemostasis. GPVI has been identified as a critical modulator of several thrombo-inflammatory disease states, including ischemic stroke, loss of vascular integrity at sites of inflammation, rheumatoid arthritis and atheroprogression[125-130], whereas CLEC-2 plays a crucial role in different (patho)physiological processes, such as tumor metastasis, maintenance of the integrity of high endothelial venules, lymph nodes development and blood/lymph vessel separation.[146-149] It would be interesting to identify the role of Syk in these processes.

Over the past years, several Syk inhibitors have been developed and have been used in the treatment of allergy,[143] B cell malignancies,[138] heparin-induced thrombocytopenia[145] and autoimmune diseases like rheumatoid arthritis[139] and immune thrombocytopenic purpura.[144] It would be of interest to determine if Syk inhibitors could be used as anti-thrombotic or anti-thrombo-inflammatory therapy in a clinical setting. Yet, knowing that GPVI and CLEC-2 have functions beyond thrombosis and hemostasis, the possibility of severe side-effects of therapeutic agents interfering with the (hem)ITAM signaling pathway, like Syk inhibitors, should be taken into account. Furthermore, since Syk is present in other cell types besides platelets, the effect of a Syk inhibitor as anti-platelet agent on these cell types should be considered, as well as the influence of the use of Syk inhibitors for other diseases, such as autoimmune diseases or cancer, on platelet function. It has also become clear that the absence of GPVI decreases infarct development, whereas GPVI/CLEC-2 double deficiency

leads to severely impaired hemostasis and blockade of platelet aggregation via $\alpha IIb\beta 3$ in the setting of acute stroke leads to intracranial hemorrhage.[97,133,272] Further studies are warranted to identify if in combination with thrombectomy, rt-PA treatment or in the absence of GPVI or CLEC-2, Syk inhibition still provides a safe anti-thrombo-inflammatory therapy without inducing intracranial hemorrhage.

The data presented here, surprisingly, also showed that thrombus formation *in vivo* can occur independently of Syk kinase function in *Syk^{ki}* mice. Zap-70 is a downstream mediator of the immunoreceptor TCR and is mainly expressed in T cells and NK cells.[184] T cells and platelet Syk contribute to the pathophysiology of ischemic stroke.[245,273] Therefore, it would be interesting to determine whether Zap-70 plays a role in ischemia reperfusion injury. Furthermore, additional studies are required to elucidate the exact signaling mechanisms downstream of GPVI and CLEC-2. Since Zap-70 was able to sustain signaling downstream of the (hem)ITAM receptors *in vivo*, it would be important to know the effects of reduced kinase activity for platelet function, if SFKs play a critical role under these conditions and whether pharmacological inhibition of Syk has to provide a complete blockade of Syk activity in order to prevent thrombosis or ischemic stroke.

6. References

1. Dzierzak E, Medvinsky A. Mouse embryonic hematopoiesis. *Trends Genet.* 1995;11(9):359-366.

2. Muller AM, Medvinsky A, Strouboulis J, Grosveld F, Dzierzak E. Development of hematopoietic stem cell activity in the mouse embryo. *Immunity.* 1994;1(4):291-301.

3. Mikkola HK, Orkin SH. The journey of developing hematopoietic stem cells. *Development.* 2006;133(19):3733-3744.

4. Lichtman MA. The ultrastructure of the hemopoietic environment of the marrow: a review. *Exp Hematol.* 1981;9(4):391-410.

5. Morrison SJ, Scadden DT. The bone marrow niche for haematopoietic stem cells. *Nature.* 2014;505(7483):327-334.

6. Weissman IL. Stem cells: units of development, units of regeneration, and units in evolution. *Cell.* 2000;100(1):157-168.

7. Wilson A, Trumpp A. Bone-marrow haematopoietic-stem-cell niches. *Nat Rev Immunol.* 2006;6(2):93-106.

8. Schofield R. The relationship between the spleen colony-forming cell and the haemopoietic stem cell. *Blood Cells.* 1978;4(1-2):7-25.

9. Ding L, Morrison SJ. Haematopoietic stem cells and early lymphoid progenitors occupy distinct bone marrow niches. *Nature.* 2013;495(7440):231-235.

10. Kunisaki Y, Bruns I, Scheiermann C, et al. Arteriolar niches maintain haematopoietic stem cell quiescence. *Nature.* 2013;502(7473):637-643.

11. Acar M, Kocherlakota KS, Murphy MM, et al. Deep imaging of bone marrow shows non-dividing stem cells are mainly perisinusoidal. *Nature.* 2015;526(7571):126-130.

12. Itkin T, Gur-Cohen S, Spencer JA, et al. Distinct bone marrow blood vessels differentially regulate haematopoiesis. *Nature.* 2016;532(7599):323-328.

13. Lord BI, Testa NG, Hendry JH. The relative spatial distributions of CFUs and CFUc in the normal mouse femur. *Blood.* 1975;46(1):65-72.

14. Calvi LM, Adams GB, Weibrecht KW, et al. Osteoblastic cells regulate the haematopoietic stem cell niche. *Nature.* 2003;425(6960):841-846.

15. Zhang J, Niu C, Ye L, et al. Identification of the haematopoietic stem cell niche and control of the niche size. *Nature.* 2003;425(6960):836-841.

16. Kiel MJ, Yilmaz OH, Iwashita T, Yilmaz OH, Terhorst C, Morrison SJ. SLAM family receptors distinguish hematopoietic stem and progenitor cells and reveal endothelial niches for stem cells. *Cell.* 2005;121(7):1109-1121.

17. Dexter TM, Allen TD, Lajtha LG. Conditions controlling the proliferation of haemopoietic stem cells in vitro. *J Cell Physiol.* 1977;91(3):335-344.

18. Avecilla ST, Hattori K, Heissig B, et al. Chemokine-mediated interaction of hematopoietic progenitors with the bone marrow vascular niche is required for thrombopoiesis. *Nat Med*. 2004;10(1):64-71.

19. Rafii S, Mohle R, Shapiro F, Frey BM, Moore MA. Regulation of hematopoiesis by microvascular endothelium. *Leuk Lymphoma*. 1997;27(5-6):375-386.

20. Sipkins DA, Wei X, Wu JW, et al. In vivo imaging of specialized bone marrow endothelial microdomains for tumour engraftment. *Nature*. 2005;435(7044):969-973.

21. Sugiyama T, Kohara H, Noda M, Nagasawa T. Maintenance of the hematopoietic stem cell pool by CXCL12-CXCR4 chemokine signaling in bone marrow stromal cell niches. *Immunity*. 2006;25(6):977-988.

22. Nagasawa T, Hirota S, Tachibana K, et al. Defects of B-cell lymphopoiesis and bone-marrow myelopoiesis in mice lacking the CXC chemokine PBSF/SDF-1. *Nature*. 1996;382(6592):635-638.

23. Ara T, Tokoyoda K, Sugiyama T, Egawa T, Kawabata K, Nagasawa T. Long-term hematopoietic stem cells require stromal cell-derived factor-1 for colonizing bone marrow during ontogeny. *Immunity*. 2003;19(2):257-267.

24. Ponomaryov T, Peled A, Petit I, et al. Induction of the chemokine stromal-derived factor-1 following DNA damage improves human stem cell function. *J Clin Invest*. 2000;106(11):1331-1339.

25. Wright DE, Bowman EP, Wagers AJ, Butcher EC, Weissman IL. Hematopoietic stem cells are uniquely selective in their migratory response to chemokines. *J Exp Med*. 2002;195(9):1145-1154.

26. Lapidot T, Petit I. Current understanding of stem cell mobilization: the roles of chemokines, proteolytic enzymes, adhesion molecules, cytokines, and stromal cells. *Exp Hematol*. 2002;30(9):973-981.

27. Zou YR, Kottmann AH, Kuroda M, Taniuchi I, Littman DR. Function of the chemokine receptor CXCR4 in haematopoiesis and in cerebellar development. *Nature*. 1998;393(6685):595-599.

28. Pang L, Weiss MJ, Poncz M. Megakaryocyte biology and related disorders. *J Clin Invest*. 2005;115(12):3332-3338.

29. Machlus KR, Thon JN, Italiano JE, Jr. Interpreting the developmental dance of the megakaryocyte: a review of the cellular and molecular processes mediating platelet formation. *Br J Haematol*. 2014;165(2):227-236.

30. Machlus KR, Italiano JE, Jr. The incredible journey: From megakaryocyte development to platelet formation. *J Cell Biol*. 2013;201(6):785-796.

31. Schulze H, Korpal M, Hurov J, et al. Characterization of the megakaryocyte demarcation membrane system and its role in thrombopoiesis. *Blood*. 2006;107(10):3868-3875.

32. Eckly A, Heijnen H, Pertuy F, et al. Biogenesis of the demarcation membrane system (DMS) in megakaryocytes. *Blood*. 2014;123(6):921-930.

33. Mahaut-Smith MP, Thomas D, Higham AB, et al. Properties of the demarcation membrane system in living rat megakaryocytes. *Biophys J*. 2003;84(4):2646-2654.

34. Behnke O. An electron microscope study of the megacaryocyte of the rat bone marrow. I. The development of the demarcation membrane system and the platelet surface coat. *J Ultrastruct Res.* 1968;24(5):412-433.

35. Yamada E. The fine structure of the megakaryocyte in the mouse spleen. *Acta Anat (Basel).* 1957;29(3):267-290.

36. Zucker-Franklin D, Kaushansky K. Effect of thrombopoietin on the development of megakaryocytes and platelets: an ultrastructural analysis. *Blood.* 1996;88(5):1632-1638.

37. Kaushansky K, Lok S, Holly RD, et al. Promotion of megakaryocyte progenitor expansion and differentiation by the c-Mpl ligand thrombopoietin. *Nature.* 1994;369(6481):568-571.

38. Grozovsky R, Begonja AJ, Liu K, et al. The Ashwell-Morell receptor regulates hepatic thrombopoietin production via JAK2-STAT3 signaling. *Nat Med.* 2015;21(1):47-54.

39. Grozovsky R, Giannini S, Falet H, Hoffmeister KM. Regulating billions of blood platelets: glycans and beyond. *Blood.* 2015;126(16):1877-1884.

40. Patel SR, Hartwig JH, Italiano JE, Jr. The biogenesis of platelets from megakaryocyte proplatelets. *J Clin Invest.* 2005;115(12):3348-3354.

41. Chang Y, Bluteau D, debili N, Vainchenker W. From hematopoietic stem cells to platelets. *Journal of Thrombosis and Haemostasis.* 2007;5(Suppl. 1):318-327.

42. Ng AP, Kauppi M, Metcalf D, et al. Mpl expression on megakaryocytes and platelets is dispensable for thrombopoiesis but essential to prevent myeloproliferation. *Proc Natl Acad Sci U S A.* 2014;111(16):5884-5889.

43. Gurney AL, de Sauvage FJ. Dissection of c-Mpl and thrombopoietin function: studies of knockout mice and receptor signal transduction. *Stem Cells.* 1996;14 Suppl 1:116-123.

44. Bunting S, Widmer R, Lipari T, et al. Normal platelets and megakaryocytes are produced in vivo in the absence of thrombopoietin. *Blood.* 1997;90(9):3423-3429.

45. Bluteau D, Lordier L, Di Stefano A, et al. Regulation of megakaryocyte maturation and platelet formation. *J Thromb Haemost.* 2009;7 Suppl 1:227-234.

46. Malara A, Gruppi C, Pallotta I, et al. Extracellular matrix structure and nano-mechanics determine megakaryocyte function. *Blood.* 2011;118(16):4449-4453.

47. Malara A, Currao M, Gruppi C, et al. Megakaryocytes contribute to the bone marrow-matrix environment by expressing fibronectin, type IV collagen, and laminin. *Stem Cells.* 2014;32(4):926-937.

48. Hamada T, Mohle R, Hesselgesser J, et al. Transendothelial migration of megakaryocytes in response to stromal cell-derived factor 1 (SDF-1) enhances platelet formation. *J Exp Med.* 1998;188(3):539-548.

49. Dhanjal TS, Pendaries C, Ross EA, et al. A novel role for PECAM-1 in megakaryocytokinesis and recovery of platelet counts in thrombocytopenic mice. *Blood.* 2007;109(10):4237-4244.

50. Niswander LM, Fegan KH, Kingsley PD, McGrath KE, Palis J. SDF-1 dynamically mediates megakaryocyte niche occupancy and thrombopoiesis at steady state and following radiation injury. *Blood*. 2014;124(2):277-286.

51. Schachtner H, Calaminus SD, Sinclair A, et al. Megakaryocytes assemble podosomes that degrade matrix and protrude through basement membrane. *Blood*. 2013;121(13):2542-2552.

52. Gawden-Bone C, Zhou Z, King E, Prescott A, Watts C, Lucocq J. Dendritic cell podosomes are protrusive and invade the extracellular matrix using metalloproteinase MMP-14. *J Cell Sci*. 2010;123(Pt 9):1427-1437.

53. Bruns I, Lucas D, Pinho S, et al. Megakaryocytes regulate hematopoietic stem cell quiescence through CXCL4 secretion. *Nat Med*. 2014;20(11):1315-1320.

54. Zhao M, Perry JM, Marshall H, et al. Megakaryocytes maintain homeostatic quiescence and promote post-injury regeneration of hematopoietic stem cells. *Nat Med*. 2014;20(11):1321-1326.

55. Rafii S, Shapiro F, Pettengell R, et al. Human bone marrow microvascular endothelial cells support long-term proliferation and differentiation of myeloid and megakaryocytic progenitors. *Blood*. 1995;86(9):3353-3363.

56. Kopp HG, Avecilla ST, Hooper AT, Rafii S. The bone marrow vascular niche: home of HSC differentiation and mobilization. *Physiology (Bethesda)*. 2005;20:349-356.

57. Junt T, Schulze H, Chen Z, et al. Dynamic visualization of thrombopoiesis within bone marrow. *Science*. 2007;317(5845):1767-1770.

58. Zhang L, Orban M, Lorenz M, et al. A novel role of sphingosine 1-phosphate receptor S1pr1 in mouse thrombopoiesis. *J Exp Med*. 2012;209(12):2165-2181.

59. Nishimura S, Nagasaki M, Kunishima S, et al. IL-1alpha induces thrombopoiesis through megakaryocyte rupture in response to acute platelet needs. *J Cell Biol*. 2015;209(3):453-466.

60. Bender M, Thon JN, Ehrlicher AJ, et al. Microtubule sliding drives proplatelet elongation and is dependent on cytoplasmic dynein. *Blood*. 2015;125(5):860-868.

61. Richardson JL, Shivdasani RA, Boers C, Hartwig JH, Italiano JE, Jr. Mechanisms of organelle transport and capture along proplatelets during platelet production. *Blood*. 2005;106(13):4066-4075.

62. Italiano JE, Jr., Lecine P, Shivdasani RA, Hartwig JH. Blood platelets are assembled principally at the ends of proplatelet processes produced by differentiated megakaryocytes. *J Cell Biol*. 1999;147(6):1299-1312.

63. Bender M, Eckly A, Hartwig JH, et al. ADF/n-cofilin-dependent actin turnover determines platelet formation and sizing. *Blood*. 2010;116(10):1767-1775.

64. Lee SH, Dominguez R. Regulation of actin cytoskeleton dynamics in cells. *Mol Cells*. 2010;29(4):311-325.

65. Carlsson L, Nystrom LE, Sundkvist I, Markey F, Lindberg U. Actin polymerizability is influenced by profilin, a low molecular weight protein in non-muscle cells. *J Mol Biol*. 1977;115(3):465-483.

66. Honore B, Madsen P, Andersen AH, Leffers H. Cloning and expression of a novel human profilin variant, profilin II. *FEBS Lett.* 1993;330(2):151-155.

67. Hu E, Chen Z, Fredrickson T, Zhu Y. Molecular cloning and characterization of profilin-3: a novel cytoskeleton-associated gene expressed in rat kidney and testes. *Exp Nephrol.* 2001;9(4):265-274.

68. Obermann H, Raabe I, Balvers M, Brunswig B, Schulze W, Kirchhoff C. Novel testis-expressed profilin IV associated with acrosome biogenesis and spermatid elongation. *Mol Hum Reprod.* 2005;11(1):53-64.

69. Goldschmidt-Clermont PJ, Furman MI, Wachsstock D, Safer D, Nachmias VT, Pollard TD. The control of actin nucleotide exchange by thymosin beta 4 and profilin. A potential regulatory mechanism for actin polymerization in cells. *Mol Biol Cell.* 1992;3(9):1015-1024.

70. Pring M, Weber A, Bubb MR. Profilin-actin complexes directly elongate actin filaments at the barbed end. *Biochemistry.* 1992;31(6):1827-1836.

71. Goldschmidt-Clermont PJ, Kim JW, Machesky LM, Rhee SG, Pollard TD. Regulation of phospholipase C-gamma 1 by profilin and tyrosine phosphorylation. *Science.* 1991;251(4998):1231-1233.

72. Witke W. The role of profilin complexes in cell motility and other cellular processes. *Trends Cell Biol.* 2004;14(8):461-469.

73. Suetsugu S, Miki H, Takenawa T. Distinct roles of profilin in cell morphological changes: microspikes, membrane ruffles, stress fibers, and cytokinesis. *FEBS Lett.* 1999;457(3):470-474.

74. Murrell M, Oakes PW, Lenz M, Gardel ML. Forcing cells into shape: the mechanics of actomyosin contractility. *Nat Rev Mol Cell Biol.* 2015;16(8):486-498.

75. Vicente-Manzanares M, Ma X, Adelstein RS, Horwitz AR. Non-muscle myosin II takes centre stage in cell adhesion and migration. *Nat Rev Mol Cell Biol.* 2009;10(11):778-790.

76. Clark K, Middelbeek J, Lasonder E, et al. TRPM7 regulates myosin IIA filament stability and protein localization by heavy chain phosphorylation. *J Mol Biol.* 2008;378(4):790-803.

77. Chubanov V, Schafer S, Ferioli S, Gudermann T. Natural and Synthetic Modulators of the TRPM7 Channel. *Cells.* 2014;3(4):1089-1101.

78. Swenson AM, Trivedi DV, Rauscher AA, et al. Magnesium modulates actin binding and ADP release in myosin motors. *J Biol Chem.* 2014;289(34):23977-23991.

79. Spinler KR, Shin JW, Lambert MP, Discher DE. Myosin-II repression favors pre/proplatelets but shear activation generates platelets and fails in macrothrombocytopenia. *Blood.* 2015;125(3):525-533.

80. Grozovsky R, Hoffmeister KM, Falet H. Novel clearance mechanisms of platelets. *Curr Opin Hematol.* 2010;17(6):585-589.

81. Stegner D, Haining EJ, Nieswandt B. Targeting glycoprotein VI and the immunoreceptor tyrosine-based activation motif signaling pathway. *Arterioscler Thromb Vasc Biol.* 2014;34(8):1615-1620.

82. Nurden AT, Nurden P, Sanchez M, Andia I, Anitua E. Platelets and wound healing. *Front Biosci*. 2008;13:3532-3548.

83. Jenne CN, Kubes P. Platelets in inflammation and infection. *Platelets*. 2015;26(4):286-292.

84. Thon JN, Italiano JE. Platelets: production, morphology and ultrastructure. *Handb Exp Pharmacol*. 2012(210):3-22.

85. Flaumenhaft R. Molecular basis of platelet granule secretion. *Arterioscler Thromb Vasc Biol*. 2003;23(7):1152-1160.

86. White JG. Interaction of membrane systems in blood platelets. *Am J Pathol*. 1972;66(2):295-312.

87. Harrison P, Cramer EM. Platelet alpha-granules. *Blood Rev*. 1993;7(1):52-62.

88. Lozano R, Naghavi M, Foreman K, et al. Global and regional mortality from 235 causes of death for 20 age groups in 1990 and 2010: a systematic analysis for the Global Burden of Disease Study 2010. *Lancet*. 2012;380(9859):2095-2128.

89. Varga-Szabo D, Pleines I, Nieswandt B. Cell adhesion mechanisms in platelets. *Arterioscler Thromb Vasc Biol*. 2008;28(3):403-412.

90. Ruggeri ZM, Orje JN, Habermann R, Federici AB, Reininger AJ. Activation-independent platelet adhesion and aggregation under elevated shear stress. *Blood*. 2006;108(6):1903-1910.

91. Maxwell MJ, Westein E, Nesbitt WS, Giuliano S, Dopheide SM, Jackson SP. Identification of a 2-stage platelet aggregation process mediating shear-dependent thrombus formation. *Blood*. 2007;109(2):566-576.

92. Nesbitt WS, Westein E, Tovar-Lopez FJ, et al. A shear gradient-dependent platelet aggregation mechanism drives thrombus formation. *Nat Med*. 2009;15(6):665-673.

93. Savage B, Almus-Jacobs F, Ruggeri ZM. Specific synergy of multiple substrate-receptor interactions in platelet thrombus formation under flow. *Cell*. 1998;94(5):657-666.

94. Nieswandt B, Watson SP. Platelet-collagen interaction: is GPVI the central receptor? *Blood*. 2003;102(2):449-461.

95. Nieswandt B, Brakebusch C, Bergmeier W, et al. Glycoprotein VI but not alpha2beta1 integrin is essential for platelet interaction with collagen. *EMBO J*. 2001;20(9):2120-2130.

96. Furie BC, Furie B. Tissue factor pathway vs. collagen pathway for in vivo platelet activation. *Blood Cells Mol Dis*. 2006;36(2):135-138.

97. Nieswandt B, Pleines I, Bender M. Platelet adhesion and activation mechanisms in arterial thrombosis and ischaemic stroke. *J Thromb Haemost*. 2011;9 Suppl 1:92-104.

98. Dutting S, Bender M, Nieswandt B. Platelet GPVI: a target for antithrombotic therapy?! *Trends Pharmacol Sci*. 2012;33(11):583-590.

99. Muller F, Mutch NJ, Schenk WA, et al. Platelet polyphosphates are proinflammatory and procoagulant mediators in vivo. *Cell*. 2009;139(6):1143-1156.

100. Offermanns S. Activation of platelet function through G protein-coupled receptors. *Circ Res.* 2006;99(12):1293-1304.

101. Clemetson KJ. Platelet activation: signal transduction via membrane receptors. *Thromb Haemost.* 1995;74(1):111-116.

102. Shattil SJ, Newman PJ. Integrins: dynamic scaffolds for adhesion and signaling in platelets. *Blood.* 2004;104(6):1606-1615.

103. Bergmeier W, Hynes RO. Extracellular matrix proteins in hemostasis and thrombosis. *Cold Spring Harb Perspect Biol.* 2012;4(2).

104. Fox JE. The platelet cytoskeleton. *Thromb Haemost.* 1993;70(6):884-893.

105. Stegner D, Nieswandt B. Platelet receptor signaling in thrombus formation. *J Mol Med (Berl).* 2011;89(2):109-121.

106. Braun A, Vogtle T, Varga-Szabo D, Nieswandt B. STIM and Orai in hemostasis and thrombosis. *Front Biosci (Landmark Ed).* 2011;16:2144-2160.

107. Coughlin SR. Thrombin signalling and protease-activated receptors. *Nature.* 2000;407(6801):258-264.

108. Heasman SJ, Ridley AJ. Mammalian Rho GTPases: new insights into their functions from in vivo studies. *Nat Rev Mol Cell Biol.* 2008;9(9):690-701.

109. Jaffe AB, Hall A. Rho GTPases: biochemistry and biology. *Annu Rev Cell Dev Biol.* 2005;21:247-269.

110. Klages B, Brandt U, Simon MI, Schultz G, Offermanns S. Activation of G12/G13 results in shape change and Rho/Rho-kinase-mediated myosin light chain phosphorylation in mouse platelets. *J Cell Biol.* 1999;144(4):745-754.

111. Pleines I, Hagedorn I, Gupta S, et al. Megakaryocyte-specific RhoA deficiency causes macrothrombocytopenia and defective platelet activation in hemostasis and thrombosis. *Blood.* 2012;119(4):1054-1063.

112. Hart MJ, Jiang X, Kozasa T, et al. Direct stimulation of the guanine nucleotide exchange activity of p115 RhoGEF by Galpha13. *Science.* 1998;280(5372):2112-2114.

113. Suzuki A, Shin JW, Wang Y, et al. RhoA is essential for maintaining normal megakaryocyte ploidy and platelet generation. *PLoS One.* 2013;8(7):e69315.

114. Underhill DM, Goodridge HS. The many faces of ITAMs. *Trends Immunol.* 2007;28(2):66-73.

115. Boylan B, Gao C, Rathore V, Gill JC, Newman DK, Newman PJ. Identification of FcgammaRIIa as the ITAM-bearing receptor mediating alphaIIbbeta3 outside-in integrin signaling in human platelets. *Blood.* 2008;112(7):2780-2786.

116. Severin S, Pollitt AY, Navarro-Nunez L, et al. Syk-dependent phosphorylation of CLEC-2: a novel mechanism of hem-immunoreceptor tyrosine-based activation motif signaling. *J Biol Chem.* 2011;286(6):4107-4116.

117. Watson SP, Herbert JM, Pollitt AY. GPVI and CLEC-2 in hemostasis and vascular integrity. *J Thromb Haemost.* 2010;8(7):1456-1467.

118. Clemetson JM, Polgar J, Magnenat E, Wells TN, Clemetson KJ. The platelet collagen receptor glycoprotein VI is a member of the immunoglobulin superfamily closely related to FcalphaR and the natural killer receptors. *J Biol Chem*. 1999;274(41):29019-29024.

119. Suzuki-Inoue K, Tulasne D, Shen Y, et al. Association of Fyn and Lyn with the proline-rich domain of glycoprotein VI regulates intracellular signaling. *J Biol Chem*. 2002;277(24):21561-21566.

120. Ezumi Y, Shindoh K, Tsuji M, Takayama H. Physical and functional association of the Src family kinases Fyn and Lyn with the collagen receptor glycoprotein VI-Fc receptor gamma chain complex on human platelets. *J Exp Med*. 1998;188(2):267-276.

121. Miura Y, Takahashi T, Jung SM, Moroi M. Analysis of the interaction of platelet collagen receptor glycoprotein VI (GPVI) with collagen. A dimeric form of GPVI, but not the monomeric form, shows affinity to fibrous collagen. *J Biol Chem*. 2002;277(48):46197-46204.

122. Watson SP, Auger JM, McCarty OJ, Pearce AC. GPVI and integrin alphaIIb beta3 signaling in platelets. *J Thromb Haemost*. 2005;3(8):1752-1762.

123. Arthur JF, Dunkley S, Andrews RK. Platelet glycoprotein VI-related clinical defects. *Br J Haematol*. 2007;139(3):363-372.

124. Vogtle T, Cherpokova D, Bender M, Nieswandt B. Targeting platelet receptors in thrombotic and thrombo-inflammatory disorders. *Hamostaseologie*. 2015;35(2).

125. Schonberger T, Siegel-Axel D, Bussl R, et al. The immunoadhesin glycoprotein VI-Fc regulates arterial remodelling after mechanical injury in ApoE-/- mice. *Cardiovasc Res*. 2008;80(1):131-137.

126. Bultmann A, Li Z, Wagner S, et al. Impact of glycoprotein VI and platelet adhesion on atherosclerosis--a possible role of fibronectin. *J Mol Cell Cardiol*. 2010;49(3):532-542.

127. Kleinschnitz C, Pozgajova M, Pham M, Bendszus M, Nieswandt B, Stoll G. Targeting platelets in acute experimental stroke: impact of glycoprotein Ib, VI, and IIb/IIIa blockade on infarct size, functional outcome, and intracranial bleeding. *Circulation*. 2007;115(17):2323-2330.

128. Boulaftali Y, Hess PR, Getz TM, et al. Platelet ITAM signaling is critical for vascular integrity in inflammation. *J Clin Invest*. 2013;123(2):908-916.

129. Boilard E, Nigrovic PA, Larabee K, et al. Platelets amplify inflammation in arthritis via collagen-dependent microparticle production. *Science*. 2010;327(5965):580-583.

130. Jain S, Russell S, Ware J. Platelet glycoprotein VI facilitates experimental lung metastasis in syngenic mouse models. *J Thromb Haemost*. 2009;7(10):1713-1717.

131. Ohlmann P, Hechler B, Ravanat C, et al. Ex vivo inhibition of thrombus formation by an anti-glycoprotein VI Fab fragment in non-human primates without modification of glycoprotein VI expression. *J Thromb Haemost*. 2008;6(6):1003-1011.

132. Schulte V, Rabie T, Prostredna M, Aktas B, Gruner S, Nieswandt B. Targeting of the collagen-binding site on glycoprotein VI is not essential for in vivo depletion of the receptor. *Blood*. 2003;101(10):3948-3952.

133. Bender M, May F, Lorenz V, et al. Combined in vivo depletion of glycoprotein VI and C-type lectin-like receptor 2 severely compromises hemostasis and abrogates arterial thrombosis in mice. *Arterioscler Thromb Vasc Biol.* 2013;33(5):926-934.

134. Nieswandt B, Schulte V, Bergmeier W, et al. Long-term antithrombotic protection by in vivo depletion of platelet glycoprotein VI in mice. *J Exp Med.* 2001;193(4):459-469.

135. Gardiner EE, Karunakaran D, Shen Y, Arthur JF, Andrews RK, Berndt MC. Controlled shedding of platelet glycoprotein (GP)VI and GPIb-IX-V by ADAM family metalloproteinases. *J Thromb Haemost.* 2007;5(7):1530-1537.

136. Rabie T, Varga-Szabo D, Bender M, et al. Diverging signaling events control the pathway of GPVI down-regulation in vivo. *Blood.* 2007;110(2):529-535.

137. Bender M, Hofmann S, Stegner D, et al. Differentially regulated GPVI ectodomain shedding by multiple platelet-expressed proteinases. *Blood.* 2010;116(17):3347-3355.

138. Friedberg JW, Sharman J, Sweetenham J, et al. Inhibition of Syk with fostamatinib disodium has significant clinical activity in non-Hodgkin lymphoma and chronic lymphocytic leukemia. *Blood.* 2010;115(13):2578-2585.

139. Weinblatt ME, Kavanaugh A, Burgos-Vargas R, et al. Treatment of rheumatoid arthritis with a Syk kinase inhibitor: a twelve-week, randomized, placebo-controlled trial. *Arthritis Rheum.* 2008;58(11):3309-3318.

140. Braselmann S, Taylor V, Zhao H, et al. R406, an orally available spleen tyrosine kinase inhibitor blocks fc receptor signaling and reduces immune complex-mediated inflammation. *J Pharmacol Exp Ther.* 2006;319(3):998-1008.

141. Currie KS, Kropf JE, Lee T, et al. Discovery of GS-9973, a selective and orally efficacious inhibitor of spleen tyrosine kinase. *J Med Chem.* 2014;57(9):3856-3873.

142. Thoma G, Smith AB, van Eis MJ, et al. Discovery and profiling of a selective and efficacious Syk inhibitor. *J Med Chem.* 2015;58(4):1950-1963.

143. Meltzer EO, Berkowitz RB, Grossbard EB. An intranasal Syk-kinase inhibitor (R112) improves the symptoms of seasonal allergic rhinitis in a park environment. *J Allergy Clin Immunol.* 2005;115(4):791-796.

144. Podolanczuk A, Lazarus AH, Crow AR, Grossbard E, Bussel JB. Of mice and men: an open-label pilot study for treatment of immune thrombocytopenic purpura by an inhibitor of Syk. *Blood.* 2009;113(14):3154-3160.

145. Reilly MP, Sinha U, Andre P, et al. PRT-060318, a novel Syk inhibitor, prevents heparin-induced thrombocytopenia and thrombosis in a transgenic mouse model. *Blood.* 2011;117(7):2241-2246.

146. Suzuki-Inoue K, Inoue O, Ozaki Y. Novel platelet activation receptor CLEC-2: from discovery to prospects. *J Thromb Haemost.* 2011;9 Suppl 1:44-55.

147. Boulaftali Y, Hess PR, Kahn ML, Bergmeier W. Platelet immunoreceptor tyrosine-based activation motif (ITAM) signaling and vascular integrity. *Circ Res.* 2014;114(7):1174-1184.

148. Herzog BH, Fu J, Wilson SJ, et al. Podoplanin maintains high endothelial venule integrity by interacting with platelet CLEC-2. *Nature.* 2013;502(7469):105-109.

149. Hess PR, Rawnsley DR, Jakus Z, et al. Platelets mediate lymphovenous hemostasis to maintain blood-lymphatic separation throughout life. *J Clin Invest*. 2014;124(1):273-284.

150. Gitz E, Pollitt AY, Gitz-Francois JJ, et al. CLEC-2 expression is maintained on activated platelets and on platelet microparticles. *Blood*. 2014;124(14):2262-2270.

151. Suzuki-Inoue K, Fuller GL, Garcia A, et al. A novel Syk-dependent mechanism of platelet activation by the C-type lectin receptor CLEC-2. *Blood*. 2006;107(2):542-549.

152. Suzuki-Inoue K, Kato Y, Inoue O, et al. Involvement of the snake toxin receptor CLEC-2, in podoplanin-mediated platelet activation, by cancer cells. *J Biol Chem*. 2007;282(36):25993-26001.

153. Navarro-Nunez L, Langan SA, Nash GB, Watson SP. The physiological and pathophysiological roles of platelet CLEC-2. *Thromb Haemost*. 2013;109(6):991-998.

154. Bertozzi CC, Schmaier AA, Mericko P, et al. Platelets regulate lymphatic vascular development through CLEC-2-SLP-76 signaling. *Blood*. 2010;116(4):661-670.

155. Suzuki-Inoue K, Inoue O, Ding G, et al. Essential in vivo roles of the C-type lectin receptor CLEC-2: embryonic/neonatal lethality of CLEC-2-deficient mice by blood/lymphatic misconnections and impaired thrombus formation of CLEC-2-deficient platelets. *J Biol Chem*. 2010;285(32):24494-24507.

156. Fu J, Gerhardt H, McDaniel JM, et al. Endothelial cell O-glycan deficiency causes blood/lymphatic misconnections and consequent fatty liver disease in mice. *J Clin Invest*. 2008;118(11):3725-3737.

157. Uhrin P, Zaujec J, Breuss JM, et al. Novel function for blood platelets and podoplanin in developmental separation of blood and lymphatic circulation. *Blood*. 2010;115(19):3997-4005.

158. Finney BA, Schweighoffer E, Navarro-Nunez L, et al. CLEC-2 and Syk in the megakaryocytic/platelet lineage are essential for development. *Blood*. 2012;119(7):1747-1756.

159. Hughes CE, Pollitt AY, Mori J, et al. CLEC-2 activates Syk through dimerization. *Blood*. 2010;115(14):2947-2955.

160. May F, Hagedorn I, Pleines I, et al. CLEC-2 is an essential platelet-activating receptor in hemostasis and thrombosis. *Blood*. 2009;114(16):3464-3472.

161. Lorenz V, Stegner D, Stritt S, et al. Targeted downregulation of platelet CLEC-2 occurs through Syk-independent internalization. *Blood*. 2015.

162. Mocsai A, Ruland J, Tybulewicz VL. The SYK tyrosine kinase: a crucial player in diverse biological functions. *Nat Rev Immunol*. 2010;10(6):387-402.

163. Poole A, Gibbins JM, Turner M, et al. The Fc receptor gamma-chain and the tyrosine kinase Syk are essential for activation of mouse platelets by collagen. *EMBO J*. 1997;16(9):2333-2341.

164. Jakus Z, Fodor S, Abram CL, Lowell CA, Mocsai A. Immunoreceptor-like signaling by beta 2 and beta 3 integrins. *Trends Cell Biol*. 2007;17(10):493-501.

165. Kerrigan AM, Brown GD. Syk-coupled C-type lectin receptors that mediate cellular activation via single tyrosine based activation motifs. *Immunol Rev*. 2010;234(1):335-352.

166. Yanagi S, Inatome R, Takano T, Yamamura H. Syk expression and novel function in a wide variety of tissues. *Biochem Biophys Res Commun*. 2001;288(3):495-498.

167. Turner M, Schweighoffer E, Colucci F, Di Santo JP, Tybulewicz VL. Tyrosine kinase SYK: essential functions for immunoreceptor signalling. *Immunol Today*. 2000;21(3):148-154.

168. Veillette A, Latour S, Davidson D. Negative regulation of immunoreceptor signaling. *Annu Rev Immunol*. 2002;20:669-707.

169. Lupher ML, Jr., Rao N, Lill NL, et al. Cbl-mediated negative regulation of the Syk tyrosine kinase. A critical role for Cbl phosphotyrosine-binding domain binding to Syk phosphotyrosine 323. *J Biol Chem*. 1998;273(52):35273-35281.

170. Turner M, Mee PJ, Costello PS, et al. Perinatal lethality and blocked B-cell development in mice lacking the tyrosine kinase Syk. *Nature*. 1995;378(6554):298-302.

171. Cheng AM, Rowley B, Pao W, Hayday A, Bolen JB, Pawson T. Syk tyrosine kinase required for mouse viability and B-cell development. *Nature*. 1995;378(6554):303-306.

172. Henderson RB, Grys K, Vehlow A, et al. A novel Rac-dependent checkpoint in B cell development controls entry into the splenic white pulp and cell survival. *J Exp Med*. 2010;207(4):837-853.

173. Costello PS, Turner M, Walters AE, et al. Critical role for the tyrosine kinase Syk in signalling through the high affinity IgE receptor of mast cells. *Oncogene*. 1996;13(12):2595-2605.

174. Crowley MT, Costello PS, Fitzer-Attas CJ, et al. A critical role for Syk in signal transduction and phagocytosis mediated by Fcgamma receptors on macrophages. *J Exp Med*. 1997;186(7):1027-1039.

175. Kiefer F, Brumell J, Al-Alawi N, et al. The Syk protein tyrosine kinase is essential for Fcgamma receptor signaling in macrophages and neutrophils. *Mol Cell Biol*. 1998;18(7):4209-4220.

176. Palacios EH, Weiss A. Distinct roles for Syk and ZAP-70 during early thymocyte development. *J Exp Med*. 2007;204(7):1703-1715.

177. Clemens GR, Schroeder RE, Magness SH, et al. Developmental toxicity associated with receptor tyrosine kinase Ret inhibition in reproductive toxicity testing. *Birth Defects Res A Clin Mol Teratol*. 2009;85(2):130-136.

178. Sharman J, Hawkins M, Kolibaba K, et al. An open-label phase 2 trial of entospletinib (GS-9973), a selective spleen tyrosine kinase inhibitor, in chronic lymphocytic leukemia. *Blood*. 2015;125(15):2336-2343.

179. Hughan SC, Hughes CE, McCarty OJ, et al. GPVI potentiation of platelet activation by thrombin and adhesion molecules independent of Src kinases and Syk. *Arterioscler Thromb Vasc Biol*. 2007;27(2):422-429.

180. Hughes CE, Finney BA, Koentgen F, Lowe KL, Watson SP. The N-terminal SH2 domain of Syk is required for (hem)ITAM, but not integrin, signaling in mouse platelets. *Blood*. 2015;125(1):144-154.

181. Obergfell A, Eto K, Mocsai A, et al. Coordinate interactions of Csk, Src, and Syk kinases with [alpha]IIb[beta]3 initiate integrin signaling to the cytoskeleton. *J Cell Biol*. 2002;157(2):265-275.

182. Law DA, Nannizzi-Alaimo L, Ministri K, et al. Genetic and pharmacological analyses of Syk function in alphaIIbbeta3 signaling in platelets. *Blood*. 1999;93(8):2645-2652.

183. Andre P, Morooka T, Sim D, et al. Critical role for Syk in responses to vascular injury. *Blood*. 2011;118(18):5000-5010.

184. Au-Yeung BB, Deindl S, Hsu LY, et al. The structure, regulation, and function of ZAP-70. *Immunol Rev*. 2009;228(1):41-57.

185. Futterer K, Wong J, Grucza RA, Chan AC, Waksman G. Structural basis for Syk tyrosine kinase ubiquity in signal transduction pathways revealed by the crystal structure of its regulatory SH2 domains bound to a dually phosphorylated ITAM peptide. *J Mol Biol*. 1998;281(3):523-537.

186. Grucza RA, Futterer K, Chan AC, Waksman G. Thermodynamic study of the binding of the tandem-SH2 domain of the Syk kinase to a dually phosphorylated ITAM peptide: evidence for two conformers. *Biochemistry*. 1999;38(16):5024-5033.

187. Deindl S, Kadlecek TA, Brdicka T, Cao X, Weiss A, Kuriyan J. Structural basis for the inhibition of tyrosine kinase activity of ZAP-70. *Cell*. 2007;129(4):735-746.

188. Deindl S, Kadlecek TA, Cao X, Kuriyan J, Weiss A. Stability of an autoinhibitory interface in the structure of the tyrosine kinase ZAP-70 impacts T cell receptor response. *Proc Natl Acad Sci U S A*. 2009;106(49):20699-20704.

189. Pao LI, Bedzyk WD, Persin C, Cambier JC. Molecular targets of CD45 in B cell antigen receptor signal transduction. *J Immunol*. 1997;158(3):1116-1124.

190. Chan AC, Kadlecek TA, Elder ME, et al. ZAP-70 deficiency in an autosomal recessive form of severe combined immunodeficiency. *Science*. 1994;264(5165):1599-1601.

191. Elder ME, Lin D, Clever J, et al. Human severe combined immunodeficiency due to a defect in ZAP-70, a T cell tyrosine kinase. *Science*. 1994;264(5165):1596-1599.

192. Negishi I, Motoyama N, Nakayama K, et al. Essential role for ZAP-70 in both positive and negative selection of thymocytes. *Nature*. 1995;376(6539):435-438.

193. Kadlecek TA, van Oers NS, Lefrancois L, et al. Differential requirements for ZAP-70 in TCR signaling and T cell development. *J Immunol*. 1998;161(9):4688-4694.

194. Schweighoffer E, Vanes L, Mathiot A, Nakamura T, Tybulewicz VL. Unexpected requirement for ZAP-70 in pre-B cell development and allelic exclusion. *Immunity*. 2003;18(4):523-533.

195. Sakaguchi N, Takahashi T, Hata H, et al. Altered thymic T-cell selection due to a mutation of the ZAP-70 gene causes autoimmune arthritis in mice. *Nature*. 2003;426(6965):454-460.

196. Mazo IB, Gutierrez-Ramos JC, Frenette PS, Hynes RO, Wagner DD, von Andrian UH. Hematopoietic progenitor cell rolling in bone marrow microvessels: parallel contributions by endothelial selectins and vascular cell adhesion molecule 1. *J Exp Med*. 1998;188(3):465-474.

197. Masters BR, So PT. Antecedents of two-photon excitation laser scanning microscopy. *Microsc Res Tech*. 2004;63(1):3-11.

198. Denk W, Strickler JH, Webb WW. Two-photon laser scanning fluorescence microscopy. *Science*. 1990;248(4951):73-76.

199. Denk W, Svoboda K. Photon upmanship: why multiphoton imaging is more than a gimmick. *Neuron*. 1997;18(3):351-357.

200. Huisken J, Stainier DY. Selective plane illumination microscopy techniques in developmental biology. *Development*. 2009;136(12):1963-1975.

201. Santi PA. Light sheet fluorescence microscopy: a review. *J Histochem Cytochem*. 2011;59(2):129-138.

202. Voie AH, Burns DH, Spelman FA. Orthogonal-plane fluorescence optical sectioning: three-dimensional imaging of macroscopic biological specimens. *J Microsc*. 1993;170(Pt 3):229-236.

203. Huisken J, Swoger J, Del Bene F, Wittbrodt J, Stelzer EH. Optical sectioning deep inside live embryos by selective plane illumination microscopy. *Science*. 2004;305(5686):1007-1009.

204. Dodt H-U, Leischner U, Schierloh A, et al. Ultramicroscopy: three-dimensional visualization of neuronal networks in the whole mouse brain. *Nature methods*. 2007;4(4):331-336.

205. Erturk A, Becker K, Jahrling N, et al. Three-dimensional imaging of solvent-cleared organs using 3DISCO. *Nat Protoc*. 2012;7(11):1983-1995.

206. Hama H, Hioki H, Namiki K, et al. ScaleS: an optical clearing palette for biological imaging. *Nat Neurosci*. 2015;18(10):1518-1529.

207. Chung K, Wallace J, Kim SY, et al. Structural and molecular interrogation of intact biological systems. *Nature*. 2013;497(7449):332-337.

208. Bergmeier W, Rackebrandt K, Schroder W, Zirngibl H, Nieswandt B. Structural and functional characterization of the mouse von Willebrand factor receptor GPIb-IX with novel monoclonal antibodies. *Blood*. 2000;95(3):886-893.

209. Bergmeier W, Schulte V, Brockhoff G, Bier U, Zirngibl H, Nieswandt B. Flow cytometric detection of activated mouse integrin alphaIIbbeta3 with a novel monoclonal antibody. *Cytometry*. 2002;48(2):80-86.

210. Nieswandt B, Bergmeier W, Rackebrandt K, Gessner JE, Zirngibl H. Identification of critical antigen-specific mechanisms in the development of immune thrombocytopenic purpura in mice. *Blood*. 2000;96(7):2520-2527.

211. Nieswandt B, Bergmeier W, Schulte V, Rackebrandt K, Gessner JE, Zirngibl H. Expression and function of the mouse collagen receptor glycoprotein VI is strictly dependent on its association with the FcRgamma chain. *J Biol Chem*. 2000;275(31):23998-24002.

212. Hofmann S, Vogtle T, Bender M, Rose-John S, Nieswandt B. The SLAM family member CD84 is regulated by ADAM10 and calpain in platelets. *J Thromb Haemost*. 2012;10(12):2581-2592.

213. Shida Y, Rydz N, Stegner D, et al. Analysis of the role of von Willebrand factor, platelet glycoprotein VI-, and alpha2beta1-mediated collagen binding in thrombus formation. *Blood*. 2014;124(11):1799-1807.

214. Stritt S, Wolf K, Lorenz V, et al. Rap1-GTP-interacting adaptor molecule (RIAM) is dispensable for platelet integrin activation and function in mice. *Blood*. 2015;125(2):219-222.

215. Nieswandt B, Echtenacher B, Wachs FP, et al. Acute systemic reaction and lung alterations induced by an antiplatelet integrin gpIIb/IIIa antibody in mice. *Blood*. 1999;94(2):684-693.

216. Jackson B, Peyrollier K, Pedersen E, et al. RhoA is dispensable for skin development, but crucial for contraction and directed migration of keratinocytes. *Mol Biol Cell*. 2011;22(5):593-605.

217. Bender M, Stritt S, Nurden P, et al. Megakaryocyte-specific Profilin1-deficiency alters microtubule stability and causes a Wiskott-Aldrich syndrome-like platelet defect. *Nat Commun*. 2014;5:4746.

218. Jin J, Desai BN, Navarro B, Donovan A, Andrews NC, Clapham DE. Deletion of Trpm7 disrupts embryonic development and thymopoiesis without altering Mg2+ homeostasis. *Science*. 2008;322(5902):756-760.

219. Tiedt R, Schomber T, Hao-Shen H, Skoda RC. Pf4-Cre transgenic mice allow the generation of lineage-restricted gene knockouts for studying megakaryocyte and platelet function in vivo. *Blood*. 2007;109(4):1503-1506.

220. Konigsberger S, Prodohl J, Stegner D, et al. Altered BCR signalling quality predisposes to autoimmune disease and a pre-diabetic state. *EMBO J*. 2012;31(15):3363-3374.

221. Larina IV, Shen W, Kelly OG, Hadjantonakis AK, Baron MH, Dickinson ME. A membrane associated mCherry fluorescent reporter line for studying vascular remodeling and cardiac function during murine embryonic development. *Anat Rec (Hoboken)*. 2009;292(3):333-341.

222. Kisanuki YY, Hammer RE, Miyazaki J, Williams SC, Richardson JA, Yanagisawa M. Tie2-Cre transgenic mice: a new model for endothelial cell-lineage analysis in vivo. *Dev Biol*. 2001;230(2):230-242.

223. Zhang J, Varas F, Stadtfeld M, Heck S, Faust N, Graf T. CD41-YFP mice allow in vivo labeling of megakaryocytic cells and reveal a subset of platelets hyperreactive to thrombin stimulation. *Exp Hematol*. 2007;35(3):490-499.

224. Faust N, Varas F, Kelly LM, Heck S, Graf T. Insertion of enhanced green fluorescent protein into the lysozyme gene creates mice with green fluorescent granulocytes and macrophages. *Blood*. 2000;96(2):719-726.

225. Feng G, Mellor RH, Bernstein M, et al. Imaging neuronal subsets in transgenic mice expressing multiple spectral variants of GFP. *Neuron*. 2000;28(1):41-51.

226. Lamb DJ, Wollin SL, Schnapp A, et al. BI 1002494, a novel potent and selective oral SYK inhibitor displays differential potency in human basophils and B-cells. *J Pharmacol Exp Ther*. 2016.

227. Braeuninger S, Kleinschnitz C, Nieswandt B, Stoll G. Focal cerebral ischemia. *Methods Mol Biol*. 2012;788:29-42.

228. Bederson JB, Pitts LH, Tsuji M, Nishimura MC, Davis RL, Bartkowski H. Rat middle cerebral artery occlusion: evaluation of the model and development of a neurologic examination. *Stroke*. 1986;17(3):472-476.

229. Moran PM, Higgins LS, Cordell B, Moser PC. Age-related learning deficits in transgenic mice expressing the 751-amino acid isoform of human beta-amyloid precursor protein. *Proc Natl Acad Sci U S A*. 1995;92(12):5341-5345.

230. Dirnagl U. Bench to bedside: the quest for quality in experimental stroke research. *J Cereb Blood Flow Metab*. 2006;26(12):1465-1478.

231. Kawamoto T. Use of a new adhesive film for the preparation of multi-purpose fresh-frozen sections from hard tissues, whole-animals, insects and plants. *Arch Histol Cytol*. 2003;66(2):123-143.

232. Schneider CA, Rasband WS, Eliceiri KW. NIH Image to ImageJ: 25 years of image analysis. *Nat Methods*. 2012;9(7):671-675.

233. Tarantino N, Tinevez JY, Crowell EF, et al. TNF and IL-1 exhibit distinct ubiquitin requirements for inducing NEMO-IKK supramolecular structures. *J Cell Biol*. 2014;204(2):231-245.

234. Grutzendler J, Yang G, Pan F, Parkhurst CN, Gan WB. Transcranial two-photon imaging of the living mouse brain. *Cold Spring Harb Protoc*. 2011;2011(9).

235. Abe T, Fujimori T. Reporter mouse lines for fluorescence imaging. *Dev Growth Differ*. 2013;55(4):390-405.

236. Heinze KG, Koltermann A, Schwille P. Simultaneous two-photon excitation of distinct labels for dual-color fluorescence crosscorrelation analysis. *Proc Natl Acad Sci U S A*. 2000;97(19):10377-10382.

237. Thrasher AJ, Burns SO. WASP: a key immunological multitasker. *Nat Rev Immunol*. 2010;10(3):182-192.

238. Stritt S, Nurden P, Favier R, et al. Defects in TRPM7 channel function deregulate thrombopoiesis through altered cellular Mg(2+) homeostasis and cytoskeletal architecture. *Nat Commun*. 2016;7:11097.

239. Yin T, Li L. The stem cell niches in bone. *J Clin Invest*. 2006;116(5):1195-1201.

240. Malara A, Abbonante V, Di Buduo CA, Tozzi L, Currao M, Balduini A. The secret life of a megakaryocyte: emerging roles in bone marrow homeostasis control. *Cell Mol Life Sci*. 2015;72(8):1517-1536.

241. Shivdasani RA, Rosenblatt MF, Zucker-Franklin D, et al. Transcription factor NF-E2 is required for platelet formation independent of the actions of thrombopoietin/MGDF in megakaryocyte development. *Cell*. 1995;81(5):695-704.

242. Brede C, Friedrich M, Jordan-Garrote AL, et al. Mapping immune processes in intact tissues at cellular resolution. *Journal of Clinical Investigation*. 2012;122(12):4439-4446.

243. Mierzejewska K, Klyachkin YM, Ratajczak J, Abdel-Latif A, Kucia M, Ratajczak MZ. Sphingosine-1-phosphate-mediated mobilization of hematopoietic stem/progenitor cells during intravascular hemolysis requires attenuation of SDF-1-CXCR4 retention signaling in bone marrow. *Biomed Res Int*. 2013;2013:814549.

244. Ma Q, Jones D, Borghesani PR, et al. Impaired B-lymphopoiesis, myelopoiesis, and derailed cerebellar neuron migration in CXCR4- and SDF-1-deficient mice. *Proc Natl Acad Sci U S A*. 1998;95(16):9448-9453.

245. van Eeuwijk JM, Stegner D, Lamb DJ, et al. The Novel Oral Syk Inhibitor, BI1002494, Protects Mice From Arterial Thrombosis and Thromboinflammatory Brain Infarction. *Arterioscler Thromb Vasc Biol*. 2016;36(6):1247-1253.

246. Jauch EC, Saver JL, Adams HP, Jr., et al. Guidelines for the early management of patients with acute ischemic stroke: a guideline for healthcare professionals from the American Heart Association/American Stroke Association. *Stroke*. 2013;44(3):870-947.

247. Berkhemer OA, Fransen PS, Beumer D, et al. A randomized trial of intraarterial treatment for acute ischemic stroke. *N Engl J Med*. 2015;372(1):11-20.

248. Soares BP, Tong E, Hom J, et al. Reperfusion is a more accurate predictor of follow-up infarct volume than recanalization: a proof of concept using CT in acute ischemic stroke patients. *Stroke*. 2010;41(1):e34-40.

249. Zinkstok SM, Beenen LF, Majoie CB, Marquering HA, de Haan RJ, Roos YB. Early deterioration after thrombolysis plus aspirin in acute stroke: a post hoc analysis of the Antiplatelet Therapy in Combination with Recombinant t-PA Thrombolysis in Ischemic Stroke trial. *Stroke*. 2014;45(10):3080-3082.

250. Yang G, Pan F, Parkhurst CN, Grutzendler J, Gan WB. Thinned-skull cranial window technique for long-term imaging of the cortex in live mice. *Nat Protoc*. 2010;5(2):201-208.

251. Grutzendler J, Kasthuri N, Gan WB. Long-term dendritic spine stability in the adult cortex. *Nature*. 2002;420(6917):812-816.

252. Holtmaat A, Bonhoeffer T, Chow DK, et al. Long-term, high-resolution imaging in the mouse neocortex through a chronic cranial window. *Nat Protoc*. 2009;4(8):1128-1144.

253. Xu HT, Pan F, Yang G, Gan WB. Choice of cranial window type for in vivo imaging affects dendritic spine turnover in the cortex. *Nat Neurosci*. 2007;10(5):549-551.

254. Holtmaat AJ, Trachtenberg JT, Wilbrecht L, et al. Transient and persistent dendritic spines in the neocortex in vivo. *Neuron*. 2005;45(2):279-291.

255. Dallas NA, Samuel S, Xia L, et al. Endoglin (CD105): a marker of tumor vasculature and potential target for therapy. *Clin Cancer Res*. 2008;14(7):1931-1937.

256. Barry FP, Boynton RE, Haynesworth S, Murphy JM, Zaia J. The monoclonal antibody SH-2, raised against human mesenchymal stem cells, recognizes an epitope on endoglin (CD105). *Biochem Biophys Res Commun*. 1999;265(1):134-139.

257. Ponzoni M, Savage DG, Ferreri AJ, et al. Chronic idiopathic myelofibrosis: independent prognostic importance of bone marrow microvascular density evaluated by CD105 (endoglin) immunostaining. *Mod Pathol*. 2004;17(12):1513-1520.

258. Herz J, Siffrin V, Hauser AE, et al. Expanding two-photon intravital microscopy to the infrared by means of optical parametric oscillator. *Biophys J*. 2010;98(4):715-723.

259. Kiel MJ, Morrison SJ. Maintaining hematopoietic stem cells in the vascular niche. *Immunity*. 2006;25(6):862-864.

260. Coskun S, Hirschi KK. Establishment and regulation of the HSC niche: Roles of osteoblastic and vascular compartments. *Birth Defects Res C Embryo Today*. 2010;90(4):229-242.

261. Wang L, Benedito R, Bixel MG, et al. Identification of a clonally expanding haematopoietic compartment in bone marrow. *EMBO J*. 2013;32(2):219-230.

262. Can A. Haematopoietic stem cells niches: interrelations between structure and function. *Transfus Apher Sci*. 2008;38(3):261-268.

263. Sanjuan-Pla A, Macaulay IC, Jensen CT, et al. Platelet-biased stem cells reside at the apex of the haematopoietic stem-cell hierarchy. *Nature*. 2013;502(7470):232-236.

264. Nakamura-Ishizu A, Takubo K, Kobayashi H, Suzuki-Inoue K, Suda T. CLEC-2 in megakaryocytes is critical for maintenance of hematopoietic stem cells in the bone marrow. *J Exp Med*. 2015;212(12):2133-2146.

265. Howell WH, Donahue DD. The Production of Blood Platelets in the Lungs. *J Exp Med*. 1937;65(2):177-203.

266. Weyrich AS, Zimmerman GA. Platelets in lung biology. *Annu Rev Physiol*. 2013;75:569-591.

267. Kato K, Kanaji T, Russell S, et al. The contribution of glycoprotein VI to stable platelet adhesion and thrombus formation illustrated by targeted gene deletion. *Blood*. 2003;102(5):1701-1707.

268. Bender M, Hagedorn I, Nieswandt B. Genetic and antibody-induced glycoprotein VI deficiency equally protects mice from mechanically and FeCl(3) -induced thrombosis. *J Thromb Haemost*. 2011;9(7):1423-1426.

269. Asazuma N, Wilde JI, Berlanga O, et al. Interaction of linker for activation of T cells with multiple adapter proteins in platelets activated by the glycoprotein VI-selective ligand, convulxin. *J Biol Chem*. 2000;275(43):33427-33434.

270. Abtahian F. Regulation of Blood and Lymphatic Vascular Separation by Signaling Proteins SLP-76 and Syk. *Science*. 2003;299.

271. Ichise H, Ichise T, Ohtani O, Yoshida N. Phospholipase Cgamma2 is necessary for separation of blood and lymphatic vasculature in mice. *Development*. 2009;136(2):191-195.

272. Nieswandt B, Kleinschnitz C, Stoll G. Ischaemic stroke: a thrombo-inflammatory disease? *J Physiol*. 2011;589(17):4115-4123.

273. Kleinschnitz C, Schwab N, Kraft P, et al. Early detrimental T-cell effects in experimental cerebral ischemia are neither related to adaptive immunity nor thrombus formation. *Blood*. 2010;115(18):3835-3842.

274. Kleinschnitz C, Stoll G, Bendszus M, et al. Targeting coagulation factor XII provides protection from pathological thrombosis in cerebral ischemia without interfering with hemostasis. *J Exp Med*. 2006;203(3):513-518.

275. Berna-Erro A, Braun A, Kraft R, et al. STIM2 regulates capacitive Ca2+ entry in neurons and plays a key role in hypoxic neuronal cell death. *Sci Signal*. 2009;2(93):ra67.

7. Appendix

7.1. Abbreviations

3D	three-dimensional
5-HT	5-hydroxytryptamine
α_{2A}	alpha-2A adrenergic receptor
AC	adenylyl cyclase
ADAM	a disintegrin and metalloprotease
ADP	adenosine diphosphate
AMD	AMD3100
ASA	acetylsalicylic acid
ATP	adenosine triphosphate
b.i.d.	*bis in die*
BABB	benzyl alcohol benzyl benzoate
BCR	B cell receptor
BFU-EM	burst-forming unit-EM
BI	BI1002494
BM	bone marrow
BMECs	BM sinusoidal endothelial cells
BSA	bovine serum albumin
Ca^{2+}	calcium
$[Ca^{2+}]_i$	intracellular calcium concentration
CAR	CXCL12 abundant reticular
CBL	casitas B-lineage lymphoma
CEACAM1	carcinoembryonic antigen-related cell adhesion molecule 1
CFU	colony-forming unit
CFU-EM	CFU-erythrocyte/megakaryocyte
CFU-GEMM	CFU-granulocyte/erythrocyte/macrophage/megakaryocyte
CLEC-2	C-type lectin-like receptor 2
CMP	common myeloid progenitor
c-Mpl	myeloproliferative leukemia virus oncogene
CRP	collagen-related peptide
CVX	convulxin
CXCL12	CXC-chemokine ligand 12
CXCR4	CXC-chemokine receptor 4
DAG	diacyl-glycerol
DAPI	4',6-diamidino-2-phenylindole
DBE	dibenzyl ether
DIC	differential interference contrast
DMEM	Dulbecco's Modified Eagle Media
DMS	demarcation membrane system
DMSO	dimethyl sulfoxide
dNTPs	deoxynucleotide triphosphates
DTS	dense tubular system
ECL	enhanced chemiluminescence
ECM	extracellular matrix
EDTA	ethylenediaminetetraacetic acid

EGTA	ethylene glycol tetraacetic acid
EM	erythrocyte/megakaryocyte
EtOH	ethanol
f.c.	final concentration
FcR	Fc receptors
FCS	fetal calf serum
FGF	fibroblast growth factor
FITC	fluorescein
GDP	guanosine diphosphate
GEFs	guanine nucleotide-exchange factors
GFP	green fluorescent protein
GM-CSF	granulocyte macrophage colony-stimulating factor
GP	glycoprotein
GPCRs	G protein-coupled receptors
GPO	glycine-proline-hydroxyproline
Grb2	growth factor receptor-bound protein 2
GTP	guanosine-5'-triphosphate
h	hour
HEPES	4-(2-hydroxyethyl)-1-piperazineethanesulfonic acid
Het	heterozygous
HSC	hematopoietic stem cell
Ig	immunoglobulin
IL	interleukin
IMS	invaginated membrane system
IP_3	inositol-1,4,5-trisphosphate
ITAM	immunoreceptor tyrosine-based activation motif
ITIM	immunoreceptor tyrosine-based inhibition motif
LAT	linker for activated T cells
LSFM	light-sheet fluorescence microscopy
MAPK	mitogen-activated protein kinase
MeOH	methanol
MFI	mean fluorescence intensities
Mg^{2+}	magnesium
$[Mg^{2+}]_i$	intracellular magnesium concentration
min	minutes
MK	megakaryocyte
MLC	myosin light chain
MMPs	matrix metalloproteases
MOPS	3-(N-morpholino)propanesulfonic acid
MP-IVM	multiphoton intravital microscopy
MRI	magnetic resonance imaging
MSCs	mesenchymal stromal cells
MSD	mean squared displacement
NK	natural killer
NMMIIA	non-muscle myosin II A
ns	not significant
o/n	overnight
OCS	open canalicular system
OPFOS	orthogonal-plane fluorescence optical sectioning

OPO	optical parametric oscillator
Orai1	Ca^{2+} release-activated calcium channel protein 1
PAR	protease-activated receptor
PBS	phosphate-buffered saline
PCR	polymerase chain reaction
PE	R-Phycoerythrin
PECAM-1	platelet endothelial cell adhesion molecule 1
PF4	platelet factor 4
PFA	paraformaldehyde
Pfn1	Profilin1
PGI_2	prostacyclin
PI3K	phosphatidylinositide 3-kinase
PIP_2	phosphatidylinositol-4,5-bisphosphate
PLC	phospholipase C
PPP	platelet-poor plasma
PRP	platelet-rich plasma
PS	phosphatidylserine
RhoA	Ras homolog gene family, member A
Rhod/RC	rhodocytin
ROCK	Rho-associated protein kinase
ROS	reactive oxygen species
RT	room temperature
rt-PA	recombinant tissue plasminogen activator
s	seconds
SCF	stem cell factor
SCID	severe combined immunodeficiency
SD	standard deviation
SDF1	stromal cell-derived factor 1
SDS-PAGE	sodium dodecyl sulfate polyacrylamide gel electrophoresis
SFKs	Src family kinases
SH	Src homology
SHP1	SH2 domain-containing protein tyrosine phosphatase 1
SimR	random simulation
SimVA	vessel associated random simulation
SLP-76	SH2 domain-containing leukocyte protein of 76 kDa
SOCE	store-operated Ca^{2+} entry
SPIM	selective plane illumination microscopy
STIM1	stromal interaction molecule 1
Syk	spleen tyrosine kinase
TBS	tris-buffered saline
TCR	T cell receptor
TEMED	N,N,N',N'-Tetramethylethylenediamine
TF	tissue factor
TGF-β1	transforming growth factor β1
THF	tetrahydrofuran
Thpo	thrombopoietin
Thr	thrombin
tMCAO	transient middle cerebral artery occlusion
TP	TxA_2 receptor

TRPM7	transient receptor potential melastatin 7
TTC	2,3,5-triphenyltetrazolium chloride
TxA$_2$	thromboxane A2
U46	U46619
VCAM1	vascular cell-adhesion molecule 1
VE-cadherin	vascular endothelial-cadherin
Veh	vehicle
vs.	versus
vWF	von Willebrand factor
WAS	Wiskott–Aldrich syndrome
WASp	Wiskott-Aldrich syndrome protein
WIP	WASp-interacting protein
Wt	wildtype
YFP	yellow fluorescent protein
Zap-70	ζ-chain-associated protein kinase of 70 kDa
Zn^{2+}	zinc

7.2. Acknowledgements

The work presented here was accomplished at the Department of Experimental Biomedicine - Vascular Medicine, University Hospital and Rudolf Virchow Center for Experimental Biomedicine, University of Würzburg, in the group of Prof. Dr. Bernhard Nieswandt between January 2011 and June 2016. Some results summarized in this thesis have been published, as indicated in the respective result sections.

Many persons supported me throughout my PhD studies, whom I would like to thank:

Prof. Dr. Bernhard Nieswandt, for giving me the opportunity to perform my PhD thesis in his laboratory, for his enthusiasm, constant support, encouragement, trust and valuable scientific discussions.

Dr. Katrin Heinze, for introducing me to the wonderful world of microscopy, for constant support, fruitful discussions and for reviewing this thesis.

Prof. Dr. Guido Stoll, for fruitful discussions and for reviewing this thesis.

Dr. David Stegner, for his critical and valuable scientific input, for his commitment to our joint projects, for inspiration, constant support and friendship.

Prof. Dr. Harald Schulze, for valuable discussions, support and great memories.

Dr. Sebastian Dütting, Dr. Markus Bender and Dr. Irina Pleines, for valuable discussions, critical input and joint efforts in different projects.

Prof. Dr. Friedemann Kiefer, Dr. Sebastian Königsberger, Prof. Dr. Andreas Beilhack, Dr. Christian Brede and all other collaborators that have not been mentioned here by name, for their support, helpful suggestions and valuable contributions.

Dr. Katharina Remer and all animal caretakers in the animal facilities in the RVZ and ZEMM, for their excellent work.

Dr. Peter Kraft, Dr. Ina Thielmann and Sarah Beck, for their support with tMCAO analyses and *in vivo* models of thrombosis.

The BioImaging team, especially Mike Friedrich, Jürgen Pinnecker, Oğuzhan Angay, Mari Gorelashvili, Patrick Schmithausen and Stephanie Hinze, for great collaboration, support and for providing technical infrastructure.

The technicians, especially Juliana Goldmann and Stefanie Hartmann, for excellent technical support.

The secretaries, Elke Hauck and Kerstin Siegmann, for great organizational support.

7.3. Publications

7.3.1. Original articles

Stegner, D.*, **van Eeuwijk, J.M.M.***, Angay, O., Gorelashvili, M., Pinnecker, J., Schmithausen, P., Semeniak, D., Friedrich, M., Brede, C., Beilhack, A., Schulze, H., Nieswandt, B., Heinze, K.G. Thrombopoiesis is spatially regulated by the bone marrow vasculature. *Submitted.*

van Eeuwijk, J.M.M.*, Stegner, D.*, Lamb, D. J., Kraft, P., Beck, S., Thielmann, I., Kiefer, F., Walzog, B., Stoll, G. and Nieswandt, B. The Novel Oral Syk Inhibitor, BI1002494, Protects Mice From Arterial Thrombosis and Thromboinflammatory Brain Infarction. *Arterioscler Thromb Vasc Biol.* 2016;36(6):1247-1253.

Stritt, S., Nurden, P., Favier, R., Favier, M., Ferioli, S., Gotru, S.K., **van Eeuwijk, J.M.M.**, Schulze, H., Nurden, A.T., Lambert, M.P., Turro, E., Burger-Stritt, S., Matsushita, M., Mittermeier, L., Ballerini, P., Zierler, S., Laffan, M.A., Chubanov, V., Gudermann, T., Nieswandt, B. and Braun, A. Defects in TRPM7 channel function deregulate thrombopoiesis through altered cellular Mg(2+) homeostasis and cytoskeletal architecture. *Nat Commun.* 2016;7:11097.

Bender, M., Stritt, S., Nurden, P., **van Eeuwijk, J.M.M.**, Zieger, B., Kentouche, K., Schulze, H., Morbach, H., Stegner, D., Heinze, K.G., Dutting, S., Gupta, S., Witke, W., Falet, H., Fischer, A., Hartwig, J.H. and Nieswandt, B. Megakaryocyte-specific Profilin1-deficiency alters microtubule stability and causes a Wiskott-Aldrich syndrome-like platelet defect. *Nat Commun.* 2014;5:4746.

Konigsberger, S., Prodohl, J., Stegner, D., Weis, V., Andreas, M., Stehling, M., Schumacher, T., Bohmer, R., Thielmann, I., **van Eeuwijk, J.M.M.**, Nieswandt, B. and Kiefer, F. Altered BCR signalling quality predisposes to autoimmune disease and a pre-diabetic state. *EMBO J.* 2012;31(15):3363-3374.

7.3.2. Oral presentations

The dense blood vessel network in the murine bone marrow spatially limits megakaryocyte migration. XXVth Congress of the International Society on Thrombosis and Haemostasis (ISTH), 2015, Toronto, Canada. (ISTH 2015 Young Investigator Award)

Syk deficiency protects mice from occlusive arterial thrombus formation and ischaemic stroke without inducing intracranial haemorrhage. 2nd European Platelet Network (EUPLAN) Conference, 2014, Le Bischenberg, France.

Thrombus formation *in vivo* can occur independently of Syk kinase function. XXIVth Congress of the International Society on Thrombosis and Haemostasis (ISTH), 2013, Amsterdam, the Netherlands.

7.3.3. Poster presentations

Thrombus formation *in vivo* can occur independently of Syk kinase function. 8th International Symposium of the Graduate School of Life Science: "SCIENTIFIC CROSSTALK", 2013, Würzburg, Germany.

Syk kinase family exchange abrogates ITAM and hemITAM signaling in platelets. 7th International Symposium of the Graduate School of Life Science: "EPOS", 2012, Würzburg, Germany.

Syk kinase family exchange abrogates ITAM and hemITAM signaling in platelets. Joint Symposium of the Collaborative Research Center (SFB) 688 and the Comprehensive Heart Failure Center Würzburg, 2012, Würzburg, Germany.

Intravital two-photon imaging of proplatelet formation and of ischemic stroke. 6th International Symposium of the Graduate School of Life Science: "BIO BANG", 2011, Würzburg, Germany.

7.4. Curriculum vitae

Name: Judith Martina Maria van Eeuwijk
Date of birth: 19.08.1987
Place of birth: Leerdam, the Netherlands
Nationality: Dutch

Postgraduate education:

2011 - present   PhD student in the group of Prof. Dr. Bernhard Nieswandt, Department of Experimental Biomedicine and Rudolf Virchow Center for Experimental Biomedicine, Julius-Maximilians-Universität Würzburg, Würzburg, Germany

Education:

2008 - 2010   Biology of Disease, Master of Science (MSc), Utrecht University, Utrecht, the Netherlands

2005 - 2008   Biomedical Sciences, Bachelor of Science (BSc), Utrecht University, Utrecht, the Netherlands

1999 - 2005   A levels, Gymnasium Camphusianum, Gorinchem, the Netherlands

1991 - 1999   Primary school, Leerdam, the Netherlands

Würzburg, August 2016   _____

                         Judith Martina Maria van Eeuwijk

7.5. Affidavit

I hereby declare that my thesis entitled, "Studies on thrombopoiesis and spleen tyrosine kinase-mediated signaling in platelets", is the result of my own work. I did not receive any help or support from commercial consultants. All sources and/or materials applied are listed and specified in the thesis.

Furthermore, I confirm that this thesis has not yet been submitted as part of another examination process neither in identical nor in similar form.

Würzburg, August 2016   _____

<div align="center">Judith Martina Maria van Eeuwijk</div>

7.6. Eidesstattliche Erklärung

Hiermit erkläre ich an Eides statt, die Dissertation „Untersuchungen der Thrombopoese und der *spleen tyrosine kinase*-vermittelten Signaltransduktion in Thrombozyten" eigenständig, d.h. insbesondere selbstständig und ohne Hilfe eines kommerziellen Promotionsberaters, angefertigt und keine anderen als die von mir angegebenen Quellen und Hilfsmittel verwendet zu haben.

Ich erkläre außerdem, dass die Dissertation weder in gleicher noch in ähnlicher Form bereits in einem anderen Prüfungsverfahren vorgelegen hat.

Würzburg, August 2016   _____

<div align="center">Judith Martina Maria van Eeuwijk</div>